27709

NATIONAL LIBRARY
OTTAWA

CANADA

BIBLIOTHÈQUE NATIONALE
OTTAWA

NAME OF AUTHOR... RICHARD D. MILROY

TITLE OF THESIS... BEAT FREQUENCY HEATING OF A PLASMA NEAR THE ELECTRON PLASMA FREQUENCY

UNIVERSITY... OF ALBERTA

DEGREE FOR WHICH THESIS WAS PRESENTED... M.Sc.

YEAR THIS DEGREE GRANTED... 1976

Permission is hereby granted to THE NATIONAL LIBRARY OF CANADA to microfilm this thesis and to lend or sell copies of the film.

The author reserves other publication rights, and neither the thesis nor extensive extracts from it may be printed or otherwise reproduced without the author's written permission.

(Signed)... Richard D. Milroy

PERMANENT ADDRESS:

#103 - 10512 - 83 Ave

Edmonton

Alta.

DATED... April 14 ... 19 76

NL-91 (10-68)

INFORMATION TO USERS

THIS DISSERTATION HAS BEEN MICROFILMED EXACTLY AS RECEIVED

This copy was produced from a microfiche copy of the original document. The quality of the copy is heavily dependent upon the quality of the original thesis submitted for microfilming. Every effort has been made to ensure the highest quality of reproduction possible.

PLEASE NOTE: Some pages may have indistinct print. Filmed as received.

Canadian Theses Division
Cataloguing Branch
National Library of Canada
Ottawa, Canada K1A 0N4

AVIS AUX USAGERS

LA THESE A ETE MICROFILMEE TELLE QUE NOUS L'AVONS RECUE

Cette copie a été faite à partir d'une microfiche du document original. La qualité de la copie dépend grandement de la qualité de la thèse soumise pour le microfimage. Nous avons tout fait pour assurer une qualité supérieure de reproduction.

NOTA BENE: La qualité d'impression de certaines pages peut laisser à désirer. Microfilmée telle que nous l'avons reçue.

Division des thèses canadiennes
Direction du catalogage
Bibliothèque nationale du Canada
Ottawa, Canada K1A 0N4

THE UNIVERSITY OF ALBERTA

BEAT FREQUENCY HEATING OF A PLASMA NEAR THE ELECTRON PLASMA FREQUENCY

by

RICHARD DOUGLAS MILROY (C)

A THESIS

SUBMITTED TO THE FACULTY OF GRADUATE STUDIES AND RESEARCH

IN PARTIAL FULFILMENT OF THE REQUIREMENTS FOR THE DEGREE OF

MASTER OF SCIENCE

DEPARTMENT OF ELECTRICAL ENGINEERING

EDMONTON, ALBERTA

SPRING, 1976

THE UNIVERSITY OF ALBERTA

FACULTY OF GRADUATE STUDIES AND RESEARCH

The undersigned certify that they have read, and recommend to the Faculty of Graduate Studies and Research, for acceptance, a thesis entitled "Beat Frequency Heating of a Plasma Near the Electron Plasma Frequency," submitted by Richard Douglas Milroy in partial fulfilment of the requirements for the degree of Master of Science in Electrical Engineering.

.....C. P. Caputch.....
Supervisor

.....

.....C. R. James.....

.....

Date ...March 4, 1976.....

ABSTRACT

The heating of a plasma in a solenoid, with a beat frequency harmonic which is excited at a frequency near to that of a Langmuir mode in a plasma, is examined. It is shown that at high temperatures the heating rate is very insensitive to changes in plasma density. The amount of energy that can be coupled to a plasma in a solenoid with this heating scheme is investigated by using a one dimensional computer code which incorporates an exact solution of the relevent MHD equations. The absorption of energy from a high powered laser is shown to be significantly enhanced with this process.

ACKNOWLEDGEMENTS

The author wishes to express his thanks to Dr. C.E. Capjack and Dr. C.R. James who supervised this project. Special thanks must also go to Dr. J. McMullin with whom many problems were discussed.

The author also wishes to thank the National Research Council of Canada and the Department of Electrical Engineering, for financial support during this work.

TABLE OF CONTENTS

CHAPTER PAGE

1. INTRODUCTION 1
2. THE HEATING MECHANISM 4
   2.1 Physical Mechanism 4
   2.2 Heating Characteristics and the Landau Dispersion Relation 9
   2.3 Comparison With Inverse Bremsstrahlung 29
3. THE M.H.D. CODE 33
   3.2 The Hydrodynamic Model 33
   3.2 Numerical Integration 38
   3.3 Alterations to the Routine 40
4. RESTRICTIONS AND ASSUMPTIONS 43
   4.1 Solenoid Length 43
   4.2 Stimulated Scattering 45
   4.3 Distortion of the Velocity Distribution Function 48
5. RESULTS 54
6. CONCLUSION 68

BIBLIOGRAPHY 70

APPENDIX 1. Computer Programs 72

LIST OF TABLES

Table	Description	Page
1.	Comparison of nonlinear heating to inverse bremsstrahlung heating.	31

LIST OF FIGURES

Figure		Page
1.	Plasma power absorption and difference frequency electric field versus density.	11
2.	Plasma power absorption and difference frequency electric field versus temperature.	12
3.	Frequency and damping rates of natural modes near the electron plasma frequency as a function of density.	15
4.	Frequency and damping rates of natural modes near the electron plasma frequency as a a function of temperature.	17
5.	Contour maps of the function $\lvert K^2 D(K,\omega) \rvert$.	22
6.	Three dimensional view of the function $1/\lvert K^2 D(K,\omega) \rvert$.	25
7.	Schematic of a beat frequency heating experiment.	33
8	Time and space positions where different quantities are known in the numerical integration.	39
9.	Plasma parameters after 40 nanoseconds of heating for initial conditions; B_0=60 kG; peak laser power=1.25 GW.	56
10.	Plasma parameters after 40 nanoseconds of heating with initial conditions; B_0=100kG; peak laser power=1.25 GW.	57
11.	Plasma parameters after 40 nanoseconds of heating with initial conditions; B_0=300 kG; peak laser power=1.25 GW.	58
12.	Plasma parameters after 40 nanoseconds of heating with initial conditions; B_0=100 kG; peak laser power=12.5 GW.	59
13.	Ion temperatures as a function of radius.	63

CHAPTER 1

INTRODUCTION

The heating of plasmas to thermonuclear temperatures is a major problem in the quest for controlled thermonuclear fusion. A problem exists with many of the heating schemes that have been used in experiments in that their efficiency drops off with increasing temperature. Plasmas in a solenoid are often heated through inverse bremsstrahlung absorption of laser radiation. It is difficult to achieve good energy coupling at high temperatures with this mechanism, since the absorption length is proportional to $T_e^{3/2}$. In this thesis a new technique of heating a plasma in a solenoid is investigated.

This new technique involves enhanced absorption of radiation by a plasma and can be achieved when a difference frequency harmonic is generated through the nonlinear mixing of two intense laser beams. The power absorption can be optimized by forcing a mode which is close to a natural mode in the plasma. In this thesis the case of two antiparallel lasers with a difference frequency close to that of the natural Langmuir mode is investigated.

Theoretical studies of heating through the nonlinear mixing of waves close to the plasma frequency have been done by Fuchs et al.[1], Cohen[2], Schmidt[3], and Capjack and James[4]. The results of Capjack and James allow a heating rate to be calculated from the laser powers, the plasma temperature,

and the plasma density.

Beat frequency heating could prove useful as a technique in heating plasmas to very high temperatures. This approach is in contrast to the normal heating approach where inverse bremsstrahlung is the only heating mechanism. The absorption length of laser radiation through inverse bremsstrahlung is very long at high temperatures, so the path length of the laser beam through the plasma must also be very long to ensure that a reasonable fraction of the laser energy is deposited in the plasma. The nonlinear heating process, however, could allow a significant fraction of the laser energy to be deposited in a short length of plasma.

Studies to date on the nonlinear heating process assume that the frequency of the difference frequency harmonic is very close to the frequency of the Langmuir mode. In most experimental situations the frequency of the Langmuir mode will change significantly during the heating process due to a change in electron temperature and density. For this reason it impossible for the frequency of the difference frequency harmonic to be close to the frequency of the Langmuir mode during the entire heating process. In this thesis an investigation is made of the sensitivity of the nonlinear heating process to changes in density. The coupling of energy to a plasma will be shown to be increased by increasing the plasma density beyond the value necessary

to make the frequency of the Langmuir mode equal to the difference frequency of the lasers.

The amount of energy that can be absorbed by a plasma in a solenoid through the nonlinear process is compared to the amount of energy that can be absorbed through inverse bremsstrahlung. A computer code which simulates the magnetohydrodynamic behavior of the plasma as it expands outwards during the heating process is used. The simulation allows an assessment to be made of the plasma conditions necessary to optimize the heating process.

CHAPTER 2

THE HEATING MECHANISM

2.1 PHYSICAL MECHANISM

In this section some of the results of a paper by Capjack and James[4] on the use of beat frequency heating at the electron plasma frequency are briefly summarized.

In their study the following assumptions are made: the heating due to the nonlinear interaction of two high frequency laser beams is considered; the source waves have a frequency much greater than the electron plasma frequency and so they can be approximated as free space waves in the plasma; the electric fields of the source waves are linearly polarized with components only in the y-direction; the dc magnetic field B_o is in the z-direction; the plasma has an isotropic Maxwellian equilibrium distribution function.

The analysis begins by finding the plasma distribution function from the Vlasov equation.

$$\frac{\partial f^{\epsilon}}{\partial t} + \underline{v} \cdot \frac{\partial f^{\epsilon}}{\partial \underline{r}} + \frac{Ze\epsilon}{m_{\epsilon}} \left(\underline{E} + \frac{\underline{v}\times\underline{B}}{c}\right) \cdot \frac{\partial f^{\epsilon}}{\partial v} = 0 \qquad (2.1)$$

where $\epsilon = +$ for ions and $-$ for electrons. The solution to equation (2.1) is expanded as

$$\begin{bmatrix} f^{\varepsilon} \\ \underline{E} \\ \underline{B} \end{bmatrix} = \begin{bmatrix} f_o^{\varepsilon} \\ \underline{E}_o \\ \underline{B}_o \end{bmatrix} + \sum_{j=1}^{3} \left\{ \begin{bmatrix} f_j^{\varepsilon} \\ \underline{E}_j \\ \underline{B}_j \end{bmatrix} \exp[i(k_j Z - \omega_j t)] + c.c. \right\} \qquad (2.2)$$

Here the frequencies and propagation vectors of the two source lasers are $(\omega_1, \underline{k}_1)$ and $(\omega_2, \underline{k}_2)$. The frequency and propagation vector of the driven beat frequency wave are $(\omega_3, \underline{k}_3)$ where

$$\begin{aligned} \omega_3 &= \omega_1 - \omega_2 \\ \underline{k}_3 &= \underline{k}_1 - \underline{k}_2 . \end{aligned} \qquad (2.3)$$

It is assumed that $\underline{B}_o$, $\underline{k}_1$, $\underline{k}_2$, and $\underline{k}_3$ are all in the z-direction.

An expression for the zero velocity moment of f_3^{ε} is found to be

$$\int f_3^{\varepsilon}(\underline{v})\, d^3v = i\varepsilon\left(\frac{e}{m_{\varepsilon}}\right) E_3 \int_{-\infty}^{\infty} \frac{\frac{\partial f_o^{\varepsilon}(u)}{\partial u}}{(\omega_3 - K_3 u)}\, du$$

$$+ 2\left(\frac{e}{m_{\varepsilon}}\right)^2 \frac{E_{1y} E_{2y} K_3}{\omega_1 \omega_2 v_{\theta\varepsilon}^2} \int_{-\infty}^{\infty} \frac{u\, f_o^{\varepsilon}(u)}{(\omega_3 - K_3 u)}\, du \qquad (2.4)$$

where u is the velocity component along the z-axis and $v_{\theta\varepsilon}$ is the thermal velocity. If this result is substituted into Poisson's equation

$$\nabla \cdot \underline{E}_3 = 4\pi n_o e \{\int f_3^+(v)\, d^3v - \int f_3^-(v)\, d^3v\} \qquad (2.5)$$

and the nonlinear term for icns is neglected, the following expression is found for E_3 .

$$E_3 = \frac{i\ 3.11\times10^{-16}\ k_3\ \lambda_1\ \lambda_2\ (1 + i\ \alpha_{o-} F_o^-)\ (P_1 P_2)^{1/2}}{[K^2 + 2 + i\ (\alpha_{o+} F_o^+ + \alpha_{o-} F_o^-)]} \qquad (2.6)$$

where

n_o = plasma density in cm^{-3},

$K = k_3 \lambda_D$ where λ_D = Debye length,

λ_1 and λ_2 are the wavelengths of the incident laser beams in microns,

P_1 and P_2 are powers of incident beams in watts/cm^2,

$$\alpha_{o\varepsilon} = \omega_3/(k_3 V_{\theta\varepsilon})$$

$$F_o^{\varepsilon} = \frac{ik_3}{\sqrt{\pi}} \int_{-\infty}^{\infty} \frac{\exp[-m_\varepsilon (u^2/2) k_B T_e]}{(\omega_3 - k_3 u)}\ du \qquad (2.7)$$

Stix[5] has shown that F_o^{ε} can be written as

$$F_o^{\varepsilon} = \sqrt{\pi}\,\frac{k_3}{|k_3|}\,\exp[-\alpha_{o\varepsilon}^2] + 2\,i\,S(\alpha_{o\varepsilon}) \tag{2.8}$$

where

$$S(z) = e^{-z^2}\int_0^z e^{-t^2}\,dt \tag{2.9}$$

The function $S(z)$ is just the complex error function. Collisional damping effects are accounted for by defining the real part of F_o^- as

$$R_e(F_o^-) = \mathrm{Max}\left(\frac{\nu_{ei}}{2\omega_3\alpha_{o-}^3}\,,\ \frac{\sqrt{\pi}\,k_3}{|k_3|}\,\exp[-\alpha_{o-}^2]\right) \tag{2.10}$$

The electron-ion collision frequency, ν_{ei} may be approximated as (see Clavier[6])

$$\nu_{ei} = \frac{2.53\times10^{-5}}{T_e^{3/2}}\,n_o \tag{2.11}$$

where the plasma density n_o is given in cm^{-3} and T_e in electron volts.

The denominator of equation (2.6) can be written as K^2D, where $D(k_3,\omega)$ is as defined in Krall and Trivelpiece[7], equation (8.3.11), as

$$D(k_3,\omega) = 1 + \sum_{\varepsilon} \frac{4\pi\, n_o e}{m_\varepsilon\, k_3} \int \frac{k_3\, \partial f_o^{\varepsilon}/\partial u}{(\omega - k_3 u)}\, du \qquad (2.12)$$

$D(k_3,\omega)$ is called the dielectric function, and its zeros correspond to natural modes of the plasma. If a Maxwellian distribution function is substituted into equation (2.12) for f_o^{ε}, and the integration is carried out it can be shown that

$$K^2 D = K^2 + 2 + i\,(\alpha_{o-} F_o^{-} + \alpha_{o+} F_o^{+}) \qquad (2.13)$$

The average power absorbed by the electrons in the plasma from the induced signal is given by

$$W_3 = R_e\,\{(J_{3z}^{-})^{*} E_3\} \qquad (2.14)$$

where J_{3z}^{-} is the induced electron current in the z-direction (see discusion in Capjack and James[8] following equation (11)).

By expressing J_{3z}^{-} in terms of the mobility tensor as given in Stix[5], the heating rate may be expressed as

$$W_3 = \frac{-\omega_{pe}^2}{2\pi\Omega-}\, R_e\,(M_{zz}^{-})\, |E_3|^2 \qquad (2.15)$$

where ω_{pe} is the electron plasma frequency, $\Omega-$ is the

electron cyclotron frequency and M^{-}_{zz} is the electron mobility tensor. Substitution for M^{-}_{zz} yields

$$W_3 = \frac{\omega_{pe}^2 \alpha_{o-}^2}{(k_3 V_{\theta-})\pi} \quad \text{Max}\left[\frac{\nu_{ei}}{2\omega_3 \alpha_{o-}} \; ; \; \sqrt{\pi}\,\frac{k_3}{|k_3|}\; e^{-\alpha_{o-}^2}\right] |E_3|^2 \quad \left(\frac{\text{ergs}}{\text{cm}^3\ \text{sec}}\right) \quad (2.16)$$

This equation is valid in the limit where either collisional or collisionless damping is dominant. The expression is only an approximation in the region where collisional and collisionless damping effects are of the same order.

2.2 HEATING CHARACTERISTICS AND THE LANDAU DISPERSION RELATION

When the central core of a plasma in a solenoid is heated, the plasma expands outwards leaving a reduced plasma density in the core. The rate at which the plasma expands outwards during the heating is dependent on the heating rate and the initial magnetic field in the solenoid. Situations can exist where the density of the central core is depleted to less than ten percent of its initial value. Thus, since the density and temperature of the plasma can vary greatly during the heating process, the frequency of the Langmuir mode can also vary greatly. Before doing a simulation of such an experiment, a knowledge of the dependence of the nonlinear heating mechanism on the plasma density and temperature is desirable. This allows the initial plasma

parameters to be chosen so as to optimize the plasma heating rate.

The heating rates can be calculated by numerically evaluating equations (2.6) and (2.14). The specific case that will be considered is one where two CO_2 laser beams with wavelengths of 9.6 and 10.6 microns are mixed in a hydrogen plasma. The heating rates calculated below are given in terms of the dimensionless quantity

$$W_3 = \left(\frac{W_3}{n_o}\right) \frac{\gamma_1}{P_1 P_2} \tag{2.17}$$

where γ_1 = 1 sec. watts^2 /(ergs cm^4). W_3 is proportional to the power absorbed/particle in ergs/sec if P_1 and P_2 are in watts/cm^2. The electric field is normalized so that the quantity, E_3, is independent of the incident laser powers.

$$E_3 = \frac{E_3}{\sqrt{P_1 P_2}} \tag{2.18}$$

The graph in Fig. 1 gives the values of W_3 and E_3 versus n_o for various values of temperature, T(eV). The graph in Fig. 2 gives the values of W_3 and E_3 versus T(eV) for various values of density, n_o.

The sharp minimum at about 50 eV in the second set of graphs corresponds to a point of minimum damping of the driven wave. Here collisional effects are becoming small and collisionless damping is just taking over.

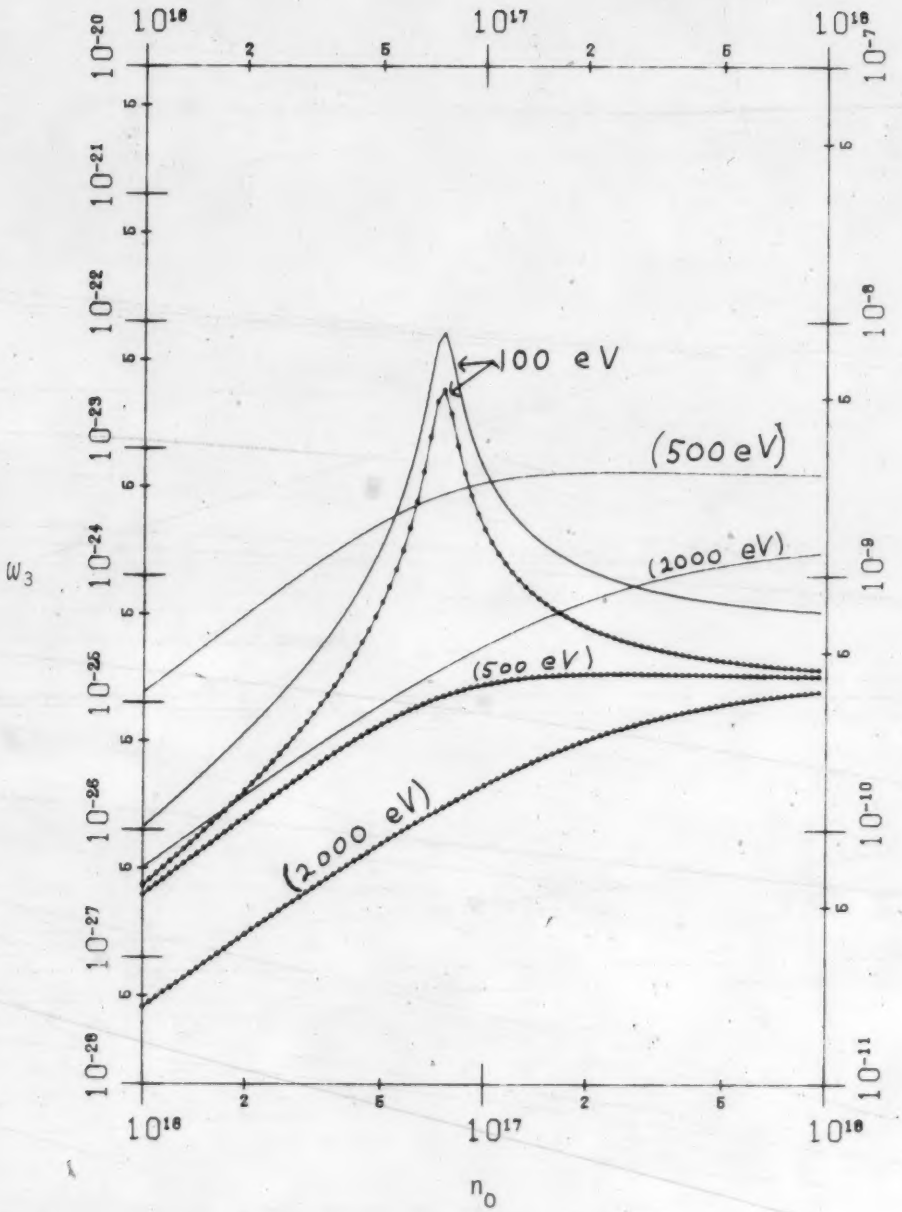

FIG. 1 Plasma power absorption (solid line) and difference frequency electric field (dotted line) versus density. The electron temperature is indicated on the curves.

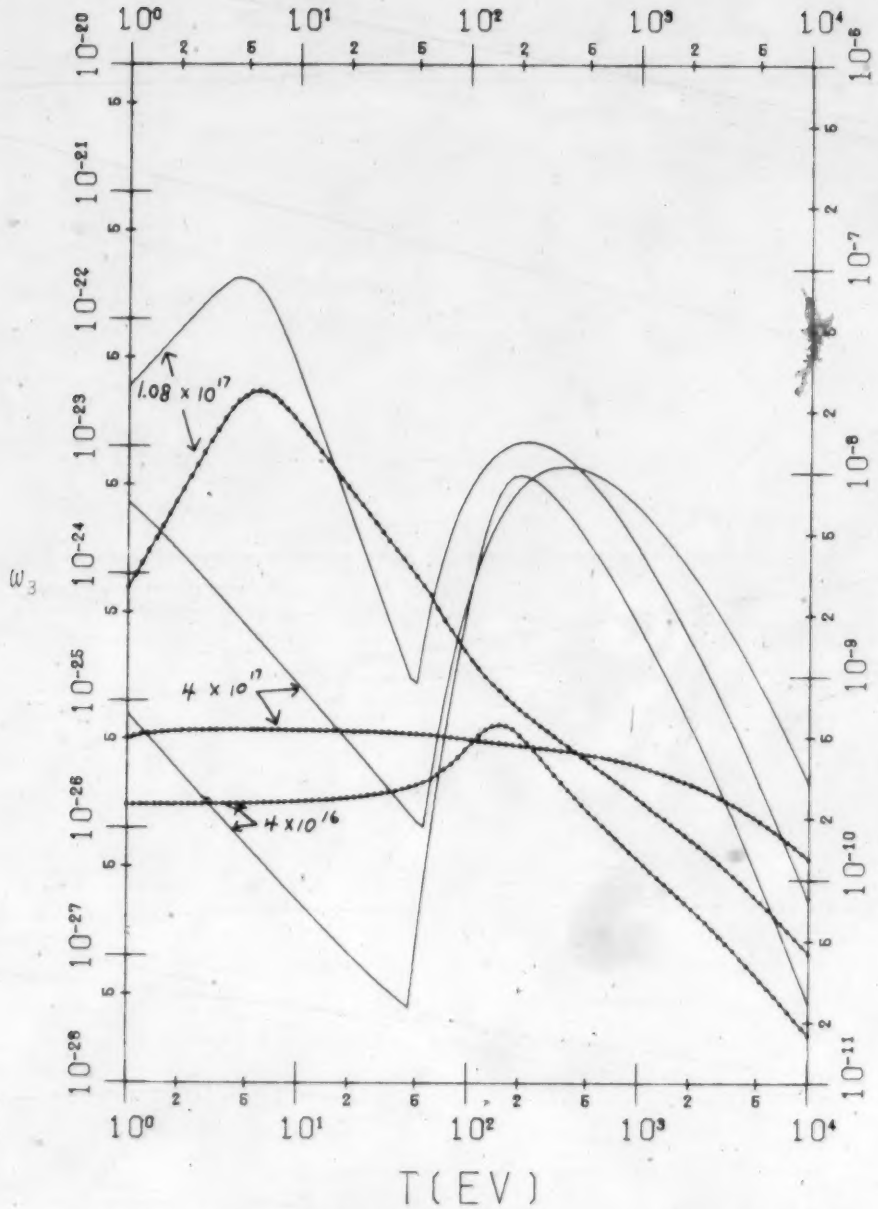

FIG. 2 Plasma power absorption (solid line) and difference frequency electric field (dotted line) versus temperature. The plasma density is indicated on the curves. The case where $n_o = 1.08 \times 10^{17}$ cm^{-17} corresponds to $\omega_3 = \omega_{p\varepsilon}$.

From equation (2.16) it may be seen that the rate of energy coupling to the plasma is maximized when $|E_3|^2$ is maximized through the selection of an operating point. With the use of equation (2.13), equation (2.6) can be written as

$$E_3 = \frac{i\ 3.11\times10^{-16}\ k_3\lambda_1\lambda_2(1+i\ \alpha_{o-}F_o^-)\ \sqrt{P_1P_2}}{K^2D(K,\omega_3)}$$

Thus $|E_3|^2$ is maximized if K^2D is minimized. Minimum values of K^2D are expected when the driving frequency, W_3, is close to a zero of D, or in other words, when the the plasma is forced at a frequency close to a natural mode in the plasma. The position of the zeros of $D(K,\omega)$ is a function of K. The parameter, K, is a function of density and temperature and can be written as

$$K = k_3\lambda_D = k_3\left(\frac{k_B}{4\pi e^2}\right)^{1/2}\left(\frac{T_e}{n_o}\right)^{1/2} = \frac{1}{\sqrt{2}}\ \frac{V_{\theta-}}{(\omega_{pe}/k_3)}$$

This suggests that the response of the heating process to varying parameters such as density and temperature can be qualitatively determined from a plot of the zeros of D.

An iterative procedure used by Capjack and James[4] was used to find the first three zeros of this expression over a range of K values. The first zero of this expression yields the complex frequency corresponding to the Langmuir mode. The other zeroes correspond to the complex frequencies of plasma oscillations which are, not normally considered as natural modes of oscillation since they damp out in

approximately one period of oscillation.

Figs. 3(a) and 3(b) are plots of complex frequencies corresponding to the first three roots of $D(K,\omega)$, normalized to ω_3, as a function of density, for temperatures of 100 eV and 500 eV. Figs. 4(a) to 4(c) are similar plots, but are plotted as a function of temperature for plasma densities of 4×10^{16} cm^{-3}, 1.08×10^{17} cm^{-3}, and 4×10^{17} cm^{-3}. The '*' at 1.0 on the real axis of these plots indicates the position of the pole corresponding to the driving frequency, ω_3.

Fig. 1 shows a sharp resonance in E_3 and W_3 for a density of about 9×10^{16} cm^{-3} when the electron temperature is 100 eV. Fig. 3(a) shows that this corresponds to the point where ω_3 is closest to the natural frequency of the Langmuir mode. Fig. 1 also shows that no such resonance exists for temperatures higher than 500 eV. From Fig. 3(b) it can be seen that the reason for this is that the Langmuir mode is heavily damped at densities that make ω_3 equal to the real part of the Langmuir mode's frequency, and thus its pole never gets close to ω_3.

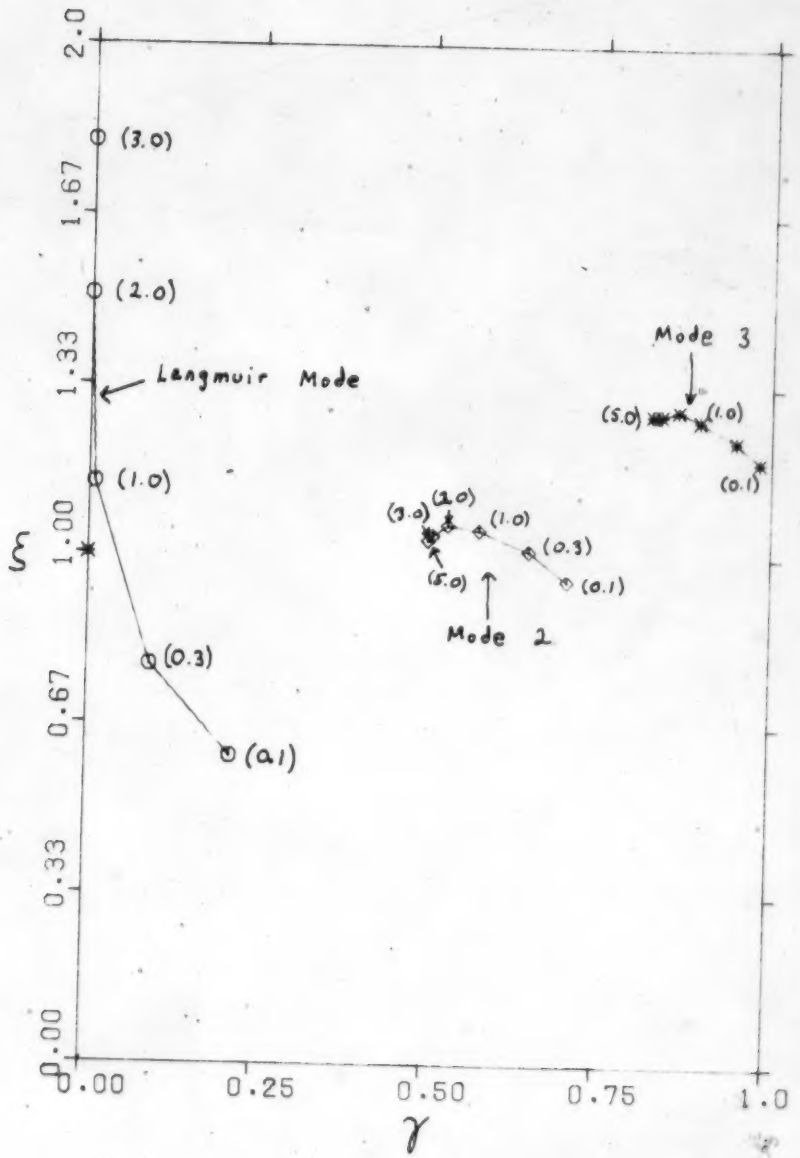

FIG. 3(a) Frequency and damping rates of natural modes near the electron plasma frequency as a function of density. The temperature is 100 eV. The complex frequencies of the natural modes in the plasma are given by $\omega = \omega_3 (\xi - i\gamma)$. Value of parameter δ is given in brackets where δ is defined so that the density, $n_o = \delta \times 1.07 \times 10^{17}$.

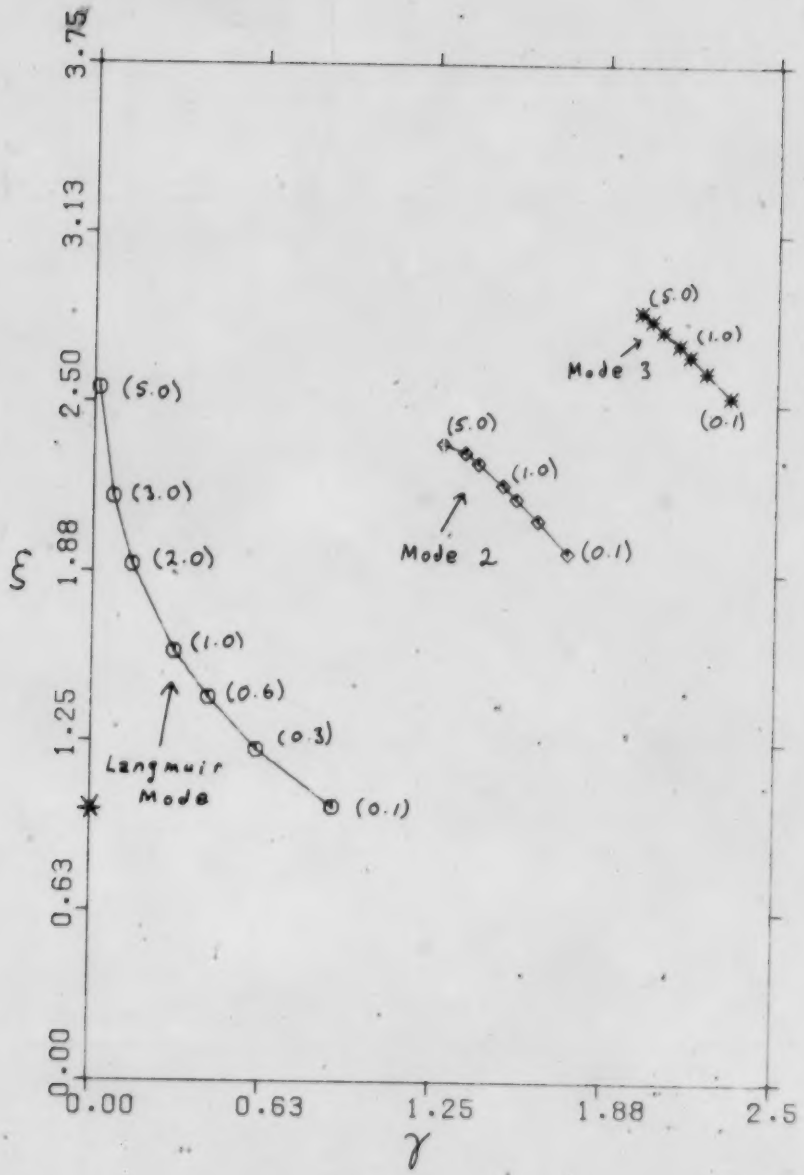

FIG. 3(b) Frequency and damping rates of natural modes near the electron plasma frequency as a function of density. The temperature is 500 eV. The complex frequencies of the natural modes in the plasma are given by $\varepsilon = \omega_3(\xi - i\gamma)$. Value of parameter δ is given in brackets where δ is defined so that the density, $n_o = \delta \times 1.07 \times 10^{17}$.

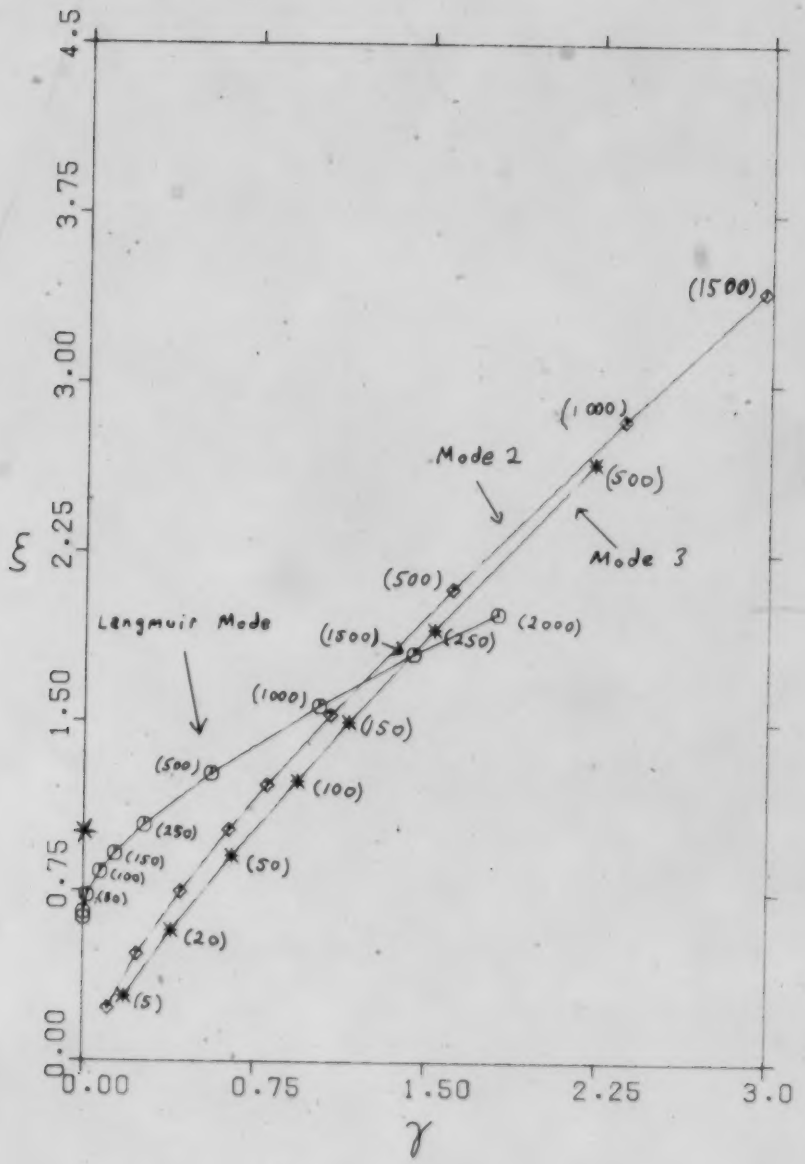

FIG. 4(a) Frequency and damping rates of natural modes near the electron plasma frequency, as a function of temperature. The density is 4.0×10^{16} cm^{-3}. The complex frequencies of the natural modes in the plasma are given by $\omega = \omega_3(\xi - i\gamma)$. Value of temperature in (eV) is given in brackets.

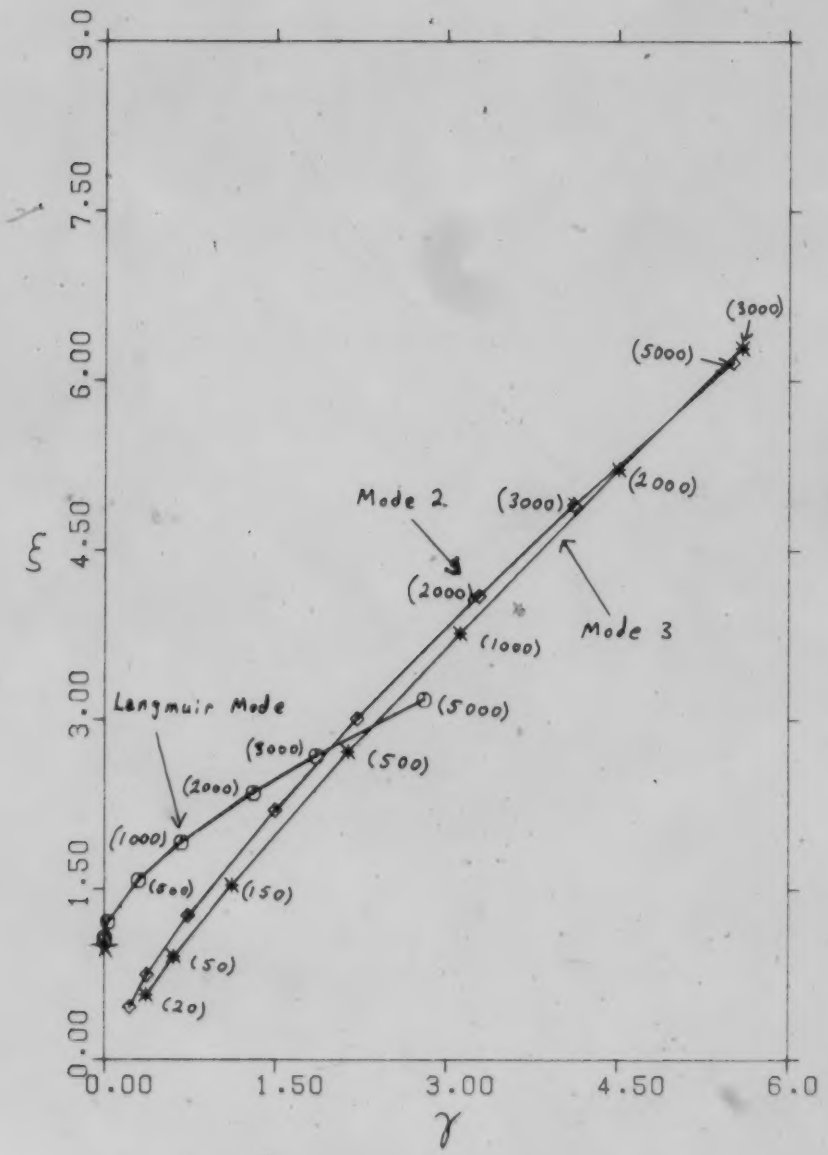

FIG. 4(b) Frequency and damping rates of natural modes near the electron plasma frequency, as a function of temperature. The density is 1.08×10^{17} cm^{-3}. The complex frequencies of the natural modes in the plasma are given by $\omega = \omega_3(\xi - i\gamma)$. Value of temperature in (eV) is given in brackets.

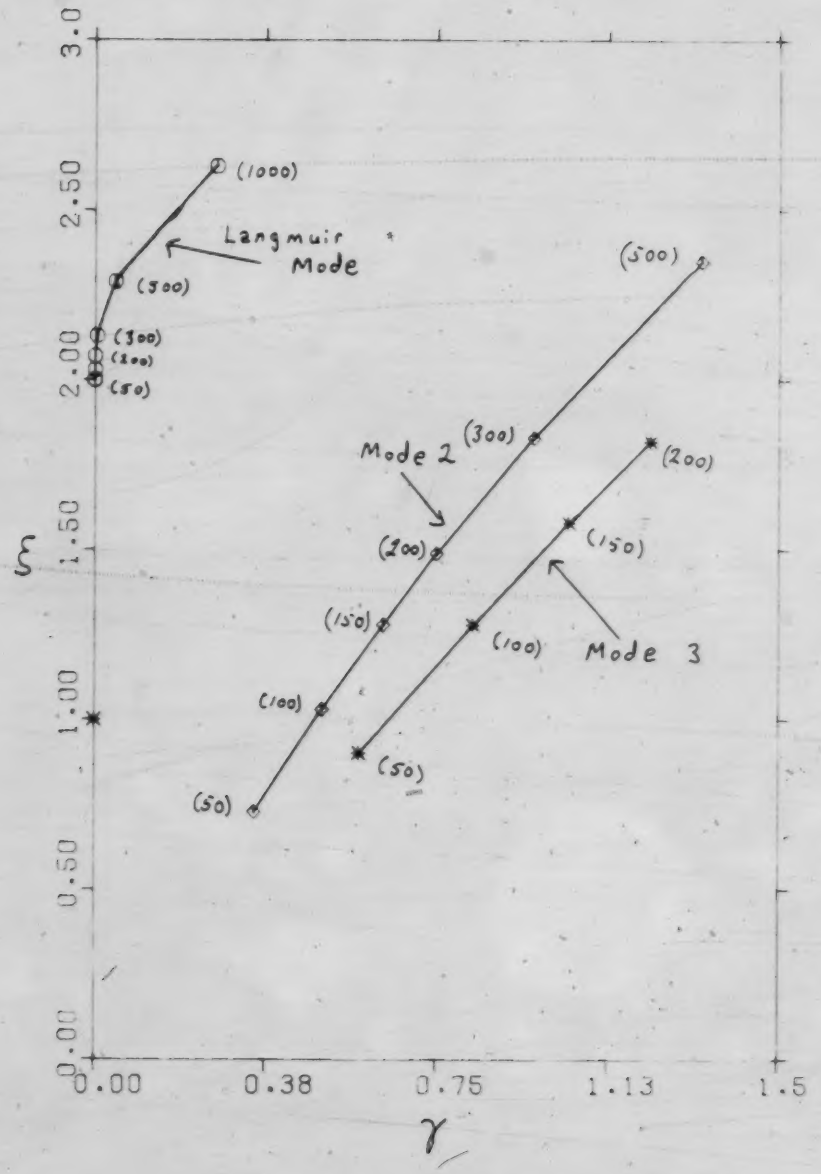

FIG. 4(c) Frequency and damping rates of natural modes near the electron plasma frequency, as a function of temperature. The density is 4.0×10^{17} cm^{-3}. The complex frequencies of the natural modes in the plasma are given by $\omega = \omega_3(\xi - i\gamma)$. Value of temperature in (eV) is given in brackets.

In Fig. 2 it can be seen that there is a resonance in E_3 for a temperature between 100 and 200 eV and a density of $4x10^{16}$ cm^{-3}. Fig. 4(a) shows that the distance between the pole at ω_3 and the pole corresponding to the Langmuir mode is minimized in this temperature range. The general shape of the graph of E_3 versus temperature for a density of $1.08x10^{17}$ cm^{-3} can be explained with the help of Fig. 4(b). The increase in E_3 as temperature increases to 6 eV is due to a decrease in collisional damping. The decrease in E_3 as temperature increases from that point can be attributed to the fact that the pole corresponding to the Langmuir mode is moving further from ω_3 with increasing temperature. Fig. 2 shows that at a density of $4x10^{17}$ cm^{-3}, E_3 is almost temperature independent from 1 to 1000 eV and then starts to drop off. Fig. 4(c) shows this to be consistent with the motion of the Langmuir pole away from ω_3. Fig. 4(c) shows, however, that at low temperatures poles corresponding to other natural modes of the plasma are close to ω_3. In fact, at a temperature of about 50 eV, the distance between ω_3 and the pole corresponding to the second mode is minimized. As the temperature increases this pole moves away from ω_3 rapidly. Thus, some sort of resonance in E_3 for a temperature close to 100 eV would be expected. This is not observed. Because of this discrepancy the importance of these higher order modes in the heating process was investigated further. Contour maps of the function $|K^2D(K,\omega)|$ for the quadrant $Re(\omega)>0$ and $Im(\omega)<0$ are shown in

Figs. 5(a) to 5(e). These contours are drawn in such a way that $|K^2D(K,\omega)|$ changes by equal amounts between contour lines. A set of computer generated three dimensional plots of $1/(|K^2D(K,\omega)|)$ is shown in Figs. 6(a) to 6(e).

Figs. 5(a) - 5(c) and 6(a) - 6(c) show that for large K, higher order poles are almost as wide as the pole corresponding to the Langmuir mode, but they are heavily damped. It is also seen that these poles correspond to a higher frequency of oscillation than the Langmuir mode. As K gets smaller these poles rapidly diminish in width compared to the Langmuir pole, move in towards the origin, and line up on a line at an angle of 45 degrees. At approximately K=0.3 the first of these poles has a frequency less than that of the Langmuir mode. As K grows even smaller, more of these poles move in with a lower frequency than the Langmuir mode.

The fact that no resonance exists in E_3 for a temperature of 100 eV and a density of 4×10^{17} cm^{-3}, as shown in Fig. 2, even though Fig. 4(c) shows that ω_3 is close to a pole, can now be understood in terms of the form of $D(K,\omega)$. This temperature and density yield, K=0.15. When K is this small the higher order poles of the function $1/(K^2D)$ are very narrow, and even though they are close to the real axis, they do not appreciably alter the shape of the function along the real axis.

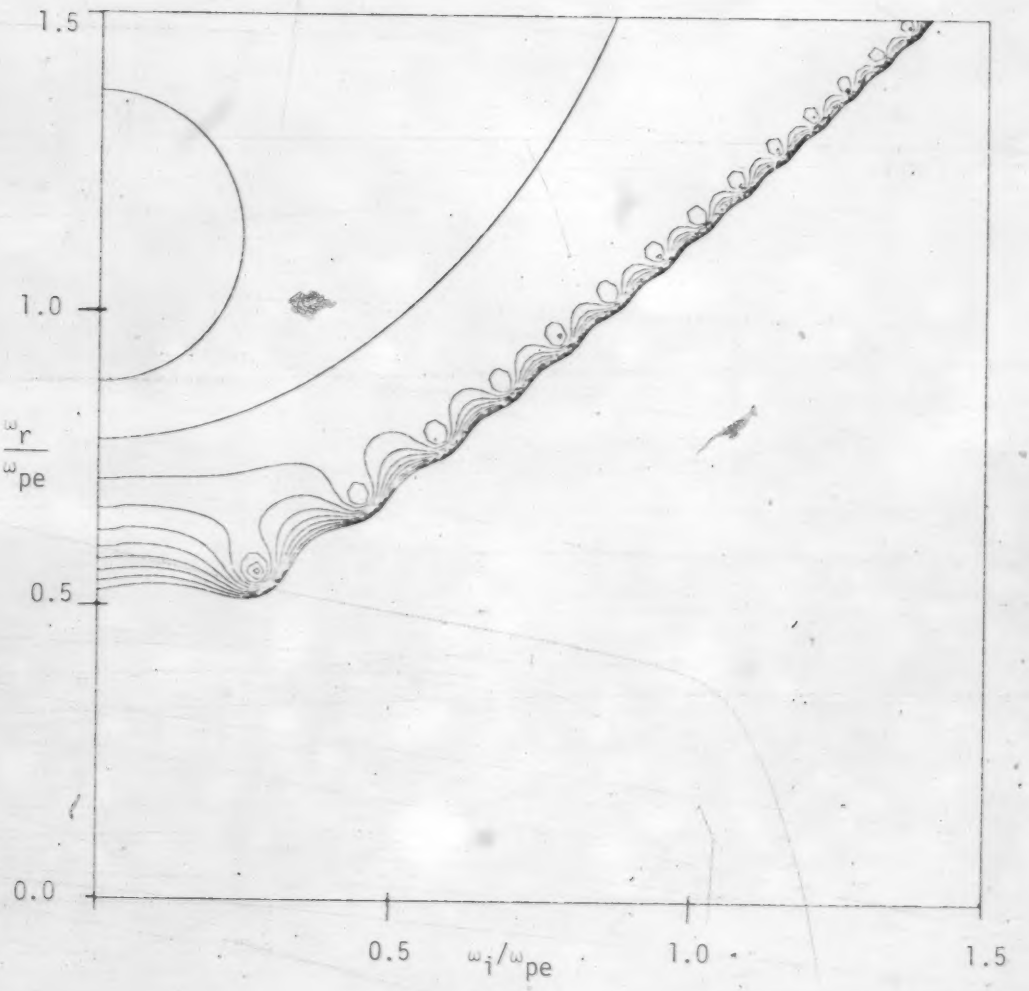

FIG. 5(a) Contour map of the function $|K^{2D}(K,\omega)|$, for K=0.15. Minimum contour value is 0.01 and each sucessive contour is increased by 0.01. Maximum value is 0.1.

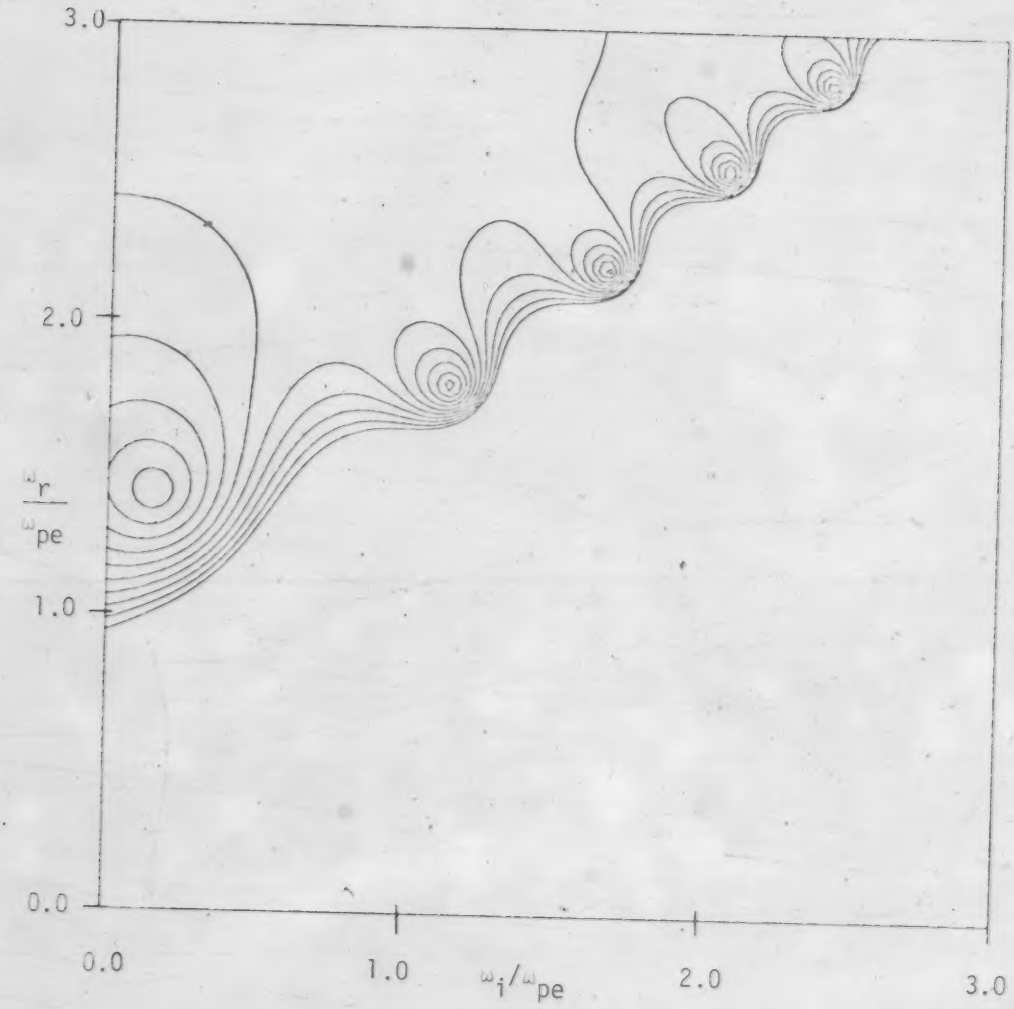

FIG. 5(b) Contour map of the function $|K^2D(K,\omega)|$, for K=0.50. Minimum contour value is 0.04 and each sucessive contour is increased by 0.04. Maximum value is 0.4.

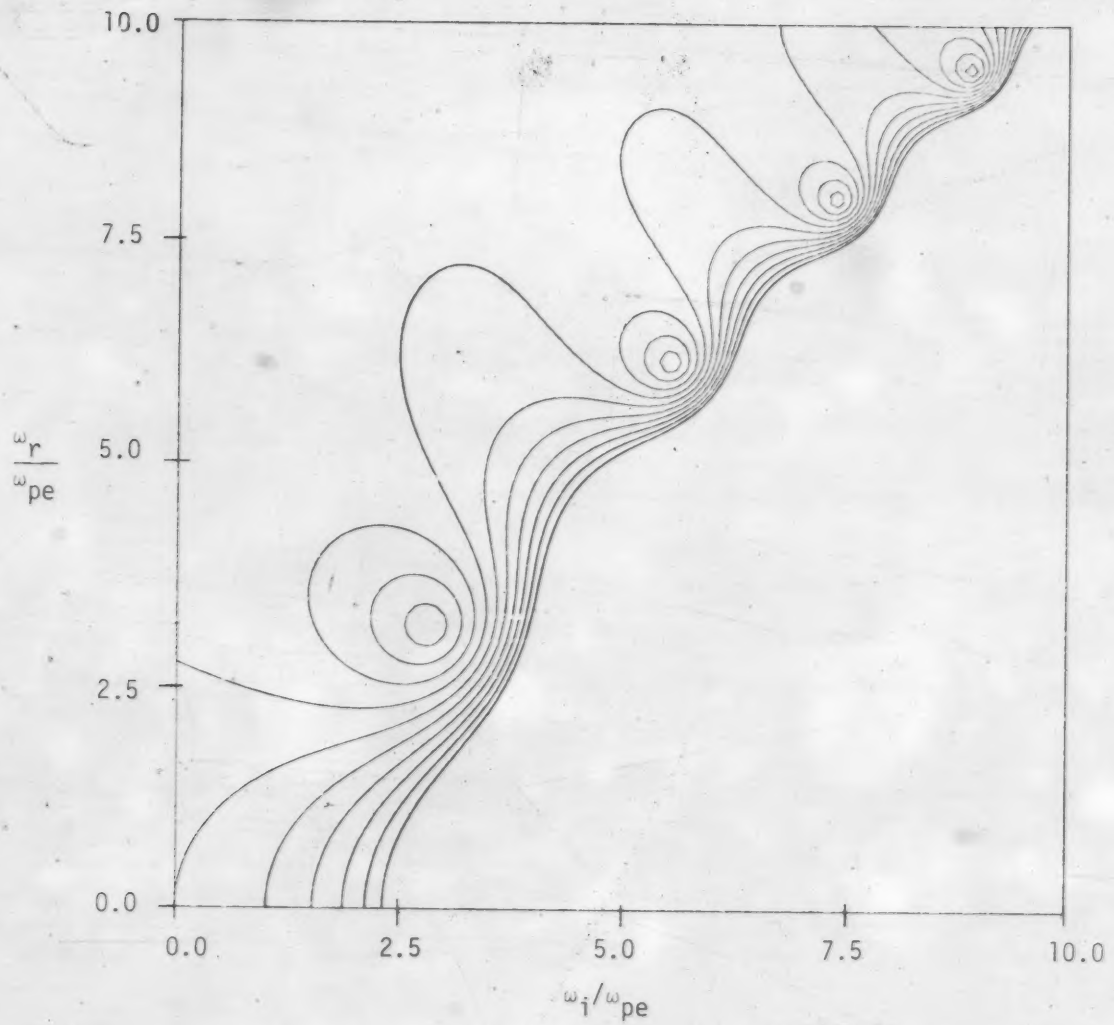

FIG. 5(c) Contour map of the function $|K^2D(K,\omega)|$, for K=2.0. Minimum contour value is 1.0 and each sucessive contour is increased by 1.0. Maximum value is 10.0.

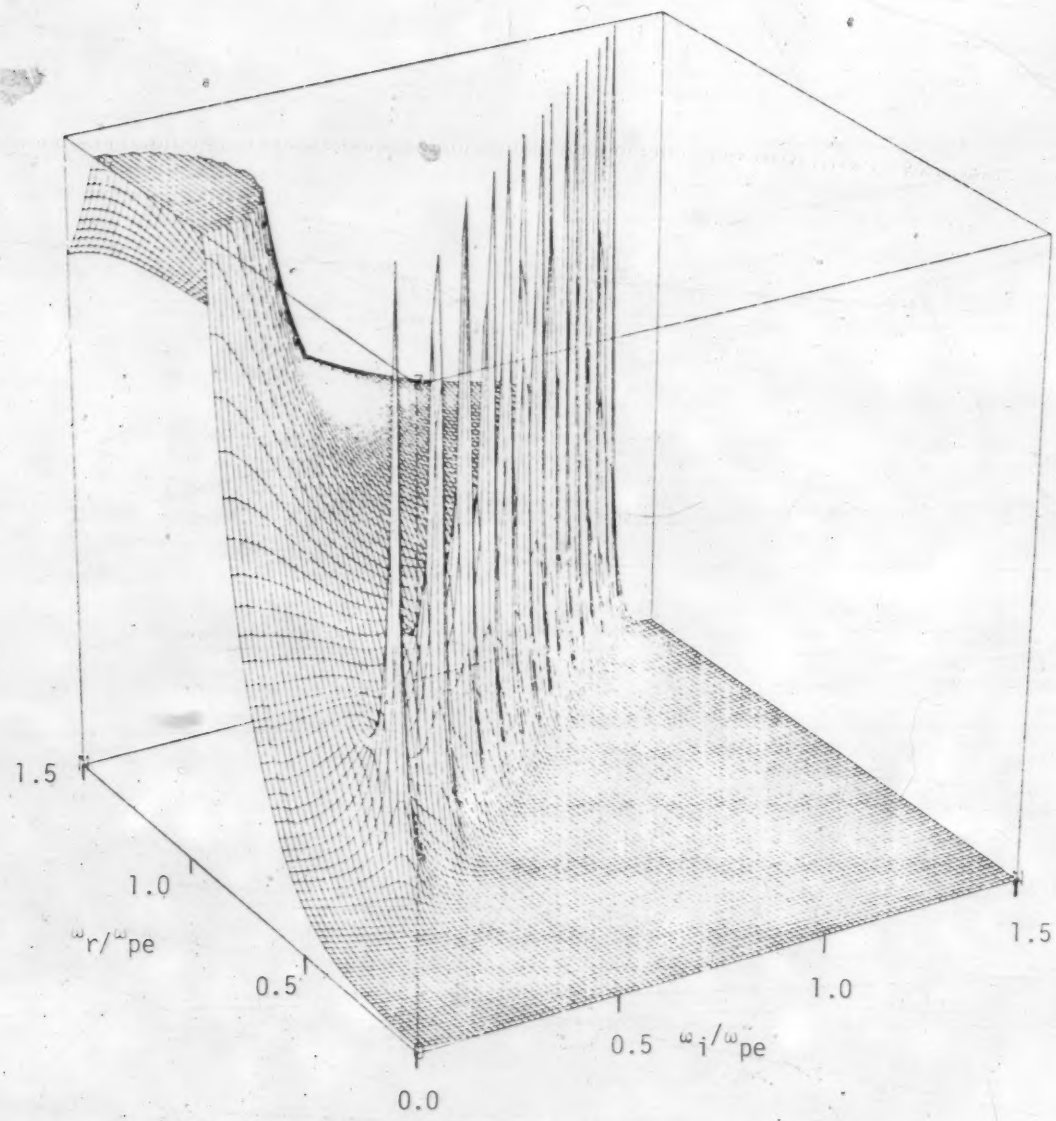

FIG. 6(a) Three dimensional view of the function $1/(|K^2D(K,\omega)|)$ as seen from 30 degrees above the bottom surface. Top surface of cube corresponds to a value of 100.0. K=0.15

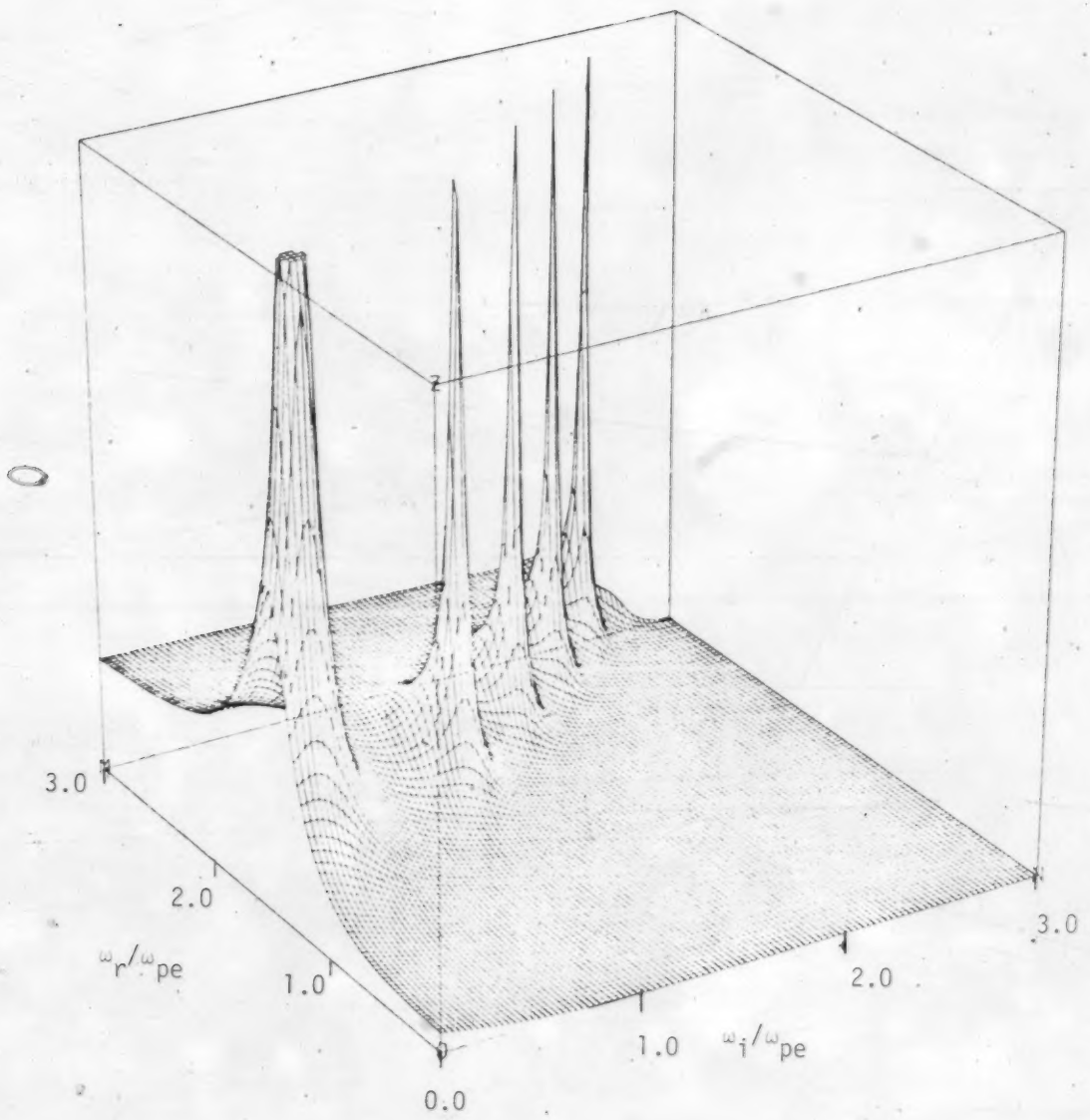

FIG. 6(b) Three dimensional view of the function $1/(|K^2D(K,\omega)|)$ as seen from 30 degrees above the bottom surface. Top surface of cube corresponds to a value of 25.0. K=0.50.

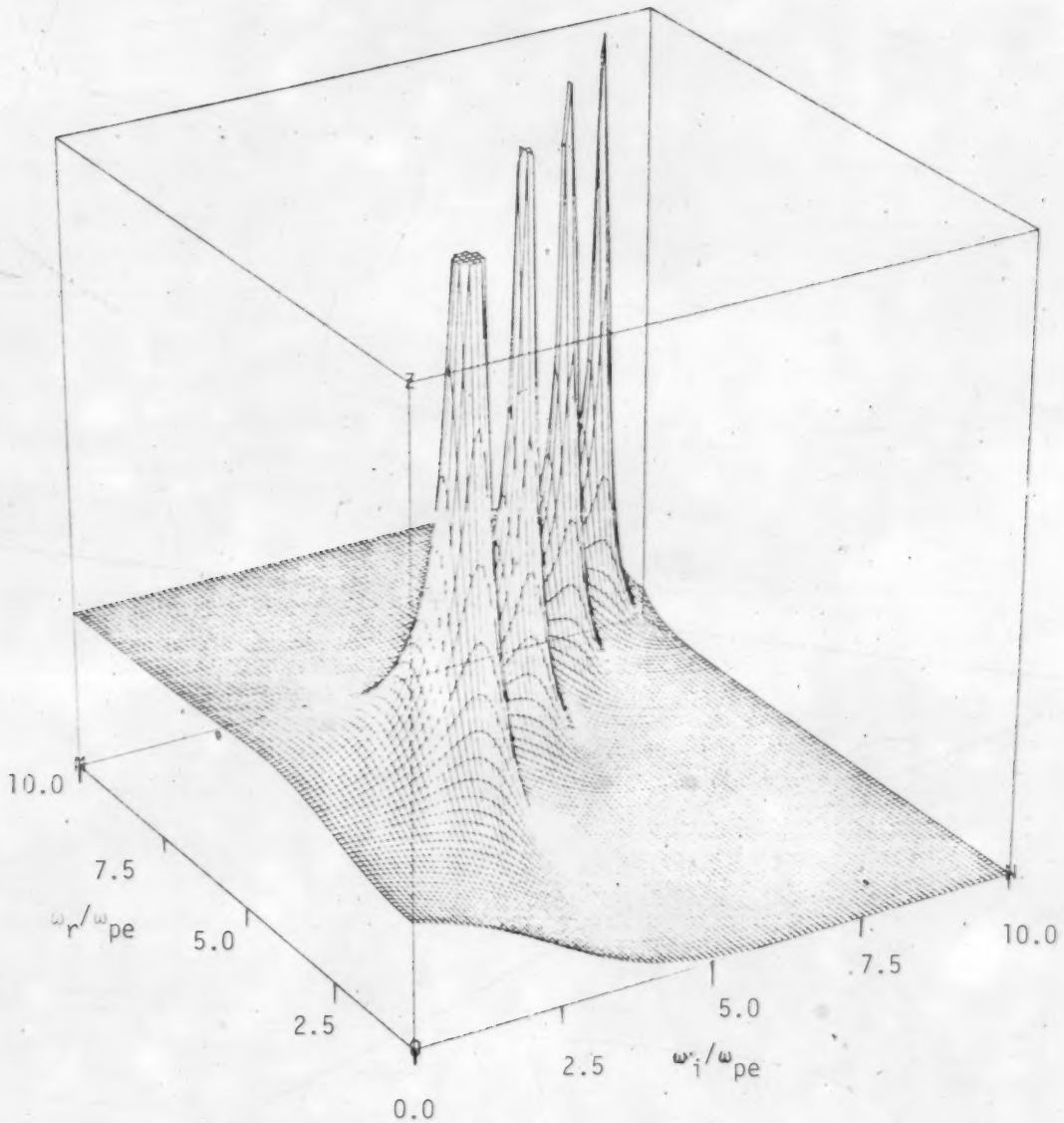

FIG. 6(c) Three dimensional view of the function $1/(|K^2D(K,\omega)|)$ as seen from 30 degrees above the bottom surface. Top surface of cube corresponds to a value of 1.0. K=2.0.

Figs. 6(a) - 6(c) also show the general dependence of E_3 on ω_3. From Fig. 6(a) it is seen that a strong resonance exists in $1/|K^2D(K,\omega_3)|$, and thus in E_3, if ω_3 is close to the frequency of the Langmuir mode. As K grows larger the strength of this resonance becomes smaller. Fig 6(b) shows that the resonance is weak when K=0.5. Fig. 6(b) also shows that the value of $1/|K^2D(K,\omega_3)|$ is much larger if ω_3 is larger rather than less than the Langmuir frequency. Fig. 6(c) shows that almost no resonance exists when K=2.0, and that the function, $1/|K^2D(K,\omega_3)|$, is almost independent of ω_3 for a wide range of ω_3 around the Langmuir frequency. Since K is large for high temperatures little importance can be placed on ω_3 being close to the frequency of the Langmuir mode for high temperatures.

The general shape of the Langmuir pole can be derived analytically for K<<1. The fact that for small K, the Langmuir pole is very close to ω_3 is used. Now,

$$\alpha_{o-} = \omega_3/k_3V_{\theta-} = \frac{1}{\sqrt{2}K} \quad (\frac{\omega}{\omega_{pe}}) \longrightarrow \qquad (2.19)$$

Thus for small K, α_{o-} is large. For large α_{o-}

$$F_o^- \approx 2\, i\, S(\alpha_{o-}) \approx i\, (\frac{1}{\alpha_{o-}} + \frac{1}{2\,\alpha_{o-}^3})$$

Thus, for this case it is found that near the Langmuir pole,

$$K_D^2 = K^2 + 1 + i\,\alpha_{o-}\,F_o^- \approx K^2 - \frac{1}{2\,\alpha_{o-}^2} \qquad (2.20)$$

Equation (2.20) has a zero at $\alpha_{o-} = 1/(\sqrt{2}\,K)$ which, by equation (2.19), corresponds to $\omega = \omega_{pe}$. Equation (2.20) shows that the Langmuir pole cannot be considered to have a simple $1/(\alpha_{o-} - (1/\sqrt{2}K))$ dependance when α_{o-} is of the same order of magnitude as K or larger.

2.3 COMPARISION WITH INVERSE BREMSSTRAHLUNG

Figs. 1 and 2 show that difference frequency heating is relatively insensitive to fluctuations in plasma density and temperature. If the powers of the input lasers are sufficiently high, a significant enhancement in the rate of plasma energy absorption over inverse bremsstrahlung absorption can be realized. This enhancement covers a wide range of temperature and density.

The rate of power absorption from the laser through inverse bremsstrahlung is given by Johnston and Dawson[9], and can be written as

$$W_{IB} \doteq \frac{8.7\times10^{-23}\; Z\, n_o^2\, \lambda^2\, \ln\Lambda\, (P_1+P_2)}{T_e^{3/2}} \quad \left(\frac{\text{ergs}}{\text{cm}^3\ \text{sec}}\right) \qquad (2.21)$$

where n_o is the plasma electron density in cm^{-3}, λ is the incident wavelength in cm, T_e is the electron temperature in

eV, P_1 and P_2 are incident laser powers in watts/cm², and

$$\Lambda = \text{Min}\{2.3\ T_e^{3/2},\ 12\ T_e\}$$

The heating rates due to inverse bremsstrahlung can be expressed in terms of the dimensionless quantity

$$W_{IB} = \left(\frac{W_{IB}}{n_o}\right) \frac{\gamma_2}{1/2(P_1+P_2)} \qquad (2.22)$$

where γ_2 = 1 sec.watts/(ergs cm²). Table 1 lists values of W_3, W_{IB} and the ratio W_3/W_{IB} for various values of density and temperature. If the power densities of both input lasers are equal, (i.e. $P_1=P_2=P$), the ratio in Table 1 multiplied by P, yields the ratio of power absorption due to the nonlinear process to the power absorption due to inverse bremsstrahlung. The inverse of this ratio yields the value of P for which $W_3=W_{IB}$. Table 1 shows that if the power densities of the input lasers are both 10^{11} watts/cm², there is an enhancement in the plasma power absorption of about one order of magnitude for an electron temperature range of 500 eV to 5000 eV and a density range of 5×10^{16} cm^{-3} to 5×10^{17} cm^{-3}. Since the nonlinear power absorption is proportional to P^2, while inverse bremsstrahlung is proportional to P, a plasma power absorption enhancement of two orders of magnitude would be experienced if the input lasers had power densities of 10^{12} watts/cm².

n_e / T(eV)	5.0×10^{16}	1.0×10^{17}	2.0×10^{17}	5.0×10^{17}
1	7.2×10^{-12} 2.2×10^{-25} 3.0×10^{-14}	1.4×10^{-11} 2.3×10^{-23} 1.6×10^{-12}	2.9×10^{-11} 4.3×10^{-24} 1.5×10^{-13}	7.2×10^{-11} 3.5×10^{-24} 5.4×10^{-14}
10	1.2×10^{-12} 7.5×10^{-27} 6.4×10^{-15}	2.4×10^{-12} 5.7×10^{-24} 2.4×10^{-12}	4.7×10^{-12} 1.6×10^{-25} 3.5×10^{-14}	1.2×10^{-11} 1.5×10^{-25} 1.3×10^{-14}
100	6.1×10^{-14} 1.8×10^{-24} 2.9×10^{-11}	1.2×10^{-13} 6.6×10^{-24} 5.4×10^{-11}	2.5×10^{-13} 1.1×10^{-24} 4.6×10^{-12}	6.1×10^{-13} 6.1×10^{-25} 1.0×10^{-12}
500	$6.7\ 10^{-15}$ 2.6×10^{-24} 3.9×10^{-10}	1.4×10^{-14} 5.4×10^{-24} 4.0×10^{-10}	2.7×10^{-14} 6.5×10^{-24} 2.4×10^{-10}	6.7×10^{-14} 6.4×10^{-24} 9.5×10^{-11}
1000	2.6×10^{-15} 5.7×10^{-25} 2.0×10^{-10}	5.1×10^{-15} 1.5×10^{-24} 2.8×10^{-10}	1.0×10^{-14} 2.6×10^{-24} 2.5×10^{-10}	2.6×10^{-14} 3.5×10^{-24} 1.3×10^{-10}
2000	9.8×10^{-16} 9.7×10^{-26} 9.9×10^{-11}	2.0×10^{-15} 2.8×10^{-25} 1.4×10^{-10}	3.9×10^{-15} 6.3×10^{-25} 1.6×10^{-10}	9.8×10^{-15} 1.2×10^{-24} 1.2×10^{-10}
5000	2.7×10^{-16} 6.3×10^{-27} 2.3×10^{-11}	5.4×10^{-16} 2.1×10^{-26} 3.9×10^{-11}	1.1×10^{-15} 6.2×10^{-26} 5.7×10^{-11}	2.7×10^{-15} 1.8×10^{-25} 6.8×10^{-11}

TABLE 1 W_{IB} (top number), W_3 (middle number), and W_3/W_{IB} (bottom number) for various values of T(eV) and n_e.

The efficiency of the transfer of laser energy to plasma energy via this nonlinear method is limited by the Manley - Rowe relations. This relation says that if P_3' is the power gained by the wave at frequency ω_3, and P_1' is the power lost by the wave of the high frequency laser at frequency ω_1, then

$$\frac{P_3'}{P_1'} \leq \frac{\omega_3}{\omega_1} \tag{2.23}$$

This relation places an upper bound of ω_3/ω_1 on the fraction of energy of the high frequency laser that can be transferred to the plasma through the nonlinear process. It is interesting to note that while the incident beam at frequency ω_1 is heavily damped by this process, the lower frequency beam at frequency ω_2 is enhanced. The energy of the high frequency beam is transferred to the lower frequency beam in such a way that $h\omega_1 = h\omega_2 + h\omega_3$. Therefore, for maximum efficiency the high frequency laser should be more powerful than the low frequency laser.

CHAPTER 3

THE M. H. D. CODE

3.1 THE HYDRODYNAMIC MODEL

Fig. 7 shows a schematic diagram for a possible experiment on the beat frequency heating of a plasma. During such an experiment both the plasma density and plasma temperature change at a rate dependent on the heating rate. The heating rate in turn is dependent on the plasma density and temperature. A prediction of the total energy that can be coupled to the plasma through the beat frequency heating process can be made with a computer code which simulates the MHD behavior of the plasma as it is heated. The MHD code used is a modified version of the code described by Burnett and Offenberger[10].

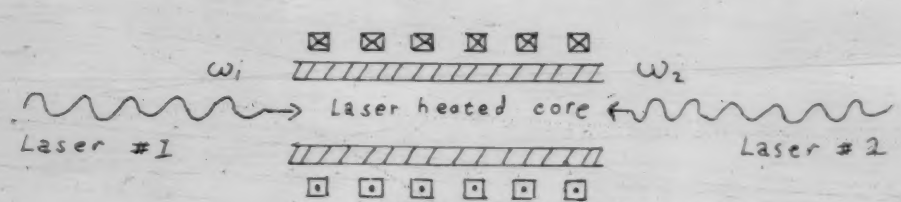

FIG. 7 Schematic of a beat frequency heating experiment.

A configuration of two antiparallel, well focused beams mixing in the center of the solenoid is assumed. The laser

radiation in the center of the solenoid will cause the gas to heat in the center and expand outwards. Since the plasma is a good conductor the magnetic field is trapped in the gas, and thus expands out with it. The computer routine incorporates an exact solution of the appropriate magnetohydrodynmic equations to describe the radial dynamics of the plasma in the solenoid.

The following discussion of the routine follows that given by Burnett and Offenberger[10]. The only major difference between this routine and that used by Burnett and Offenberger is that this version separates parallel and perpendicular electron temperatures.

A fully ionized three temperature plasma with a parallel electron temperature of $T_{\parallel}$, a perpendicular electron temperature of $T_{\perp}$, and an isotropic ion temperature of T_i is assumed. The ions and electrons are assumed to have the same local number density, n_0, and the same radial fluid velocity v. Apart from hydrodynamic terms, energy is transported by electron and ion thermal conduction. Radiation transport is neglected. The magnetic field is assumed to diffuse due to a classical electrical resistivity with joule heating being absorbed by the electrons. In addition to electron heating due to inverse bremsstrahlung absorption, the present version of the routine includes the nonlinear heating process discussed in chapter two. The power absorbed through the nonlinear process is converted

into the component of electron thermal energy parallel to the magnetic field. This makes it necessary to calculate the perpendicular and parallel electron temperatures separately. Parallel and perpendicular thermal energies are assumed to be exchanged according to electron-ion and electron-electron collision rates. Electrons and ions are assumed to exchange energy at the classical equipartition rate. An artificial viscosity is introduced to numerically handle the shock wave which is generated by strong expansion. The artificial viscosity has the effect of spreading the shock front over several mesh points. This technique is described by Richmeyer and Morton[11].

In this code the z-dependence of the variables is neglected. The implications of this assumption are discussed later. The differential equations that are solved numerically to determine the M.H.D. behavior of the plasma are given below.

Continuity or Conservation of Mass

$$\frac{\partial n_o}{\partial t} + \frac{1}{r} \frac{\partial}{\partial r} (r\, n_o\, v) = 0 \qquad (3.1)$$

where r=radius as measured from the center of the solenoid and v is the fluid velocity (which is defined to be in the radial direction).

Conservation of Momentum

$$m_i n_o\left(\frac{\partial v}{\partial t}\right) + v\frac{\partial v}{\partial r}\Big) + \frac{\partial}{\partial r}[n_o k_B(T_\perp + T_i) + P_p + Q] = \frac{-B}{4\pi}\frac{\partial B}{\partial r} \qquad (3.2)$$

where $P_p = \omega_{pe}^2\,\omega_i^2\,(E^2/8\pi)$ is the ponderomotive pressure of the light and Q is the artificial viscosity term discussed above. As given by Richtmeyer and Morton[11] this term is

$$Q = A\, m_i n_o\left(\frac{\partial v}{\partial r}\right)^2 \qquad \partial v/\partial r < 0$$

$$Q = 0 \qquad \partial v/\partial r > 0$$

where A is a constant chosen in such a way as to cause the shock front to spread over a distance of about three times the width of the spacial net used in the routine. Except at a shock front, this term is very close to zero and is totally insignificant. For the case of a strong magnetic field in the solenoid, shock fronts do not form and this term could be dropped from the routine.

Energy Conservation for the Electron Gas

$$\frac{\partial T_\perp}{\partial t} + \frac{\partial T_\perp}{\partial r} = \frac{-2}{3}T_\perp\frac{1}{r}\frac{\partial}{\partial r}(rv) + \frac{2}{3}\,\frac{1}{n_o r}\frac{\partial}{\partial r}\left(k_e\, r\,\frac{\partial T_\perp}{\partial r}\right)$$

$$+\frac{2}{3}\,\frac{\varepsilon_j}{n_o} - \frac{(2/3\,T_\perp + 1/3\,T_{//} - T_i}{\tau_{eq}} + \frac{2}{3}\frac{\varepsilon_L}{n_o} + \frac{1}{3}\,\frac{(\delta T_{//})}{\tau_c} \qquad (3.3a)$$

where k_e is thermal conductivity divided by k_B,

$\varepsilon_j=[c^2\eta/(4\pi)^2]\,(\frac{\partial B}{\partial r})^2$ is power from joule heating, η is the electrical resistivity, τ_{eq} is electron-ion thermal equalization time, ε_L is inverse bremsstrahlung power input, and τ_c is electron collision time.

Sucessive terms on the right hand side denote work done by expansion, thermal conduction losses, joule heating, energy transfer to ions, inverse bremsstrahlung energy input, and energy transfer from parallel electron energy to the perpendicular electron energy. $\delta T_{\parallel}$ is the difference between the electron parallel tenperature and the electron perpendicular temperature. ($\delta T_{\parallel} = T_{\parallel} - T_{\perp}$) It is calculated from,

$$\frac{\partial}{\partial t}(\delta T_{\parallel}) + \frac{v\partial}{\partial r}(\delta T_{\parallel}) = \frac{2\varepsilon_{NL}}{n_o} - \frac{(\delta T_{\parallel})}{\tau_c} \qquad (3.3b)$$

where ε_{NL} is the power input due to the nonlinear heating process.

Energy Conservation For The Proton Gas.

$$\frac{\partial T_i}{\partial t} + v\frac{\partial T_i}{\partial r} = -\frac{2}{3}(T_i + \frac{Q}{n_o})\frac{1}{r}\frac{\partial}{\partial r}(rv) + \frac{2}{3}\frac{1}{rn_o}\frac{\partial}{\partial r}(k_i r\frac{\partial T_i}{\partial r}) + \frac{(2/3\,T_{\perp} + \frac{1}{3}T_{\parallel}) - T_i}{\tau_{eq}} \qquad (3.4)$$

The various terms in equation (3.4) denote quantities analogous to those defined in equation (3.3a). The first term has been modified by the shock heating. The parameter,

K_i, is the ion thermal conductivity divided by Boltzmann's constant.

Magnetic Field Transport And Diffusion

$$\frac{\partial B}{\partial t} + v \frac{\partial B}{\partial r} = \frac{-B}{r} \frac{\partial}{\partial r} (rv) + \frac{1}{r} \frac{\partial}{\partial r} \left(\frac{rc^2}{4\pi} n \frac{\partial B}{\partial r}\right) \qquad (3.5)$$

3.2 NUMERICAL INTEGRATION

The MHD equations are numerically integrated by a Lagrangian scheme. The solenoid is divided into 50 to 100 concentric shells. In a Lagrangian scheme the boundaries of the shells move with the fluid velocity and must be adjusted with each time increment. The difference equations are written in such a way that all quantities except v are taken at half-integral space steps and integral time steps. The shell velocity, v, is computed at half-integral time steps and integral space steps. The hydrodynamic equations (3.1) and (3.2) are treated explicitly and the diffusion equations (3.3), (3.4), and (3.5) are treated implicitly. The method of solution of the implicit difference equations is discussed by Richmeyer and Morton[11]. Since the properly centered difference equations require knowledge of the transport coefficients at half-integral time steps, equations (3.3) to (3.5) are solved with an iterative procedure. The time and space positions, in which different

quantities are known, is shown in Fig. 8.

The boundary conditions applied are;

$$\begin{aligned} T_e &= T_0 && \text{at } r=R_0 \\ \partial B/\partial r &= 0 && \text{at } r=R_0 \\ v &= 0 && \text{at } r=R_0 \\ \partial T/\partial r &= 0 && \text{at } r=0 \\ \partial B/\partial r &= 0 && \text{at } r=0 \end{aligned} \qquad (3.6)$$

These boundary conditions correspond to what would be experienced if the solenoid was surrounded by a copper shell. The plasma temperature at the shell would go to the shell temperature. The second boundary condition would occur due to the high conductivity of copper and corresponds to conservation of magnetic flux. These boundary conditions also apply to the case of a larger solenoid, where the laser heated region is much smaller than R_0.

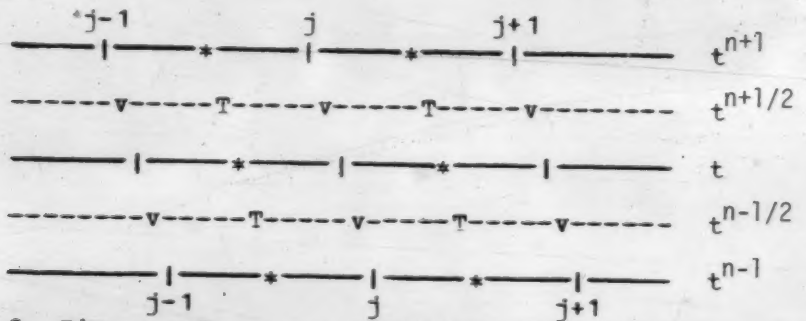

Fig. 8 Time and space positions where different quantities are known. '|' denotes positions and times where shell radii are known. '*' denotes positions and times where the parameters, T_u, $T_\perp$, T_i, n_0, and B are known. 'v' denotes positions and times where shell velocities are known. 'T' denotes positions and times where transport coeficients are known.

3.3 ALTERATIONS TO ROUTINE

A number of changes have been made to the routine as described by Burnett and Offenberger[10]. The program efficiency has been increased, and other changes were necessary to accommodate the nonlinear heating process. A small error was found in the calculation of the joule heating term of the original routine, but its correction made an insignificant difference to the results. Also changes made in the calculation of the transport coefficients made little difference to the final results. The contribution to heating from inverse bremsstrahlung was changed to that given by Johnston and Dawson[9].

One major change already discussed was the inclusion of $(\delta T_{//})$ seperate from the electron temperature, which was made necessary by the nonlinear heating process. The factor, τ_c, which is the electron collision time is calculated from

$$\frac{1}{\tau_c} = \frac{1}{\tau_{ei}} + \frac{1}{\tau_{ee}} \qquad (3.7)$$

where τ_{ei} is the electron-ion collision time and τ_{ee} is the electron-electron collision time. τ_{ee} is given in (5.26) of Spitzer[12], and τ_{ei} can be calculated from (5.22) of Spitzer.

Another major change, which greatly increased the efficiency of the routine, was the inclusion of a subroutine which made the program adjust its time step size to the maximum size allowed by the plasma conditions at that time

step.

This was accomplished by choosing the time step, Δt, such that the following conditions are satisfied:

1. Δt must be less than a specified fraction A_o of the maximum time step allowed by the stability condition. (The stability condition is discussed below.)
2. The radius of any shell boundary cannot change by more than ten percent in a single time step.
3. The shell thickness of any shell cannot change by more than ten percent in a single time step.
4. The electron or ion temperature cannot change by more than ten percent in a single time step.
5. The size of a time step cannot increase by more than fifty percent in a single time step.

The size of the time step used is usually limited by the first condition above. The stability condition used was one derived by Richmeyer and Morton[11] and can be written as:

$$\Delta t \leq A_o \, \mathrm{Min}\{\Delta r_i (C^2 + C_A^{\,2})^{-1}\} \qquad (3.8)$$

where C is the adiabatic sound speed and C_A is the Alfven velocity. Essentially all this condition says is that the time step must be smaller than the time necessary for a pressure wave to travel a distance equal to the smallest space step.

The stability condition was derived for a case in which no input power was given up to the plasma. Equation (3.8) is found to be quite adequate when the laser power input is low if A_0 is set to 0.8. When the laser power input is large (i.e. an input laser power density of 10^{12} watts/cm^2) or when there is good nonlinear energy coupling between the laser and the plasma, it is found that A_0 must be reduced to 0.5. For a larger A_0 the routine will generate oscillations near the center of the solenoid, with a time period equal to the time step size and a space period equal to the space step size. For economy it is desirable to make A_0 as large as possible. It is found experimentally that the results are unaffected by the choice of A_0 as long as it is small enough to prevent the oscillations previously mentioned.

Finally the boundary condition for B at $r=R_0$ was changed from $B=0$ at $r=R_0$ as in the original version of the routine to $\partial B/\partial r = 0$ at $r=R_0$. This is easily derived as being the boundary condition for a cylinder surrounded by a copper sheet with the use of Ampere's Law.

This last change implies conservation of magnetic flux in the routine. It allows the use of conservation of energy and conservation of magnetic flux as two checks on the numerical procedure. It is found that in a 40 ns run both of these quantities are conserved to 5 significant digits. For longer runs the temperature starts to rise at the boundaries and energy can be lost from the plasma.

CHAPTER 4

RESTRICTIONS AND ASSUMPTIONS

4.1 SOLENOID LENGTH

For the one-dimensional M.H.D. routine to give a reasonable approximation to reality, it must be assumed that the solenoid's length is much greater than its radius, and that the heating is reasonably constant over its length. In the M.H.D. simulations made for this thesis the radius of the solenoid was assumed to be 0.5 cm, so if its length is about 5 cm or greater the first of the above conditions will be satisfied. The model may be valid for a shorter solenoid if calculations are made for a short enough time to prevent significant disturbances to reach the outer radius of 0.5 cm.

The heating in the solenoid is greatest close to where the high frequency laser enters the plasma. Here both lasers would have maximum intensity; the first one because it hasn't had time to damp, and the second because its power grows as it propagates through the plasma. The power lost by the first beam is approximately ten times as great as the power absorbed by the plasma, and the power gained by the second beam is approximately nine times as great as the power absorbed by the plasma. Using this information the length over which the product $P_1 P_2$ is reasonably constant can be calculated with the use of Table 1 of chapter two,

for specific values of $P_1, P_2, T_{\parallel}$, and n_o. The power intensity of the first laser P_1 must satisfy the equation

$$\frac{\partial P_1}{\partial x} = -\alpha P_1(x) P_2(x) \qquad (4.1)$$

where $\alpha = 10^{-6} W_3 n_o$. The constant α is equal to ten times the power absorbed by the plasma in watts/cm³ divided by the product of the laser intensities in watts/cm². Assuming the laser beams are insignificantly damped by inverse bremsstrahlung absorption, $P_2(x)$ can be written in terms of $P_1(x)$ as

$$P_2(x) = P_1(x) + P_2(\infty) - P_1(\infty) \qquad (4.2)$$

where $P_2(\infty)$ is the power of the second laser beam before it enters the plasma and $P_1(\infty)$ is the power of the first laser beam after it has passed through the plasma. Using equation (4.2) the solution to equation (4.1) is

$$P_1(x) = \frac{b P_1(o) \exp[-bx]}{[\alpha P_1(o) (1 - \exp[-bx]) + b]} \qquad (4.3)$$

where $b = \alpha(P_2(\infty) - P_1(\infty))$ and $P_1(0)$ is the power of the first laser before it enters the plasma. With this solution for $P_1(x)$, $P_2(x)$ can be calculated from equation (4.2). Approximate values of α for different temperatures and densities can be found with Table 1 or with Figs. 1 and 2. Equations (4.2) and (4.3) are used in chapter 5 to find the

distance over which P_1P_2 is reasonably constant for the conditions experienced in the MHD simulation.

4.2 STIMULATED SCATTERING

When an intense electromagnetic wave is present in a plasma, two new waves can be parametrically excited by the incident or pump wave. If one of the excited modes is electromagnetic it can escape from the plasma and appear as stimulated scattering of the incident wave. The process of stimulated scattering is very closely related to the nonlinear heating process studied in chapter two. In the process of stimulated scattering, the incident wave of frequency ω_o and wavenumber k_o interacts with a propagating density perturbation (ω,k) associated with an electrostatic wave. This results in an electromagnetic wave of frequency $\omega_o - \omega$ and wave vector $k_o - k$ being scattered. This scattered wave can then interact with the incident wave in much the same way as the waves from the two lasers described in chapter two. This interaction then amplifies the original density perturbation. An unstable situation can result if the energy transfer to the scattered electromagnetic wave and the electrostatic wave exceeds their natural damping rate. Some energy is deposited in the plasma via the electrostatic wave, but the amount is limited by the Manley - Rowe relations.

Theoretical studies of this process, assuming all waves

are coherent have been made by Drake et al.[13]. A similar study, but assuming incoherent waves has been made by Tsytovich[14].

Theory shows that the incident wave intensity has to exceed a threshold value before significant scattering will occur. After the threshold intensity has been exceeded, the scattered wave amplitude grows exponentially according to $e^{\gamma t}$, where γ is known as the growth rate and t is the time over which the wave can grow. The time t is limited to $t=\ell/c$, where ℓ is the interaction length and c is the speed of light.

Stimulated Brillouin scattering (the scattering of light from ion-acoustic waves) could possibly present a problem in a solenoid such as the one described in this thesis. Experiments have been made on stimulated Brillouin scattering by Offenberger, Cervenan, Yam, and Pasternak[15]. The Manley - Rowe relations tell us that very little energy can get into the plasma through stimulated Brillouin scattering since the ion-acoustic wave frequency is small for the values of wave vector, k, which occur in such a process. For example, if the electron temperature is 100 eV and the plasma density is 4×10^{17} cm^{-3} a maximum of the fraction 6.4×10^{-4} of the incident beam's power can be transferred to the plasma through this process.

The theory from Drake et al.[13], and the experiment by Offenberger et al.[15] both indicate that for power

intensities of 10^{11} to 10^{12} watts/cm^2, and for temperatures and densities assumed in this thesis, growth rates for stimulated Brillouin scattering of about 10^{11} to 10^{12} sec^{-1} can be expected. Such growth rates over several centimeters would ensure that almost all the light would be scattered. However the interaction length, ℓ, over which the scattered beam can grow will not be larger than the coherence length of the ion-acoustic wave from which it scatters. In a rapidly heated plasma a certain amount of turbulence would be expected. This would limit the coherence length of the ion-acoustic wave. Experimental evidence given by Offenberger et al.[15] indicates that the coherence length of the ion-acoustic wave may be sufficiently small, so that only a small amount of light will be scattered.

The process of scattering from electron plasma waves, or stimulated Raman scattering, is also very closely related to the heating process of chapter two. In this process the scattered wave would propagate antiparallel to the incident wave, and its frequency would match the electron plasma frequency. The Manley - Rowe relations would impose approximately the same maximum energy transfer condition that was imposed in chapter two. This process would appear also as a method of enhancing heating. The usefulness of this process to enhance heating is limited by the fact that the growth rate of stimulated Raman scattering is smaller than the growth rate of stimulated Brillouin scattering for the plasma conditions assumed in this thesis, and by short

natural coherence lengths of plasma waves.

4.3 DISTORTION OF THE VELOCITY DISTRIBUTION FUNCTION

The equations which describe the nonlinear heating were derived assuming a Maxwellian velocity distribution function. It might be expected, however, that the continual Landau damping of the driven wave would cause the distribution function to flatten near the phase velocity of the difference frequency wave, ω_3/k_3. This flattening of the distribution function would cause a decrease in the Landau damping.

It turns out that the distribution function remains much closer to Maxwellian than would be predicted as a result of collisions. Theory shows that collective electrostatic interactions have an effect similar to collisions on the distribution function, and that a thermal velocity distribution can be maintained, even in the absence of collisions. Bernstein and Trehan[16] show how a limit is placed on the magnitude of plasma oscillations in a cold plasma. At this limit a process similar to the breaking of water waves takes place. This process causes ordered motion to go over into unordered thermal motion. One dimensional many body computer models (see Bernstein and Trehan[16]) allow this process to be investigated in warm plasmas. It is seen that in this case, energy is fed even faster into thermal motion from the organized wave energy. A discussion of this

process can also be found in chapter 7 of Schmidt[17]

Computer models by Dawson[18], and Dawson and Shanny[19], show that the distribution function will maintain a Maxwellian form in the presence of Landau damping much better than would be predicted on the basis of collisions alone, but if the amplitude of the plasma wave is sufficiently high, the damping rate will deviate from that predicted by linear Landau theory.

Most of the theoretical work done in this area has been done as an investigation of the time development of finite initial value amplitude electron waves, rather than the steady state solution of a driven wave as is the case at hand. Three approaches have been used to investigate the time development of these electron waves. The results of these have been summarized in an experimental paper by Franklin, Hamberger, and Smith[20]. The first approach is that of the one dimensional computer model and has already been discussed.

The second method, used by Armstrong[21], is to solve simultaneously Vlasov's and Poissons's equations using numerical techniques. The results, summarized by Franklin et al.[20], are that the damping rate, γ_L, is correctly predicted by linear Landau theory if the amplitude of the plasma wave is small. The condition can be expressed quantitatively as

$$\frac{e\phi}{k_B T_{\parallel}} \ll 1 \qquad (4.4)$$

ϕ is the potential of the electrostatic wave. When ϕ increases, violating equation (4.4), the damping rate decreases. When $e\phi/k_B T_{\parallel} \approx 1$ the damping rate is no longer exponential, and the instantaneous rate exceeds the value predicted by linear Landau theory. This behavior can be associated with the "wave breaking" process in a cold plasma.

The third method separates the electron distribution function into a resonant part and a non-resonant part, and solves exactly the Vlasov equation in the resonant region. This technique was used by O'Neil[22], and later by Bailey and Denavit[23]. Their results showed a decrease in Landau damping if

$$q \equiv \frac{\gamma_L}{\omega_B} \to 0 \qquad (4.5)$$

where $\omega_B = k_3 (e\phi/m_e)$ is the frequency of oscillation of the trapped electrons. k_3 and ϕ are the wave vector and potential respectively of the electrostatic wave. Sugihara and Kamimura[24] computed self-consistent equilibrium solutions to the initial value problem for a range of $0<q<\infty$. They found the same result as O'Neil for $q \to 0$ and linear Landau damping for $q \to \infty$.

An experiment to test the damping behavior of plasma waves for various values of $e\phi/k_B T_{//}$ and q was done by Franklin, Hamberger, and Smith[20]. They did the experiment on a sodium column, with an electron temperature of 2500 °K and a density of about 2×10^{7} cm^{-3}. The experimental results indicate that linear Landau damping could be expected for

$$\frac{e\phi}{k_B T_{//}} \lesssim 2\times10^{-3} \qquad (4.6)$$

It should be noted here that this condition was derived and tested only for the case where K is of the order of unity.

When K is of order unity it is assumed that relation (4.6) is an approximate condition which must be imposed on the difference frequency wave before the equations for the nonlinear heating are to be accurate. For the specific case of difference frequency heating with lasers of wavelengths of 9.6 and 10.6 microns condition (4.6) becomes

$$\frac{e\phi}{k_B T_{//}} = 2.4\times10^{-2}\, E_3/T_{//} \lesssim 2\times10^{-3} \qquad (4.7)$$

Values of E_3 for different values of n_o, $T_{//}$, and laser powers can be found from Figs. 1 and 2 of chapter two. When using this condition to find restrictions that must be placed on the routine, it must be remembered that by the time the laser power, and thus E_3, reach a maximum, the temperature of the electrons is high. It should also be

remembered that this condition was derived by neglecting the role of collisions in thermalization. At low temperatures collisions can play an important role in maintaining the Maxwellian distribution. If the electron temperature is sufficiently high to make K of the order unity, relations (4.6) and (4.7) can be used to check the validity of the results. For example, at a density of $n_o = 4 \times 10^{17}$, an electron temperature of $T_{//} = 1000$ eV, and input laser intensities of 2.5×10^{11} watts/cm^2 it is found that $E_3 = 30$ statvolts/cm. For this temperature and density, $K = k_3 \lambda_D = 0.46$. Relation (4.7) then yeilds $e\phi / k_B T_{//} = 7.2 \times 10^{-4}$. This implies that the driven wave should be experiencing damping as predicted by linear Landau theory. If the electron temperature is lowered significantly from this value, K will decrease, and relation (4.7) cannot be used to test the validity of the theory.

The effect of E_3 exceeding the restrictions placed on it by relation (4.6) can be predicted qualitatively, with the aid of Figures 3 and 4 of chapter two. When E_3 gets large the Landau damping will decrease and the poles associated with $D(K,\omega)$ will move towards the real axis. If ω_3 is very close to the frequency of the Langmuir mode, a stronger field resonance could be expected leading to a greater heating rate than that predicted in chapter two. If, on the other hand, ω_3 is not close to the frequency of the Langmuir mode, the motion of the poles towards the real axis would have little effect on the value of E_3, but the

decreased damping would lead to a reduction in power absorption.

CHAPTER 5

RESULTS

The M.H.D. code discussed in chapter 3 has been used to compare the heating of a plasma when two lasers are mixed with a difference frequency near that of the Langmuir mode, with the heating that is obtained when inverse bremsstrahlung is the only energy absorption mechanism.

The laser energy pulse assumed in the routine is 40 nsec long and of triangular shape. The pulse starts with zero power, reaches peak power at 20 nsec, and falls off to zero again at 40 nsec. The radial intensity distribution of the focused laser pulse is assumed to be Gaussian. The intensity as a function of radius, r, can be expressed as,

$$I_L(r) = P_L/(2\pi\sigma^2)\exp[-r^2/2\sigma^2] \qquad (5.1)$$

where P_L is the laser power, and σ is the radius of the beam. σ has been set of 0.045 cm. For all the runs reported in this thesis both lasers were assumed to be of equal power.

The spatial mesh in each case consisted of 50 shells. Initially the inner shell had a radius of 3×10^{-3} cm. The thickness of the n'th shell is given by $3\times10^{-3}\times A^n$ where A is chosen in such a way as to make the radius of the outer shell 0.5 cm.

Initially, a fully ionized hydrogen plasma with electron and ion temperatures of 1 eV is assumed. The plasma has a uniform electron and proton density of 7×10^{17} cm^{-3}. The magnetic field is longitudinal and uniformly distributed throughout the solenoid. Several runs were made with different initial magnetic fields and different laser powers.

Figures 9 to 12 are plots of $T_{\parallel}$, $T_{\perp}$, T_i, B, and n_0 versus radius at a time of 40 nsec. In Figs. 9(a), 10(a), 11(a), and 12(a) energy is assumed to be absorbed by inverse bremsstrahlung only, while in Figs. 9(b), 10(b), 11(b), and 12(b) it is assumed that energy is absorbed by both inverse bremsstrahlung and the nonlinear process. In all figures the plotted value of magnetic field is normalized to the initial plasma density. The plotted value is given by B/B_0 x initial plasma density.

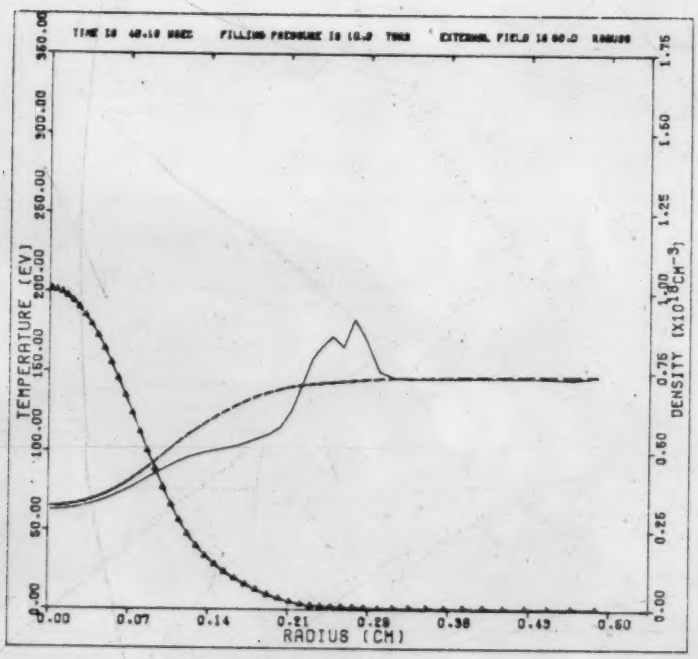

(a) Inverse bremsstrahlung only.

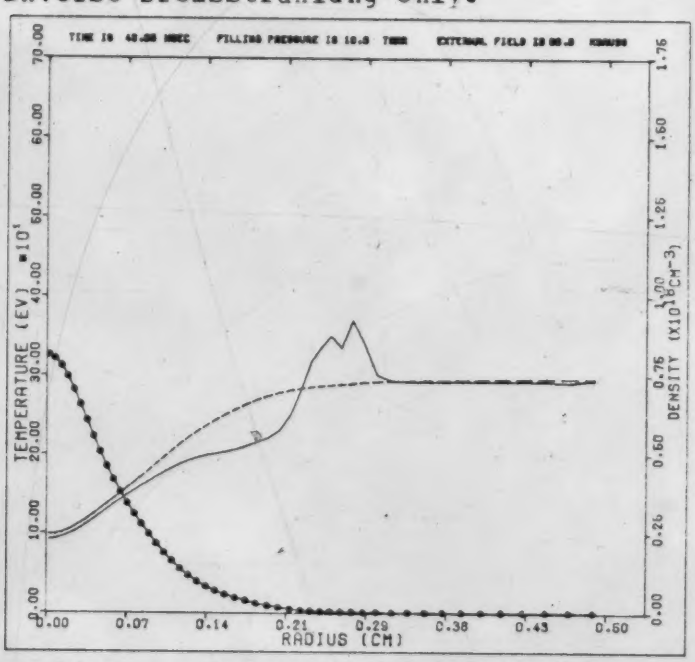

(b) Nonlinear + inverse bremsstrahlung.

Fig. 9 Plasma parameters $T_{\parallel}$ and $T_{\perp}$ (dotted curve), n_0 (solid curve), and B normalized to initial density (dashed curve) as a function of radius, at 40 ns. Initial conditions are $n_0=7\times10^{17}$ cm^{-3}, $B_0=60$ kG, and peak laser power=1.25 GW.

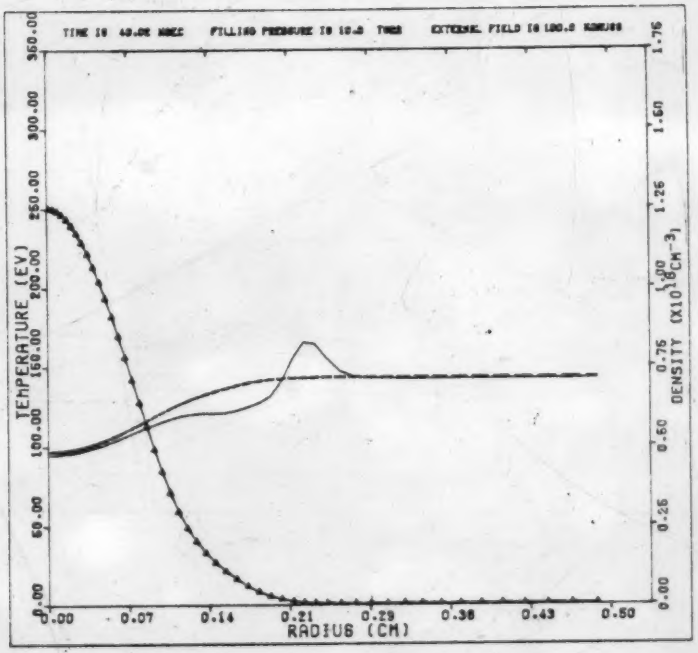

(a) Inverse bremsstrahlung only.

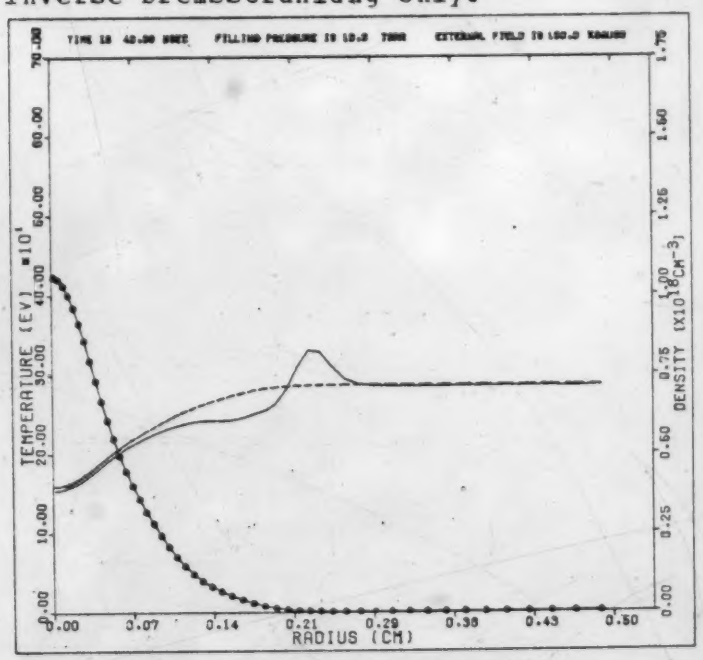

(b) Nonlinear + inverse bremsstrahlung.

Fig. 10 Plasma parameters $T_{\parallel}$ and $T_{\perp}$ (dotted curve), n_e (solid curve), and B normalized to initial density (dashed curve) as a function of radius, at 40 ns. Initial conditions are $n_0 = 7 \times 10^{17}$ cm^{-3}, $B_0 = 100$ kG, and peak laser power = 1.25 GW.

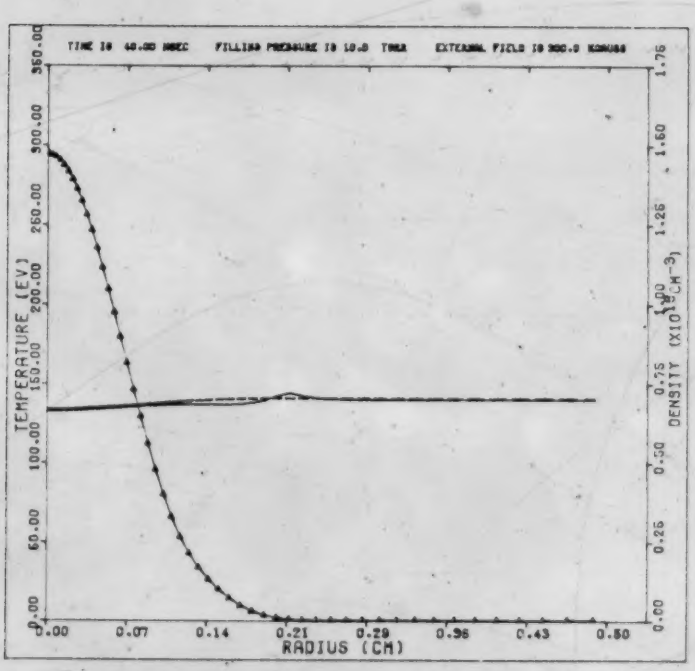

(a) Inverse bremsstrahlung only.

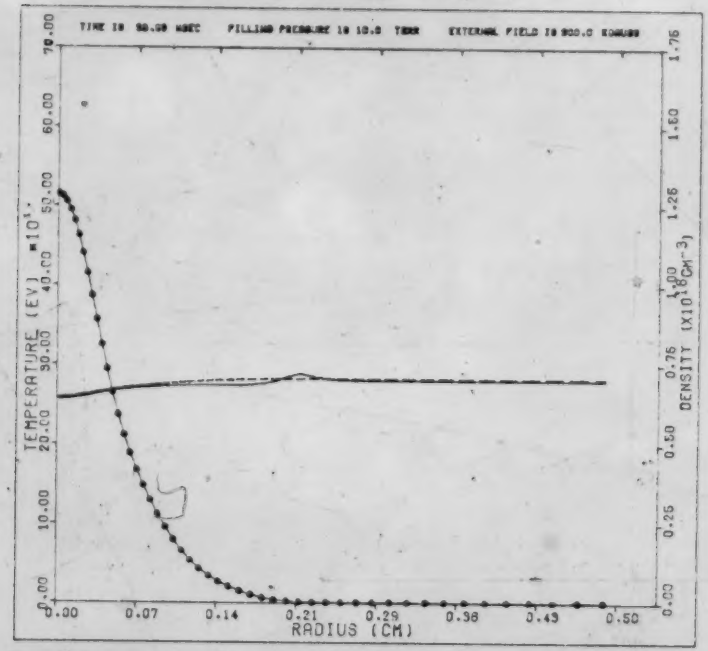

(b) Nonlinear + inverse bremsstrahlung.

Fig. 11 Plasma parameters $T_{\parallel}$ and $T_{\perp}$ (dotted curve), n_0 (solid curve), and B normalized to initial density (dashed curve) as a function of radius, at 40 ns. Initial conditions are $n_0 = 7 \times 10^{17}$ cm^{-3}, $B_0 = 300$ kG, and peak laser power = 1.25 GW.

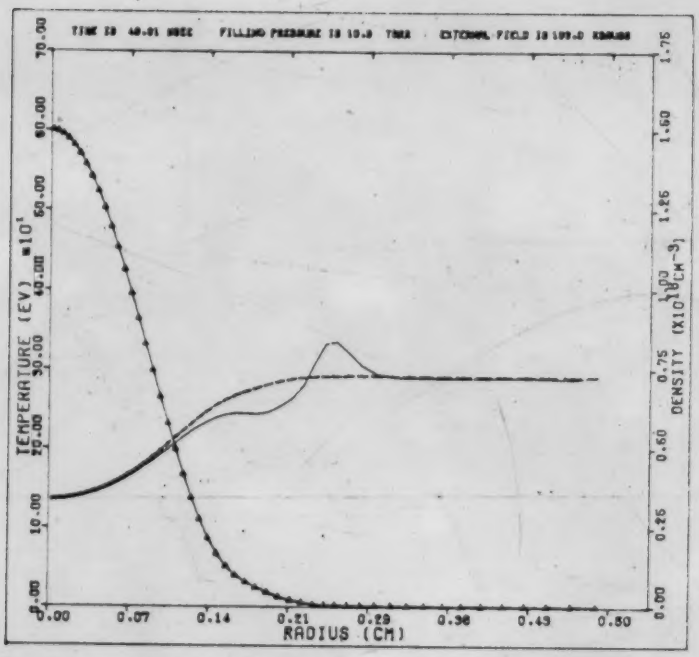

(a) Inverse bremsstrahlung only.

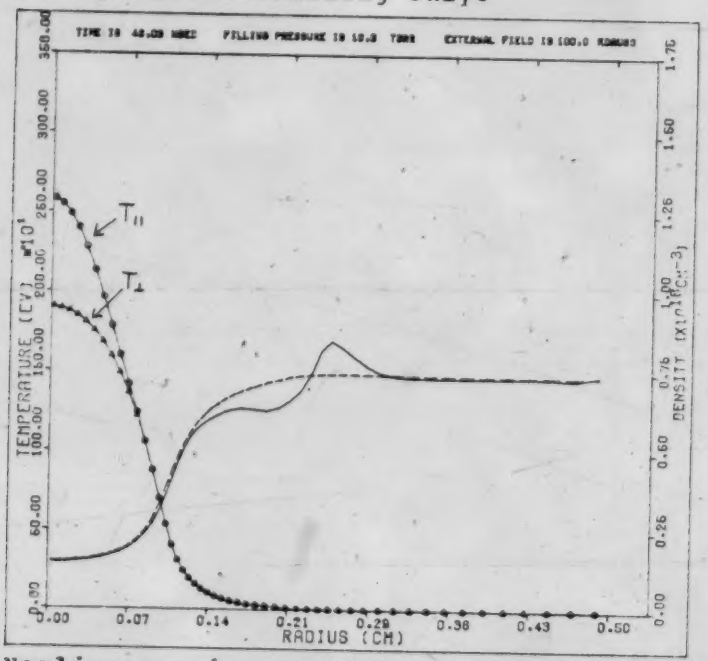

(b) Nonlinear + inverse bremsstrahlung.

Fig. 12 Plasma parameters $T_{\parallel}$ and $T_{\perp}$ (dotted curve), n_0 (solid curve), and B normalized to initial density (dashed curve) as a function of radius, at 40 ns. Initial conditions are $n_0 = 7 \times 10^{17}$ cm^{-3}, $B_0 = 100$ kG, and peak laser power = 12.5 GW.

In Figs. 9(a) and 9(b) the following parameters were used; initial magnetic field, B_0=60 kG.; initial plasma density, n_0=7x10^{17} cm^{-3}; peak laser power, P_L=1.25 GW. Total laser energy is 25 joules. Comparing these two figures, it is seen that the temperature of the electrons in the center of the solenoid is about 330 eV after the nonlinear heating mechanism is used, and about 200 eV after only inverse bremsstrahlung absorption is used. For this run the parallel and perpendicular electron temperatures remained within ten eV of each other throughout the simulation, and were essentially equal at 40 ns. It was found that in the center shell the ratio, W_3/W_{IB}, varied from 5 to 8 during the time period of 18 ns to 35 ns, where W_3 is the heating rate due to the nonlinear process and W_{IB} is the heating rate due to inverse bremsstrahlung absorption.

Figures 10(a) and 10(b) come from a simulation where the parameters are all the same as those in Fig. 9 except for the magnetic field which has been increased to 100 kG for this run. Increasing the magnetic field makes it more difficult for the plasma to expand outwards during the simulation. This results in the density staying higher in the center of the solenoid, which increases the coupling of laser energy to the plasma through both inverse bremsstrahlung and the nonlinear processes. This is shown in Fig. 10 where the electron temperatures and plasma densities are higher than those shown in Fig. 9. Again, the

electron temperature in the center of the solenoid is significantly higher for the case where nonlinear heating is assumed.

Bethe and Vlases[25] have suggested that one of the requirements to heat a plasma to thermonuclear temperatures in a long solenoid is a magnetic field of 300 to 500 kG. Thus, it is of interest to make a simulation of a laser heated solenoid with fields of this strength. Figs. 11(a) and 11(b) show the results of such a simulation, at a time of 40 ns. Again, the laser power is the same as in previous runs; total laser energy is 25 joules, peak laser power is 1.25 GW. These plots show that the density stays almost constant throughout the simulation. The nonlinear process is able to heat the electrons in the center of the column to about 1.75 times as high a temperature as inverse bremsstrahlung absorption alone.

As explained in chapter two, the power absorption due to the nonlinear process is proportional to the product of the powers of the two lasers, while the power absorption due to inverse bremsstrahlung absorption is proportional to the sum of the powers. Thus W_3/W_{IB} increases as laser powers increase. The effect of increasing the laser power was investigated by making a simulation where the lasers had a peak power of 12.5 GW and a total energy of 250 joules. The initial magnetic field was set to 100 kG. The results of this simulation are shown in Figs. 12(a) and 12(b). The

final electron temperature for the case of nonlinear heating is more than three times the electron temperature with only inverse bremsstrahlung absorption. Fig. 12(b) shows that the parallel and perpendicular electron temperatures have not yet equalized at 40 ns. It is interesting to note the sharp density minimum in the center of the solenoid (Fig. 12(b)) caused by the rapid nonlinear heating. In the center shell the ratio, W_3/W_{IB}, was between 8 and 40 for the period of 5ns to 35 ns.

So far no mention has been made of the resulting ion temperatures in these simulations. Fig. 13 shows a plot of the ion temperatures for all the simulations made. These plots show that in the more rapidly heated plasmas, decoupling between electrons and ions is greater than in the plasmas that are heated more slowly. These plots also show an advantage in having a large magnetic field. The large magnetic fields maintain a higher plasma density in the center of the solenoid, and this makes the electron-ion equipartition time smaller. Spitzer[12], shows that the equipartition time is approximately proportional to $T_e^{3/2}/n_o$. The very rapid heating experienced in the simulation with the 250 joule laser and the nonlinear heating resulted in almost complete decoupling between electrons and ions in the center of the solenoid. This is seen as a steep minimum in ion temperature in the center of the solenoid.

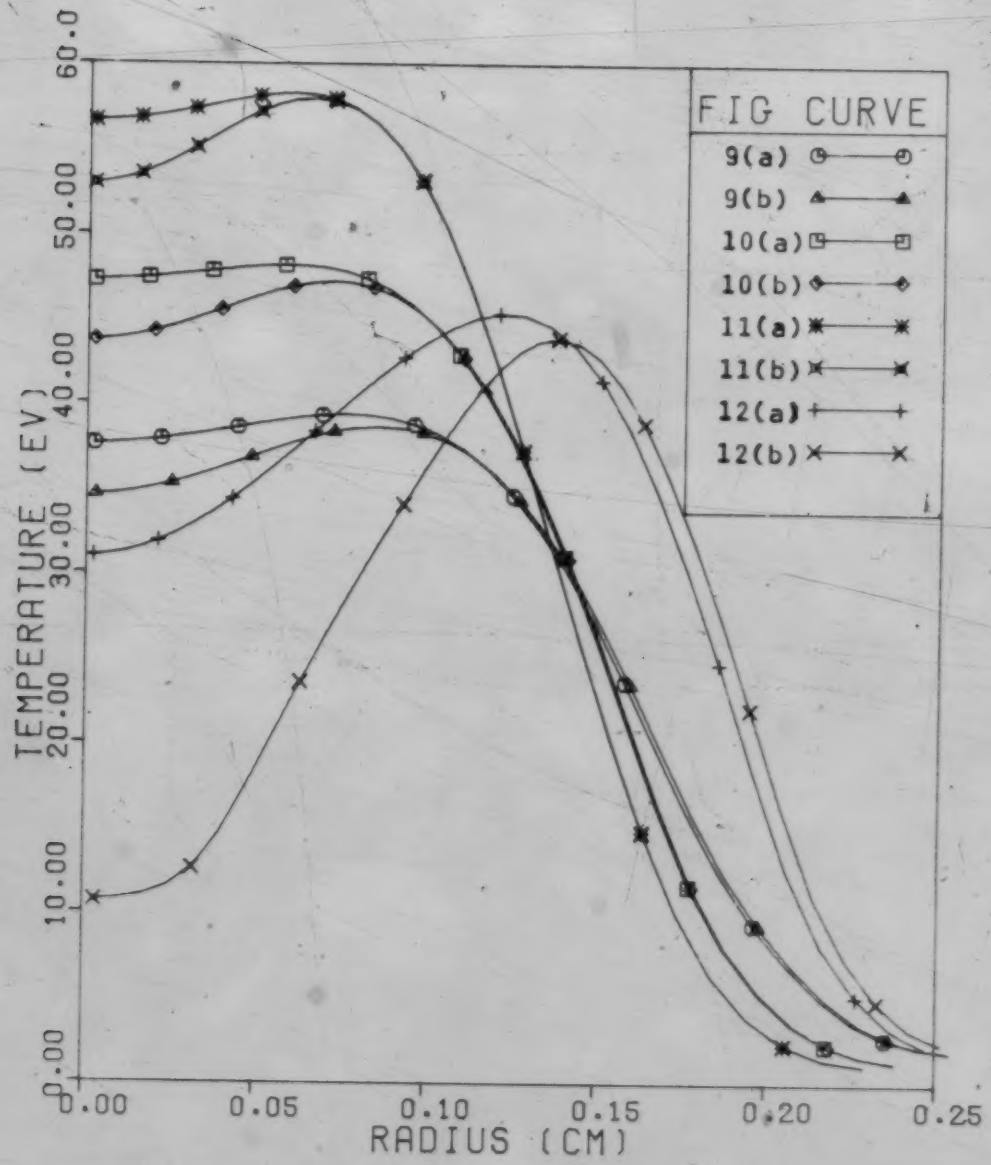

Fig. 13 Ion temperature versus radius at a time of 40 ns. Curves originate from simulations associated with previous figures as indicated on the graph.

The value of $e\phi/k_B T_{//}$ has been calculated at several times in the simulations. In general, the value of $e\phi/k_B T_{//}$ is so close to the critical value defined in relation (4.7) that it is impossible to predict the accuracy of the damping rate of the beat frequency wave, as given by linear Landau theory, under these conditions.

For example, in the simulation where the laser energy is 25 joules and the initial magnetic field is 100 kG, $K=0.17$ and $e\phi/k_B T_{//}=4.3\times10^{-3}$ at 15 ns; at 35 ns, $K=0.3$ and $e\phi/k_B T_{//}=5.8\times10^{-4}$. Similarly for the simulation with the higher powered lasers (laser energy of 250 joules, and initial magnetic field of 100 kG) $K=0.68$ and $e\phi/k_B T_{//}=3.4\times10^{-3}$ at 15ns; and $K=1.3$, and $e\phi/k_B T_{//}=5.5\times10^{-4}$ at 30 ns. For both of these simulations, the values of $e\phi/k_B T_{//}$ found at 15 ns is larger than the critical value defined in relation (4.7). However, since relation (4.7) is only an approximate condition it is difficult to estimate the accuracy of the nonlinear heating equations given in chapter two under these conditions. Relation (4.7), however, does predict that the calculated nonlinear heating rate should be accurate under the conditions experienced at 35 ns.

The total energy absorbed by the plasma can be calculated by adding up the total thermal, kinetic, and magnetic energy in the plasma initially, and after 40 ns. The absorbed energy is expressed in ergs/cm length of

solenoid. The increase in total absorbed energy due to the nonlinear process is surprisingly small. For the simulation with 25 joule lasers and 60 kG magnetic fields the total power absorbed was 1.29×10^7 ergs/cm for inverse bremsstrahlung absorption alone, and 1.34×10^7 ergs/cm when the nonlinear process was used. This is an increase in total energy by a factor of only 1.04. This is partially caused by the fact that power absorption from both mechanisms decreases as the temperature rises and density falls. Another factor to be considered is that, because the nonlinear power absorption is proportional to the product of the laser powers, the heating takes place over a smaller cross sectional area of the solenoid than does inverse bremsstrahlung heating. It must also be remembered that the thermal energy is proportional to the product of plasma density and temperature. Thus, even though the temperature is much greater in the center of the solenoid for the case in which nonlinear heating is used, the total thermal energy in the center of the solenoid is not that much greater, since the plasma density is lower.

In the simulations where the initial magnetic field is 100 kG and laser energies are 25 joules, 1.59×10^7 ergs/cm are absorbed when only inverse bremsstrahlung absorption is used, and 1.69×10^7 ergs/cm are absorbed when nonlinear heating is used. For this case the nonlinear heating results in a total energy absorption enhancement of a factor of only 1.06. For the simulations with a 300 kG field,

1.89×10^7 ergs/cm are absorbed for the case of only accounting for inverse bremsstrahlung absorption and 2.06×10^7 ergs /cm for the case including nonlinear heating. This represents a total energy absorption enhancement of a factor of 1.09.

The simulation with 250 joule lasers and an initial field of 100 kG shows that nonlinear heating results in 1.5 times as much energy being absorbed by the plasma. With only inverse bremsstrahlung absorption, 3.28×10^7 ergs/cm are absorbed, while 4.89×10^7 ergs/cm are absorbed when the nonlinear process is used. Thus, if the laser powers are sufficiently high the nonlinear process can produce a significant enhancement in total energy absorption.

These simulations are most accurate for a solenoid of about 3 cm in length. If it is much shorter than this, the one-dimensional approximation is no longer valid. If it is much longer than this, there would be times in the simulations when the high frequency laser beam would be depleted at one end of the solenoid. Even for the case of a 3 cm solenoid there are times that the nonlinear process deposits much more energy at one end of the solenoid than the other. For example, in the run with the 25 joule lasers and a magnetic field of 100 kG, the high frequency laser is depleted to about 40% of its initial value in 3 cm, at a time of 16 ns. The low frequency beam grows to about 150% of its initial value. Consequently, at one end of the

solenoid the actual heating rate is 150% of the rate used in the simulation, while at the other end it is only 40% of the rate used in the simulation. At this time in the simulation, the electron temperature in the central shell of the solenoid is about 200 eV. The parallel thermal conductivity (calculated from equations (5.47) and (5.48) of Spitzer[12]) is 4.2×10^7 watts/cm eV. The calculated value of power being deposited in the plasma is about 2.3×10^9 watts/cm^3. Thus, it may be expected that one end of the solenoid will start to heat faster than the rate calculated in the simulation. But, if the temperature increases significantly, the nonlinear coupling between the laser and plasma decreases, allowing the laser to penetrate further into the plasma. The thermal conductivity is then sufficiently large to keep the temperature of the solenoid reasonably uniform along its length. At later times in the simulation there is no problem in maintaining a constant temperature along the length of the solenoid since the thermal conductivity rises according to $T_e^{5/2}$ and the high frequency laser penetrates the plasma more easily as the temperature rises.

For the simulation with higher powered lasers, the parallel thermal conductivity is much higher due to the higher electron temperature. As a result a fairly uniform temperature distribution is maintained along the length of the solenoid, even when the first laser beam is depleted significantly as it propagates through the plasma.

CHAPTER 6

CONCLUSION

The analysis in this thesis indicates that the mixing of two laser beams to generate a beat frequency harmonic near the electron plasma frequency can provide a useful technique of heating the electrons in a plasma. It has been shown that this process is insensitive to changes in density and temperature.

At low temperatures a serious limitation in the theory arises due to the difficulty in estimating the accuracy of the damping rate of the beat frequency wave as predicted by linear Landau theory. However, at electron temperatures of 300 eV and higher, theory predicts that the damping rate will be very close to that predicted by linear Landau theory.

The results of the M.H.D. simulations show that this nonlinear process can greatly enhance the heating of electrons in a short experimental solenoid. In particular, if the laser beam intensity reaches values of 10^{12} watts/cm^2, a significant fraction of the laser energy can be deposited in a short solenoid. This is demonstrated in the simulation where two 250 joule laser pulses raise the electron temperature in the center of the solenoid to over 2000 eV. When one considers that the absorption length of inverse bremsstrahlung absorption has a $T_e^{3/2}/n_o$ dependence, it is seen that it would take a much higher powered beam to

achieve this temperature if inverse bremsstrahlung were the only energy absorption mechanism.

The results of this thesis suggest further work should be done in the investigation of the use of beat frequency heating of a plasma in a long solenoid. An example of how beat frequency heating may lead to enhanced absorption in a long solenoid is given below. A laser fires a high powered beam of radiation with a wavelength of 9.6 microns down the center of a plasma filled solenoid. Just before this beam reaches the far end of the solenoid, another laser fires a short, but high intensity pulse of 10.6 micron radiation down the solenoid antiparallel to the first beam. When this pulse meets the beam of 9.6 micron radiation it will interact with it. The 9.6 micron beam will be depleted, and the 10.6 micron pulse will grow in amplitude. Thus, about 90% of the energy of the 9.6 micron beam is converted into a pulse of 10.6 micron radiation travelling in the opposite direction to the original beam and 10% of the energy is deposited in the thermal energy of the plasma electrons. Turning the beam around like this makes the laser radiation travel through a greater length of plasma so that more energy will be absorbed by inverse bremsstrahlung absorption. However, if all the energy of the 9.6 micron beam becomes compressed in the first few cm of the 10.6 micron pulse as this theory would suggest, the intensity of this pulse would grow to such a size that other nonlinear processes may become dominant.

BIBLIOGRAPHY

[1] V. Fuchs, C.R. Neufeld, J. Telchmann, and A.G. Engelhardt, ''Nonlinear Absorption of Radiation by Optical Mixing in a Plasma'', Physical Review Letters, 31, 1110 (1973)

[2] B.I. Cohen, ''Space-time Interaction of Opposed Transverse Waves in a Plasma'', The Physics of Fluids, 17, 496 (1973)

[3] G. Schmidt, ''Resonant Excitation of Electrostatic Modes With Electromagnetic Waves'', The Physics of Fluids, 16, 1676 (1972)

[4] C.E. Capjack and C.R. James, ''Heating Rates for a Beat Frequency Laser Heated Plasma'', Canadian Journal of Physics, (in print)

[5] T.H. Stix, Theory of Plasma Waves, McGraw Hill (1962)

[6] P.A. Clavier, ''Plasma Ripple'', Proceedings of IEEE, 1198 (1966)

[7] N.A. Krall and A.W. Trivelpiece, Principles of Plasma Physics, McGraw Hill (1973)

[8] C.E. Capjack and C.R. James, ''Optical Frequency Mixing Near the Cyclotron Frequency for Plasma Heating'', The Physics of Fluids, 17, 948 (1974)

[9] T.W. Johnston and J.M. Dawson, ''Correct Values For High-frequency Power Absorbtion by Inverse Bremsstrahlung in Plasmas'', The Physics of Fluids, 16, 722 (1974)

[10] N.H. Burnett and A.A. Offenberger, ''Magnetohydrodynamic Behavior of a Laser-Heated Solenoid'', Journal of Applied Physics, 45, 2155 (1974)

[11] R.D. Richtmeyer and K.W. Morton, Difference Methods for Initial Value Problems, Interscience Publishers (1957)

[12] L. Spitzer, Physics of Fully Ionized Gases, Interscience Publishers (1957)

[13] J.F. Drake, P.K. Kaw, Y.C. Lee, G. Schmidt, C.S. Liu, and M.N. Rosenbluth, ''Parametric Instabilities of Electromagnetic Waves in Plasmas'', The Physics of Fluids, 17, 778 (1974)

[14] V.N. Tsytovich, Nonlinear Effects in Plasmas, Plenum Press (1970)

[15] A.A. Offenberger, M.R. Cervenan, A.M. Yam, and A.W. Pasternak, ''Stimulated Brillouin Scattering of CO_2 Laser Radiation From Underdense Plasma'', (to be published)

[16] I.B. Bernstein and S.K. Trehan, ''Plasma Oscillations (I)'', Nuclear Fusion, 1, 3 (1960)

[17] G. Schmidt, Physics of High Temperature Plasmas, Academic Press (1966)

[18] J.M. Dawson, ''One-dimensional Plasma Model'', The Physics of Fluids, 5,445 (1962)

[19] J.M. Dawson and R. Shanny, ''Some Investigations of Nonlinear Behavior in One Dimensional Plasmas'', The Physics of Fluids, 11, 1506 (1968)

[20] R.N. Franklin, S.M. Hamberger, and G.J. Smith, ''Damping of Finite Amplitude Electron Plasma Waves in Collisionless Plasma'', Physical Review Letters, 29, 914 (1972)

[21] T.P. Armstrong, ''Numerical Studies of the Nonlinear Vlasov Equation'', The Physics of Fluids, 10, 1269 (1967)

[22] T. O'Neil, ''Collisionless Damping of Nonlinear Plasma Oscillations'', The Physics of Fluids, 8, 2255 (1965)

[23] V.L. Bailey and J. Denavit, ''Nonlinear Oscillations in a Collisionless Plasma'', The Physics of Fluids, 13, 451 (1970)

[24] R. Sugihara and T. Kamimura, ''An Asymptotic Method for the Vlasov Equation'', Journal of the Physical Society of Japan, 33, 206 (1972)

[25] H.A. Bethe and G.C. Vlases, ''Transverse Diffusion of Particles and Energy in a Laser-Heated Plasma Column'', The Physics of Fluids, 18, 982 (1975)

APPENDIX 1

COMPUTER ROUTINES

This routine and associated subroutines constitute the main M.H.D. code.

```
      INTEGER P,PRTFR
      COMMON PO,BZ,R,P,T,TF
C     FOR ITAPE=1 OUTPUT IS ON TAPE. SPECIFY FILE NAME IN CONTROL CARDS.
C     NPRT IS THE RATIO OF (TAPE OUTPUT)/(PRINT OUTPUT).
C     NTEST (=0 FOR ORIGINAL START AT TIME 0)  (=1 FOR RESTART WITHOUT
C     CHANGING SHELL SPACING)  (=2 FOR RESTART REORGANIZING DATA)
C     NREC IS THE RECORD NUMBER TO BE READ IN FOR RESTART OFF UNIT 4.
C     NCYCH IS ZERO FOR INVERSE BREMSTRAULUNG ONLY. IS 1 FOR
C     NON-LINEAR HEATING.
      R=0.5
      W=3.0E-03
      IT=3
      P=50
      VI=0.9
      BZ=3.0E+05
      PO=10.0
      DT=0.25E-10
      TF=40.0E-09
      PRTFR=1
      ITAPE=1
      NPRT=20
      NTEST=1
      NREC=1
      NCYCH=1
      CALL ALAS2(VI,W,DT,IT,PRTFR,ITAPE,NPRT,NTEST,NREC,NCYCH)
      STOP
      END
      SUBROUTINE ALAS2(VI,W,DT,IT,PRTFR,ITAPE,NPRT,NTEST,NREC,NCYCH)
      INTEGER P,O,Q,PRTFR
      REAL*8       RC(101),U0(101),TE0(100),DT0(100),BC(100),N0(100)
     1,R1(101),U1(101),TE1(100),B1(100),DT1(100),N1(100),    DN(100),
     2                  AA(100),BB(100),CC(100),DD(100),E(100),F(100),
     3Q0(100),           PA(100),DR(100),EE,FF,GG,VIS(100)
     4,                      AAB(100),BBB(100),CCB(100),DDB(100),
     5AAI(100),BBI(100),CCI(100),DDI(100),AAE(100),BBE(100),CCE(100),
     6DDE(100),DR1(100),DR2(100),DR3(100),R4(100),DX1(100),DX2(100),
     7DX3(100),DX4(100),DX5(100),DX6(100),DX7(100),PP(100),AR(100),
     8U2(101),HH,II,TI0(100),HJUL(100)
      REAL    N2(100),TE2(100),TI2(100),DT2(100),B2(100),LIN(100),HEAT(1
     1 00),HRATIO(100)/100*C.0/,RC(100),KE2(100),KI2(100),TEQ2(100)
     2,KR2(100),ETH0(100),EKE0(100),EB0(100),PB(100),PKE(100),PABS(100)
     3,PTH(100),MI,KB ,TP0(100),TPF(100),TP2(100),E322(100),POWER(100)
```

```
     4,W3M1(100),TPARD(100),W3M(100)
      COMMON PO,BZ,R,P,T,TF/COMTH0/TE0,DT0,N0,B0/COMTH1/TE1,DT1,N1,B1
     1/COMHY0/U0,R0    /COMHY1/U1,R1/COMTH2/TE2,N2,B2    /COMLAS/LIN,HEAT
     2/COMEN/DN,ETH0,EKE0,EB0,PABS,PB,PTH,PKE,PABST,PTHT,PKET,PBT
     3/PARAL/TP0,TPP,TP2,E3ZZ,W3M1,TPARD,W3M
C     SUBROUTINE ALAS WILL SOLVE THE TWO FLUID MAGNETOHYDRODYNAMIC
C     EQUATIONS IN CYLINDRICAL SYMMETRY ASSUMING QUASINEUTRALITY BY
C     MEANS OF A LAGRANGIAN DIFFERENCE SCHEME
C     THE EQUATIONS FOR THE MAGNETIC FIELD AND ELECTRON AND ION
C     TEMPERATURES  ARE A NONLINEAR COUPLED SET AND ARE SOLVED
C     BY AN ITERATIVE PROCEDURE WITH THE TRANSPORT COEFFICIENTS
C     EVALUATED AT TIME T+.5DT COMPUTED ANEW AT THE START OF EACH
C     ITERATION
C     BZ DENOTES AN EXTERNAL MAGNETIC FIELD
C     PO DENOTES THE FILLING PRESSURE(HYDROGEN MOLECULES)
C     VI DENOTES A VON-NEUMAN VISCOSITY PARAMETER (SHOCK THICKNESS)
C     P (<100) DENOTES THE NUMBER OF CYLINDRICAL SHELLS USED IN THE INT.
C     A REPRESENTS THE OUTER LIMIT OF THE SPATIAL MESH
C     W REPRESENTS THE THICKNESS OF THE CENTRAL CORE
C     DT REPRESENTS THE TIME INCREMENT (HELD CONSTANT IN ALAS2 )
C     TF REPRESENTS THE TOTAL DURATION OF THE INTEGRATION
C     IT DENOTES THE NUMBER OF ITERATIONS IN THE LOOP FOR TE1,DT1,B1.
C     PRTFR = PRINTING FREQUENCY.
C     THE FOLLOWING PRECAUTIONS MUST BE OBSERVED WITH ALAS2:
C     (1) IF DT IS CHOSEN LARGER THAN THE STABILITY LIMIT AN INSTABILITY
C     WILL RESULT IN NEGATIVE DENSITIES AND AN ARITHMETIC ERROR
C     WILL TERMINATE EXECUTION. IN GENERAL IT IS SAFE TO WORK WITH
C     DT UP TO ONE-HALF OF THE STABILITY LIMIT.
C     (2) THE CONVERGENCE OF B1,TE1,DT1 IS DETERMINED BY THE PARAMETER
C     'IT'. USUALLY A REASONABLE DEGREE OF ACCUACY IS OBTAINED BY
C     SETTING 'IT'=3 ,HOWEVER, 'IT'=1 WILL SAVE TIME FOR SURVEY
C     CALCULATIONS.
C     (3) IN CASES WHERE IT IS EXPECTED THAT TI WILL BE << TE,
C     CONVERGENCE IS SOMETIMES SPEEDED BY WRITING THE SECOND TEMPERATURE
C     EQUATION IN TERMS OF TI(I) RATHER THAN DT(I),(DT(I)=(TE(I-TI(I)))
      ITINC=0
      NLC=0
      O=P-1
      Q=P+1
      R0(1)=0.1D-12
      R0(2)=W
      A=(R/W)**(1.0/(P-1.0))
      DO 99 I=1,10
      A=(((R*(A-1.0))+W)/W)**(1.0/P)
   99 CONTINUE
      U0(1)=0.0D0
      U0(2)=0.0D0
      DO 1 I=3,Q
      U0(I)=0.0D0
      R0(I)=R0(I-1)  +A*(R0(I-1-R0(I-2))
    1 CONTINUE
      R0(P+2)=2*R0(P+1-R0(P)
      KB=1.6E-12
      H=13.6
      AV=7.0E16
```

```
      PI=3.1416
      MI=1.6725E-24
      C=3.0E+10
      WL2=3.17E+28
C     ASSUMES INITIALLY THAT TE=TI=1EV.
      BC(P+1)=BZ
      DO 2 I=1,P
      DR(I)=RO(I+1-RO(I)
      VIS(I)=DR(I)*VI
      TEO(I)=1.0D0
      TPO(I)=0.0
      TP2(I)=0.0
      TIO(I)=1.0D0
      DTO(I)=0.0D0
      BC(I)=BZ
      NO(I)=AV*PO
      DN(I)=AV*PO*PI*((RO(I+1)**2.0-(RO(I)**2.0))
      QO(I)=0.0
    2 CONTINUE
      T=0.0
      CALL REST(TIO,T,P,NTEST,NREC,W,R,DN,TPO)
      WRITE (6,101) PO,BZ,T
      WRITE (6,102)
      WRITE (6,103)
      WRITE (6,104) (I,RO(I),RO(I+1), UO(I),NO(I),TEO(I),DTO(I),BO(I),
     1I=1,P)
  101 FORMAT (1H1,' FILLING PRESSURE IS',E10.3,10X,' AXIAL MAGNETIC FIEL
     1D IS',E10.3,'   TIME IS',E12.5,'  SEC.'///)
  102 FORMAT ( ' THE INITIAL CONDITIONS ARE'/)
  103 FORMAT ( ' I',5X,' RO(I)',7X,' RO(I+1)',5X,'  UO(I)',6X,' NO(I)',
     17X,' TEO(I)',6X,' DTO(I)',6X,' BO(I)'/)
  104 FORMAT (I4,7D13.4)
      J=0
      L=1
      M=0
      NLOOP=0
      NPRT1=NPRT
      ITEST=0
      CALL FLUX(P,BO,RO)
    4 CONTINUE
      NLOOP=NLOOP+1
      DTN=DT
C CALCULATE TIMESTEP DT
      CALL TIME(P,DT,TI2,ITEST,KB,TIO,MI,QO,PP,PI)
C     TEMP,DENSITY, AND MAGNETIC FIELD AT T+DT/2 INITIALIZED TO VALUES AT T.
      CALL ENERGY(DT,P,0)
      DO 3 I=1,P
      RC(I)=(RO(I)+RO(I+1))/2.0
      TE2(I)=TEO(I)
      DT2(I)=DTO(I)
      TI2(I)=TIO(I)
      N2(I)=NO(I)
      B2(I)=BO(I)
    3 CONTINUE
C     FIRST APPROX. FOR ELECTRON ION THERMALIZATION TIME + ELECTRICAL
```

```
C     CONDUCTIVITIES AT T+DT/2. (VALUES AT TIME T USED AS AN APPROX.)
      CALL ETCOND(KE2,P)
      CALL ITCOND(KI2,TI2,P)
      CALL EITT(TEQ2,P)
      CALL ECOND(KR2,P)
C     CALCULATION OF VARIABLES TE1,TI1,B1,R1,U1,N1,NE1, AT TIME T+DT:
C     CALCULATION OF PONDEROMOTIVE PRESSURE
      CALL LHEAT(I,RC,HRATIO,P,1,C,TI2,NCYCH,J,IT,DT)
      DO 44 I=1,P
      PP(I)=3.18E+C9*NO(I)*LIN(I)/(C*WL2)
   44 CONTINUE
C     SOLUTION FOR THE FLUID VELOCITIES AT T+.5DT:
C     SOLUTION FOR THE SHELL BOUNDRIES AT T+DT:
      U1(1)=C.000
      U1(Q)=UO(Q)
      R1(1)=RO(1)
      R1(Q)=RO(Q)
C      WILL DEFINE A NEW TIMESTEP 'DTN' WHICH IS AN AVERAGE OF THE OLD
C     TIMESTEP USED AND THE NEW TIMESTEP TO BE USED.  DTN WILL BE USED
C      FOR CALCULATION OF U1(I) ONLY.   FOR FIRST TIMESTEP DTN=DT .
      DTN=(DTN+DT)/2.0
      IF(ITEST.EQ.0) DTN=DT
      ITEST=1
      DO 5 I=2,P
      U1(I)=UO(I-(4.0D0*DTN*((KB*NO(I)*(TIO(I)+TEO(I))+MI*QO(I)+PP(I))
     1-(KB*NO(I-1)*(TIO(I-1)+TEO(I-1))+MI*QO(I-1)+PP(I-1)))/((RO(I+1-
     2RO(I-1))*(NO(I-1)+NO(I))*MI))
     3-(DTN*2.0*(BO(I-1)+BO(I))*(1.C/(4.0*PI))*(BO(I-BO(I-1))/
     4(RO(I+1-RO(I-1))*(NO(I-1)+NO(I))*MI))
      R1(I)=RO(I)+(DT*(U1(I)))
    5 CONTINUE
      R1(P+2)=2*R1(P+1-R1(P)
C     SOLUTION FOR THE NEW DENSITIES AT TIME T+DT:
C     CALCULATION OF VISCOSITY AT TIME T+.5DT:
      DO 73 I=1,P
      N1(I)=DN(I)/(((R1(I+1)*R1(I+1)-(R1(I)*R1(I)))*PI)
      N2 (I)=(N1(I)+NO(I))/2.0
   73 CONTINUE
C     CALCULATES DIFFERENCE QUANTITIES NEEDED FOR CALCULATING B1,TE1,DT1
      R4(1)=RO(1)+RO(2)+R1(1)+R1(2)
      RC(1)=R4(1)/4.0
      DR1(1)=RO(2)+R1(2-(RO(1)+R1(1))
      DR1(P+1)=(RO(P+2)+R1(P+2)-(RO(P+1)+R1(P+1))
      DR2(1)=RO(3)+R1(3-(RO(1)+R1(1))
      RC(P)=R
      QO(P)=0.
      DO 74 I=2,P
      DR1(I)=(RO(I+1)+R1(I+1)-(RO(I)+R1(I))
      DR2(I)=(R1(I+2)+RO(I+2)-(R1(I)+RO(I))
      DR3(I)=(R1(I+1)+RO(I+1)-(R1(I-1)+RO(I-1))
      R4(I)=RO(I+1)+R1(I+1)+RO(I)+R1(I)
      RC(I)=R4(I)/4.0
C     VISCOSITY AT T+DT/2. USED FOR NEXT TIME INTERVAL AS WELL.
      QO(I)=0.0
C     IF(U1(I+1).LT.U1(I))QO(I)=0.25*VIS(I)*VIS(I)*N2(I)*((U1(I+1U1(I)
```

```
C     .1)/DR1(I))**2
      DX2(I)=(R1(I+1)+R0(I+1))*U1(I+1)/(R4(I)*DR1(I))
      DX3(I)=(R1(I)+R0(I))*U1(I)/(R4(I)*DR1(I))
      DX4(I)=(R1(I+1)+R0(I+1))/(R4(I)*DR2(I)*DR1(I))
      DX5(I)=(R1(I)+R0(I))/(R4(I)*DR3(I)*DR1(I))
      DX6(I)=(R1(I+1)+R0(I+1))/(R4(I)*DR2(I)*DR1(I)*N2(I))
      DX7(I)=(R1(I)+R0(I))/(R4(I)*DR1(I)*DR3(I)*N2(I))
      BBB(I)= (1.0D0/DT) + ((2.0D0)*(DX2(I-DX3(I))))
      DDB(I)=(B0(I)/DT) - ((2.0D0)*B0(I)*(DX2(I-DX3(I))))
      BBI(I)=(1.0D0/DT)+((4.0D0/3.0D0)*(DX2(I-DX3(I))))
      DDI(I)= (DTO(I)/DT) - ((4.0D0/3.0D0)*DTO(I)*(DX2(I-DX3(I)))
     1+((8.0D0/3.0D0)*MI*Q0(I)*(DX2(I-DX3(I))/N2(I))
      BBE(I)=(1.0D0/DT) + ((4.0D0/3.0D0)*(DX2(I-DX3(I))))
      DDE(I)= (TE0(I)/DT) - ((4.0D0/3.0D0)*TE0(I)*(DX2(I-DX3(I))))
   74 CONTINUE
      T2=T+0.5*DT
C     ITERATION LOOP FOR B1,TE1,TI1 STARTS:
      J=-1
   77 CONTINUE
      J=J+1
      CALL LHEAT(T2,BC,HRATIO,P,2,1,TI2,NCYCH,J,IT,DT)
C     SOLUTION FOR THE MAGNETIC FIELD AT TIME T+DT:
C     EQUATION FOR THE MAGNETIC FIELD WILL BE WRITTEN IN THE FORM:
C     -AA(I)B1(I+1) + BB(I)B1(I) - CC(I)B1(I-1) = DD(I)
      KR2(P+1)=KR2(P)
      DO 8 I=2,P
      AA(I)=          (DX4(I)*(KR2(I+1)+KR2(I))/PI)
      BB(I)= BBB(I)+((1.0D0/PI)*(DX4(I)*(KR2(I+1)+KR2(I))+DX5(I)*
     1(KR2(I)+KR2(I-1))))
      CC(I)=          (DX5(I)*(KR2(I)+KR2(I-1))/PI)
      DD(I)=DDB(I)+((1.0D0/PI)*(DX4(I)*(KR2(I+1)+KR2(I))*(B0(I+1-B0(I))
     1-DX5(I)*(KR2(I)+KR2(I-1))*(B0(I-B0(I-1)))))
    8 CONTINUE
C     CALCULATES MAGNETIC FIELD IN CENTRAL CORE:
      GG=2.0*(R0(2)+R1(2))*U1(2)/(DR1(1)*R4(1))+8.0*(R0(2)+R1(2))*(KR2(
     12)+KR2(1))/(12.566*DR2(1)*DR1(1)*R4(1))+1.0/DT
      EE=8.0*(R0(2)+R1(2))*(KR2(1)+KR2(2))/(DR2(1)*12.566*DR1(1)*R4(1))
      FF=8.0*(R0(2)+R1(2))*(KR2(1)+KR2(2))*(B0(2-B0(1))/(12.566*DR1(1)
     1*R4(1)*DR2(1)-2.0*B0(1)*(R0(2)+R1(2))*U1(2)/(R4(1)*DR1(1))+B0(1)/
     2DT
      E(1)=EE/GG
      F(1)=FF/GG
      DO 9 I=2,P
      E(I)=AA(I)/(BB(I-(CC(I)*E(I-1))))
      F(I)=(DD(I)+(CC(I)*F(I-1)))/(BB(I-(CC(I)*E(I-1))))
    9 CONTINUE
      B1(P+1)=F(P)/(1.0-E(P))
      B1(P)=E(P)*B1(P+1)+F(P)
      DO 10 I=1,0
      B1(P-I)=E(P-I)*B1(Q-I)+F(P-I)
   10 CONTINUE
C     SOLUTION FOR ELECTRON TEMPERATURE AT TIME T+DT;
C     EQUATION FOR TE(T+DT) WILL BE WRITTEN IN THE FORM:
C     -AA(I)TE1(I+1) + BB(I)TE1(I) - CC(I)TE1(I-1) = DD(I)
      DO 11 I=2,0
```

```
      AA(I) = (8.0D0/3.0D0)*(KE2(I+1)+KE2(I))*DX6(I)
      BB(I) =BBE(I) +((8.0D0/3.0D0)*((KE2(I+1)+KE2(I))*DX6(I)+(KE2(I)+
     1KE2(I-1))*DX7(I)))
      CC(I) = (8.0D0/3.0D0)*(KE2(I)+KE2(I-1))*DX7(I)
      HJUL(I) =((2.0*KR2(I))/(3.0*KB*N2(I)*(4.0*PI)**2))
     1*((((B1(I+1)+B0(I+1)-(B1(I-1)+B0(I-1)))/DR3(I))**2)
      DD(I) =DDE(I) +((8.0D0/3.0D0)*((KE2(I+1)+KE2(I))*DX6(I)*(TE0(I+1-
     1TE0(I))-(KE2(I)+KE2(I-1))*DX7(I)*(TE0(I-TE0(I-1))))
     2-(DT2(I)/TEQ2(I))+HEAT(I)+HJUL(I)
   11 CONTINUE
C     CALCULATES TEMPERATURE RISE OF CENTRAL CORE:
      GG=1.333*(R0(2)+R1(2))*U1(2)/(DR1(1)*R4(1))+5.333*(R0(2)+R1(2))*
     1(KE2(2)+KE2(1))/((N1(1)+N0(1))*DR2(1)*DR1(1)*R4(1))+1.0/DT
      EE=5.333*(R0(2)+R1(2))*(KE2(1)+KE2(2))/(DR2(1)*(N1(1)+N0(1))
     1*DR1(1)*R4(1))
      FF=5.333        *(R0(2)+R1(2))*(KE2(1)+KE2(2))*(TE0(2-TE0(1))
      FF=5.333*(R0(2)+R1(2))*(KE2(1)+KE2(2))*(TE0(2-TE0(1)))/((N1(1)+N0
     1(1))*DR1(1)*R4(1)*DR2(1)-1.333*TE0(1)*(R0(2)+R1(2))*U1(2)/(R4(1)
     2*DR1(1))+(TE0(1)/DT-(DT2(1)/TEQ2(1))
     3+(8.0/(3.0*((4.0*PI)**2.0)*KB))*(KR2(1)+KR2(2))*((B0(2)+B1(2)-(
     4B0(1)+B1(1)))*((B0(2)+B1(2)-(B0(1)+B1(1)))/((N1(1)+N0(1))*DR2(1)
     5*DR2(1))+HEAT(1)
      E(1)=EE/GG
      F(1)=FF/GG
      DO 12 I=2,0
      E(I)=AA(I)/(BB(I-(CC(I)*E(I-1))))
      F(I)=(DD(I)+(CC(I)*F(I-1)))/(BB(I-(CC(I)*E(I-1))))
   12 CONTINUE
      TE1(P)=TE0(P)
      DO 13 I=1,0
      TE1(P-I)=(E(P-I)*TE1(Q-I))+F(P-I)
   13 CONTINUE
C     SOLUTION FOR RELATIVE TEMPERATURE, DT=TE-TI, AT TIME T+DT:
      DO 14 I=2,0
      AA(I)=  (8.0D0/3.0D0)*(KI2(I+1)+KI2(I))*DX6(I)
      BB(I)=BBI(I)+((8.0D0/3.0D0)*((KI2(I+1)+KI2(I))*DX6(I)+(KI2(I)+
     1KI2(I-1))*DX7(I)))  +(1.0D0/TEQ2(I))
      CC(I)=(8.0D0/3.0D0)*(KI2(I)+KI2(I-1))*DX7(I)
      DD(I)=DDI(I)+((8.0D0/3.0D0)*((KI2(I+1)+KI2(I))*DX6(I)*(DT0(I+1-
     1DT0(I))-(KI2(I)+KI2(I-1))*DX7(I)*(DT0(I-DT0(I-1))))
     2 -(1.0D0*DT0(I)/TEQ2(I))+HEAT(I)+HJUL(I)
     7-((8.0D0/3.0D0)*((KI2(I+1)+KI2(I))*DX6(I)*((TE1(I+1)+TE0(I+1))
     8-(TE1(I)+TE0(I)))-(KI2(I)+KI2(I-1))*DX7(I)*((TE0(I)+TE1(I)-
     9(TE0(I-1)+TE1(I-1)))))
     A+((8.0D0/3.0D0)*((KE2(I+1)+KE2(I))*DX6(I)*((TE1(I+1)+TE0(I+1))
     B-(TE1(I)+TE0(I)))-(KE2(I)+KE2(I-1))*DX7(I)*((TE0(I)+TE1(I)-
     C(TE0(I-1)+TE1(I-1)))))
   14 CONTINUE
C     CALCULATES RELATIVE TEMPERATURE IN CENTRAL CORE:
      HH=5.333        *(R0(2)+R1(2))*(KI2(1)+KI2(2))*((TE0(2)+TE1(2)-
     1(TE0(1)+TE1(1)))/((N1(1)+N0(1))*DR1(1)*R4(1)*DR2(1))
      II=5.333        *(R0(2)+R1(2))*(KE2(1)+KE2(2))*((TE0(2)+TE1(2)-
     1(TE0(1)+TE1(1)))/((N1(1)+N0(1))*DR1(1)*R4(1)*DR2(1))
      GG=1.333*(R0(2)+R1(2))*U1(2)/(DR1(1)*R4(1))+5.333*(R0(2)+R1(2))
     1*(KI2(2)+KI2(1))/((N1(1)+N0(1))*DR2(1)*DR1(1)*R4(1))+1.0/DT+1.0/
```

```
     2TEQ2(1)
      EE=5.333*(RO(2)+R1(2))*(KI2(1)+KI2(2))/(DR2(1)*(N1(1)+NO(1))*DR1
     1(1)*R4(1))
      FF=5.333       *(RO(2)+R1(2))*(KI2(1)+KI2(2))*(DTO(2-DTO(1))
     1/((N1(1)+NO(1))*DR1(1)*R4(1)*DR2(1)-1.333*DTO(1)*(RO(2)+R1(2))*
     2U1(2)/(R4(1)*DR1(1)))+DTO(1)/DT-DTO(1)/TEQ2(1)
     4+ (8.0/(3.0*((4.0*PI)**2.0)*KB))*(KR2(1)+KR2(2))*((BO(2)+B1(2)-(
     5BO(1)+B1(1)))*((BO(2)+B1(2)-(BO(1)+B1(1)))/((N1(1)+NO(1))*DR2(1)
     6*DR2(1))+HEAT(1-HH+II
      E(1)=EE/GG
      F(1)=FF/GG
      DO 15 I=2,O
      E(I)=AA(I)/(BB(I-(CC(I)*E(I-1)))
      F(I)=(DD(I)+(CC(I)*F(I-1)))/(BB(I-(CC(I)*E(I-1)))
   15 CONTINUE
      DT1(P)=DTO(P)
      DT1(O)=E(O)*DT1(P)+F(O)
      DO 16 I=2,O
      DT1(P-I)=E(P-I)*DT1(Q-I)+F(P-I)
   16 CONTINUE
C     CALCULATION OF TRANSPORT COEF AT TIME T+DT/2.
      DO17 I=1,P
      TE2(I)=(TEO(I)+TE1(I))/2.0
      DT2(I)=(DTO(I)+DT1(I))/2.0
      TI2(I)=TE2(I-DT2(I)
      B2(I)=(BO(I)+B1(I))/2.0
   17 CONTINUE
      CALL ECOND(KE2,P)
      CALL ETCOND(KE2,P)
      CALL ITCOND(KI2,TI2,P)
      CALL EITT(TEQ2,P)
C     RETURNS TO CALCULATE TE1,B1,DT1 ONCE MORE
C     GENERALLY FOUR ITERATIONS WILL SUFFICE
      IF (J-IT) 77,20,20
   20 CONTINUE
C     NOW HAS FINAL VALUES FOR B1,TE1,DT1
      ITINC=ITINC+1
      T=T+DT
C     RELABEL VARIABLES    VARIABLE1 BECOMES VARIABLEO.
      RO(Q)=R1(Q)
      RO(P+2)=R1(P+2)
      BO(P+1)=B1(P+1)
      UO(Q)=U1(Q)
      DO 21 I=1,P
      RO(I)=R1(I)
      UO(I)=U1(I)
      NO(I)=N1(I)
      TEO(I)=TE1(I)
      DTO(I)=DT1(I)
      TIO(I)=TE1(I-DT1(I)
      BO(I)=B1(I)
   21 CONTINUE
      IF (L-PSTPR) 223,222,222
  222 CONTINUE
      CALL ENERGY(DT,P,1)
```

```
      DO 505 I=1,P
      POWER(I)=PABS(I)/(3.14*(R1(I+1)**2-R1(I)**2))
  505 CONTINUE
      NPRT1=NPRT1+1
      IF(NPRT1.LT.NPRT) GO TO 881
      NPRT1=0
      WRITE (6,105) T,NLOOP
  105 FORMAT('1','TIME = ',E12.6,' SEC',
     1'     THIS IS THE ',I4,' TH TIMESTEP'/)
      WRITE (6,106)
  106 FORMAT(' ',' (I)',T10,'RO(I)',T20,'UO(I)',T31,'TEO(I)',T42,'DTO(I)
     1',T54,'NO(I)',T65,'BO(I)',T75,'PABS(I)',T87,'PTH(I)',T97,'PKE(I)'
     2,T108,'PB(I)',T118,'HRATIO(I)'/)
      DO225 I=1,P
      WRITE(6,107)I,RO(I),UO(I),TEO(I),DTO(I),NO(I),BO(I),PABS(I),PTH(I)
     1,PKE(I),PB(I),HRATIO(I)
  225 CONTINUE
  107 FORMAT(' ',I4,6(1X,D10.3),5(1X,E10.3))
      WRITE(6,108) PABST,PTHT,PKET,PBT
  108 FORMAT('0','PABST =',E10.3,'  PTHT =',E10.3,'  PKET =',E10.3
     1,'  PBT =',E10.3)
C     CALCULATE AND PRINT OUT VALUES USED AS AN ENERGY CHECK ON PARALLEL
C     TO PERPENDICULAR ENERGY TRANSFER.
      WRITE(6,501)
  501 FORMAT('1',' (I) PAR. TEMP   POWER IN    POWER OUT POWER ABS. TOTAL
     1 POWER    E3')
      TW3M=0.0
      TW3M1=0.0
      TDPAR=0.0
      DO 508 I=1,P
      W3MW=W3M(I)*1.0E-07*DN(I)/N2(I)
      W3M1W=W3M1(I)*1.0E-07*DN(I)/N2(I)
      DEPAR=0.8E-19*TPARD(I)*DN(I)/DT
      TW3M=TW3M+W3MW
      TW3M1=TW3M1+W3M1W
      TDPAR=TDPAR+DEPAR
      WRITE(6,502) I,TPF(I),W3MW,W3M1W,DEPAR,POWER(I),E3ZZ(I)
  508 CONTINUE
  502 FORMAT(' ',I4,6E11.3)
      WRITE (6,507)
  507 FORMAT('0','TOTAL VALUES FOR POWER ABSORBED AND RELEASED BY PARALL
     1EL TEMP.')
      WRITE (6,506) TW3M,TW3M1,TDPAR
  506 FORMAT(' ','POWER IN=',E10.3,'      POWER OUT=',E10.3,
     1'     POWER ABSORBED=',E10.3)
  881 CONTINUE
      L=0
C     DATA READ ONTO A TAPE IF ITAPE= 1.
      IF(ITAPE.EQ.0) GO TO 223
      CALL TPDATA
  223 CONTINUE
      IF (T-TF) 23,23,24
   23 L=L+1
      GO TO 4
   24 CONTINUE
```

```
      IF(ITAPE.EQ.1) ENDFILE3
      CALL FLUX(P,B0,R0)
      RETURN
      END
      SUBROUTINE LHEAT(T,RC,HRATIO,NCELL,NLASER,IHRT,TI2,NCYCH,J,IT,DT)
      REAL LIN(100),HEAT(100),RC(100),TE2(100),N2(100),B2(100),HRATIO(10
     10),LMDA,K3,PWR1(100),PWR2(100),W3M(100),TI2(100)
     1,TPF(100),TPO(100),TP2(100),W3M1(100),E3ZZ(100),TPARD(100)
      COMMON/COMTH2/TE2,N2,B2   /COMLAS/LIN,HEAT/COMDIF/WAVE1,WAVE2,PWR1
     1,PWR2 /PARAL/TPO,TPF,TP2,E3ZZ,W3M1,TPARD,W3M
C     LHEAT CALCULATES LASER INTENSITY LIN(I) (ERGS/CM2.SEC) (REQUIRED
C     FOR PONDEROMOTIVE PRESSURE AND HEATING RATE/PARTICLE (EV/SEC)
C     IHRT=1 IF HEATING RATES ARE TO BE CALCULATED.
C     NCELL = NO. OF CELLS USED IN DIFFERENCE SHCHEME (=P IN NEAL'S NOT.)
C     NLASER = NO. OF LASERS USED IN HEATING.
C     HRATIO(I) = DIFF FREQ. HEAT/INVERSE BREMSSTRAHLUNG HEATING BY
C     INCIDENT BEAMS.
C     DEFN OF LASER PARAMETERS.
C     WAVE1, WAVE2  -  WAVELENGTH (MICRONS) S1, S2 - SPOT SIZE(CM),
C     PD = PULSE DURATION (SEC)
      WAVE1=9.6
      WAVE2=10.6
      S1=0.045
      S2=0.045
      P1=1.25E+9
      P2=1.25E+9
      PD=40.0E-09
C     LASER AMPLITUDE VS. TIME  (AF= AMPLITUDE FACTOR)
      AF=2.0-2.0*T/PD
      IF(T.LE.PD/2.)AF=2.0*T/PD
      P1A=P1*AF
      P2A=P2*AF
      A1=2.0*S1*S1
      A2=2.0*S2*S2
C     SPATIAL DISTRIBUTION OF LASER POWER.
C     PWR1(I) = INTENSITY (W/CM2)
C     LIN = TOTAL LASER (1+2) INTENSITY (ERGS/CM2.SEC)
      DO2 I=1,NCELL
      PWR1(I)=P1A/(3.142*A1)*EXP(-RC(I)*RC(I)/A1)
      LIN(I)=1.0E+07*PWR1(I)
      GO TO (2,1),NLASER
    1 PWR2(I)=P2A/(3.142*A2)*EXP(-RC(I)*RC(I)/A2)
      LIN(I)=LIN(I)+1.E+07*PWR2(I)
    2 CONTINUE
      IF(IHRT.NE.1)GO TO 3
C     CALCULATION OF HEATING RATE FROM INCIDENT LASER BEAMS VIA INVERSE
C     BREMSSTRAHLUNG ABSORPTION. HEAT IS IN ERGS/CM3.SEC.
      Z=1.0
      DO5 I=1,NCELL
      TX=TE2(I)**1.5
      LMDA=12.0*TE2(I)
      IF(TE2(I).LT.27.0)  LMDA=2.3*TX
      HEAT(I)=8.67E-31*((N2(I)*WAVE1)**2)*Z*ALOG(LMDA)*PWR1(I)/TX
      GO TO (5,4),NLASER
    4 HEAT(I)=HEAT(I)+8.67E-31/TX*((N2(I)*WAVE2)**2)*Z*ALOG(LMDA)*PWR2(I
```

```
     1)
      W3M1(I)=0.0
    5 CONTINUE
      IF(NLASER.NE.2)GO TO 7
      IF(NCYCH.EQ.0) GO TO 10
      CALL DFHH(NCELL)
      DO 11 I=1,NCELL
      TCOL=(1.8E+04*(TE2(I)+0.333333*TP2(I))**1.5)/N2(I)
      IF(TCOL.LT.(2.0*DT)) GO TO 15
      TPF(I)=(TPO(I)*(1.0-0.5*DT/TCOL)+2.0*W3M(I)*DT/(1.6E-12*N2(I)))
     1/(1.0+0.5*DT/TCOL)
      TP2(I)=0.5*(TPO(I)+TPF(I))
      W3M1(I)=1.6E-12*TP2(I)*N2(I)/(2.0*TCOL)
      GO TO 11
   15 TPF(I)=0.0
      TP2(I)=0.0
      W3M1(I)=W3M(I)+0.5*1.6E-12*TPO(I)*N2(I)
   11 CONTINUE
      IF(J-IT) 12,13,13
   13 CONTINUE
      DO 14 I=1,NCELL
      TPARD(I)=TPF(I-TPO(I)
   14 TPO(I)=TPF(I)
   12 CONTINUE
   10 CONTINUE
      DO6 I=1,NCELL
      IF(HEAT(I).LT.1.0E-65) HEAT(I)=1.0E-65
      HRATIO(I)=W3M(I)/HEAT(I)
      HEAT(I)=HEAT(I)+W3M1(I)
    6 CONTINUE
C     2/3 . HEATING RATE (EV.SEC)/PARTICLE   VALUE STORED IN HEAT(I).
    7 DO8 I=1,NCELL
      HEAT(I)=0.6667*0.625E+12*HEAT(I)/N2(I)
    8 CONTINUE
    3 RETURN
      END
      SUBROUTINE DFHH(NCELL)
C     DIFF. FREQ. HARMONIC HEATING VERSION 2
C     ROUTINE CALCULATES HEATING RATE DUE TO MIXING OF TWO ANTIPARALLEL
C     LASERS.
      COMPLEX E32,EO,J/(0.0,1.0)/
      REAL T(100),N(100),B(100),PWR1(100),PWR2(100),W3M(100),A3,KZ,K
     1,FOSPL(12,5) ,TP2(100),E3ZZ(100),TPO(100),TPF(100),W3M1(100),
     1TPARD(100)
      COMMON/COMTH2/T,N,B/COMDIF/WAVE1,WAVE2,PWR1,PWR2
     1/PARAL/TPO,TPF,TP2,E3ZZ,W3M1,TPARD,W3M
      DATA FOSPL/0.2,0.5,0.8,1.0,1.2,1.4,1.7,2.0,2.5,3.0,3.5,4.0,
     1 .3895,0.7199,1.064,1.076,1.015,0.913,0.7451,0.6027,0.4462,0.3565
     2,0.2992,0.2567,1.003,1.299,0.5474,-0.2165,-0.4162,-0.5635,-0.532,
     3-0.4114,-0.2316,-0.1393,-0.0931,0.0,0.0,0.987,-3.4911,-0.3284,
     4-0.6701,-0.06606,0.1709,0.231,0.1287,0.5593E-1,0.03642,0.0,1.097
     5,-4.976 ,5.272,-0.5696,1.007,0.2633,0.06673,-0.06821,-0.0485,
     6-0.01301,-0.02428,0.0/
C     CALCULATION OF BEAT FREQ. LASER HEATING.
C     PARAMETERS FOR THE DIFF. FREQ. WAVE (ANTIPARALLEL BEAMS)
```

```
      K3=6.283E+04*(1.0/WAVE1+1.0/WAVE2)
      W3=1.885E+15*(1.0/WAVE1-1.0/WAVE2)
      KZ=ABS(K3)
      DO1 II=1,NCELL
      WPE=5.63E+04*SQRT(N(II))
      VOE=5.93E+07* SQRT((T(II)+TP2(II)))
      VEI=2.53E-05*N (II)/((T(II)+0.333333*TP2(II))**1.5)
      K=KZ*VOE/(1.4142*WPE)
      AO=W3/(KZ*VOE)
      AOE=AO
      IF(AOE.GT.10.)AOE=10.0
      AOES=AOE*AOE
C
C     SPLINE APPROXIMATION FOR FO
      IF(AO.GT.3.25)GO TO 12
      DO7 I=1,12
      IF(AO.LT.FOSPL(I,1))GO TO 8
    7 CONTINUE
    8 I=I-1
      DA=AO-FOSPL(I,1)
      FO=FOSPL(I,2)+FOSPL(I,3)*DA+FOSPL(I,4)*DA*DA+FOSPL(I,5)*DA**3
      FO=J*FO
      GO TO 11
   12 FO=J/AO*(1.0+0.5/(AO*AO)+0.75/(AO**4)+1.875/(AO**6)+6.563/(AO**8))
   11 DAMP=AMAX1(VEI/(2.0*W3*AO**3),1.772*EXP(-AOES))
      FO=FO+DAMP
      E3Z=J*3.0E-16*KZ*WAVE1*WAVE2*(1.0+J*AO*FO)/(K*K+1.0+J*AO*FO
     .1-2.72E-04/(AO*AO))*1.0343
      E3ZZ(II)=(CABS(E3Z))*SQRT(PWR1(II)*PWR2(II))
      W3M(II)=WPE*WPE*AO*AO/(3.142*KZ*VOE)*REAL(FO)*(CABS(E3Z)**2)
     1*PWR1(II)*PWR2(II)
    1 CONTINUE
      RETURN
      END
      SUBROUTINE REST(TIO,T,P2,ITEST,NREC,W2,R,DN,TPO)
C     THIS ROUTINE WILL READ DATA FROM SEQ. FILE AND PASS IT BACK TO
C     ALAS2.
C     AS INITAL CONDITIONS.
C     IF ITEST=0 NOTHING IS DONE.
C     IF ITEST=1 ROUTINE RESTARTS WITH INITIAL CONDITIONS AS ON FILE.
C     IF ITEST=2 ROUTINE REORGANIZES DATA TO CHANGE NUMBER OF SHELLS.
      REAL*8 RO(101),UO(101),TEO(100),DTO(100),TIO(100),BO(100),
     1NO(100),DBLE,DN(100)
      REAL RS(102),TES(102),TIS(102),NS(102),VS(102),BS(102),
     1RCS(100),RCN(100),TPS(102),TPO(100)
      INTEGER P1,P2,Q
      COMMON/COUTHO/TEO,DTO,NO,BO/COMHYO/UO,RO
      IF(ITEST.EQ.0) GO TO 1
      DO 2 I=1,NREC
      READ(4)T,TF,PO,R,BZ,P1,RS,TES,TIS,NS,VS,BS,TPS
    2 CONTINUE
      IF(ITEST.EQ.2) GO TO 9
      DO 3 I=1,P1
      RO(I)=DBLE(RS(I))
      UO(I)=DBLE(VS(I))
```

```
      TEO(I)=DBLE(TES(I))
      TIO(I)=DBLE(TIS(I))
      TPO(I)=TPS(I)
      BO(I)=DBLE(BS(I))
      NO(I)=DBLE(NS(I))
      DTO(I)=TEO(I-TIO(I)
    3 CONTINUE
      BO(P1+1)=DBLE(BS(P1))
      RO(P1+1)=DBLE(RS(P1+1))
      RO(P1+2)=DBLE(2.0*RS(P1+1-RS(P1))
      UO(P1+1)=DBLE(VS(P1+1))
      DO 14 I=1,P1
      DN(I)=NO(I)*3.1416*((RO(I+1)**2-(RO(I)**2))
   14 CONTINUE
      GO TO 1
    9 RO(1)=0.1D-12
      RO(2)=W2
      A=(R/W2)**(1.0/(P2-1.0))
      DO 4 I=1,10
      A=(((R*(A-1.0))+W2)/W2)**(1.0/P2)
    4 CONTINUE
      Q=P2+1
      DO 5 I=3,Q
      RO(I)=RO(I-1)+A*(RO(I-1-RO(I-2))
    5 CONTINUE
      RO(Q+1)=2.0*RO(P2+1-RO(P2)
      DO 6 I=1,P1
    6 RCS(I)=(RS(I)+RS(I+1))/2.0
      DO 7 I=1,P2
    7 RCN(I)=(RO(I)+RO(I+1))/2.0
      N1=1
      DO 8 I=1,P2
      N=N1
      DO 10 J=N,P1
      N1=J
      IF(RCN(I).LT.RCS(J)) GO TO 11
   10 CONTINUE
CC    ONLY COMES HERE IF RCN(I) .GT. RCS(P1)
      UO(I)=DBLE(VS(P1))
      TPO(I)=TPS(P1)
      TEO(I)=DBLE(TES(P1))
      TIO(I)=DBLE(TIS(P1))
      BO(I)=DBLE(BS(P1))
      NO(I)=DBLE(NS(P1))
      DTO(I)=TEO(I-TIO(I)
      GO TO 8
   11 IF(N1.EQ.1) GO TO 12
C     RCN(I) IS BETWEEN RCS(N1-1) AND RCS(N1)
      BO(I)=BS(N1-1)+((RCN(I-RCS(N1-1))/(RCS(N1-RCS(N1-1)))
     1*(BS(N1-BS(N1-1))
      UO(I)=VS(N1-1)+((RCN(I-RCS(N1-1))/(RCS(N1-RCS(N1-1)))
     1*(VS(N1-VS(N1-1))
      TEO(I)=TES(N1-1)+((RCN(I-RCS(N1-1))/(RCS(N1-RCS(N1-1)))
     1*(TES(N1-TES(N1-1))
      TIO(I)=TIS(N1-1)+((RCN(I-RCS(N1-1))/(RCS(N1-RCS(N1-1)))
```

```
     1*(TIS(N1-TIS(N1-1))
      TPO(I)=TPS(N1-1)+((RCN(I-RCS(N1-1))/(RCS(N1-RCS(N1-1)))
     1*(TPS(N1-TPS(N1-1))
      NO(I)=NS(N1-1)+((RCN(I-RCS(N1-1))/(RCS(N1-RCS(N1-1)))
     1*(NS(N1-NS(N1-1))
      DTO(I)=TEO(I-TIO(I)
      GO TO 8
   12 UO(I)=DBLE(VS(1))
      TEO(I)=DBLE(TES(1))
      TPO(I)=TPS(I)
      TIO(I)=DBLE(TIS(1))
      BO(I)=DBLE(BS(1))
      NO(I)=DBLE(NS(1))
      DTO(I)=TEO(I-TIO(I)
    8 CONTINUE
      BO(P2+1)=BO(P2)
      UO(P2+1)=0.0D0
      DO 13 I=1,P2
      DN(I)=NO(I)*3.1416*((RO(I+1)**2.0-(RO(I)**2.0))
   13 CONTINUE
    1 RETURN
      END
      SUBROUTINE TIME(P,TSF,TI2,ITEST,KB,TIO,MI,QO,PP,PI)
      REAL*8 TE1(100),DT1(100),N1(100),B1(100),U1(101),R1(101),
     1RO(101),UO(101),TEO(100),DTO(100),BO(100),NO(100)
     2,TIO(100),QO(100),PP(100),DABS
      REAL TE2(100),N2(100),TI2(100),B2(100),KB,MI,AA(101),ZZ(6)
      INTEGER P,Q
      COMMON/COMTH1/TE1,DT1,N1,B1/COMHY1/U1,R1/COMTH2/TE2,N2
     1,B2/COMHY0/UO,RO/COMTH0/TEO,DTO,NO,BO
C SUBROUTINE CALCULATES TIME INCREMENTS FOR NEXT STEP IN MHD CODE
C P=NO. OF CYLINDRICAL SHELLS USED
C FIRST CALCULATE TIME STEP FOR EQNS. TO BE STABLE.
C TSF=FINAL TIME STEP TO BE USED
C TSI=TIME STEP USED IN PREVIOUS LOOP
C CS2=(SPEED OF SOUND)**2
C CA2=(ALFVEN VELOCITY)**2
      TZ(1)=1000.0
      TZ(2)=1000.0
      TZ(3)=1000.0
      TZ(4)=1000.0
      TZ(5)=1000.0
      TZ(6)=1000.0
      A0=0.8
      A1=0.2
      A2=1.0
      A3=1.0
      A4=10
      A5=20.0
      A6=0.2
      TSI=TSF
      TSF=1.0
      IF (ITEST.EQ.0) GO TO 601
      GO TO 602
  601 CONTINUE
```

```
      DO 3 I=1,P
      TE1(I)=TE0(I)
      DT1(I)=DT0(I)
      N1(I)=N0(I)
      B1(I)=B0(I)
      R1(I)=R0(I)
    3 CONTINUE
      A0=0.1
      R1(P+1)=R0(P+1)
  602 CONTINUE
C     LIMIT TS SO STABILITY CONDITION IS SATISFIED.
      DO 1 I=1,P
      PRESS=N1(I)*(1.38D-16)*(TE1(I)+(TE1(I-DT1(I)))
      RHO=(1.67D-24)*N1(I)
      CS2=(5.0/3.0)*PRESS/RHO
      CA2=(B1(I)**2)/(4.0*3.14159*RHO)
      C=SQRT(CS2+CA2)
      TS=A0*(R1(I+1-R1(I))/C
      IF(TS.LT.TZ(1)) TZ(1)=TS
    1 CONTINUE
      IF (ITEST.EQ.0) GO TO 99
      Q=P+1
C  CALCULATE AA(I)=ACCELERATION OF THE I'TH SHELL BOUNDARY.
      AA(1)=0.0
      AA(P+1)=0.0
      DO 6 I=2,11
      AA(I)=-(4.0D0*((KB*N0(I)*(TI0(I)+TE0(I))+MI*Q0(I)+PP(I))
     1-(KB*N0(I-1)*(TI0(I-1)+TE0(I-1))+MI*Q0(I-1)+PP(I-1)))/((R0(I+1-
     2R0(I-1))*(N0(I-1)+N0(I))*MI))
     3-(2.0*(B0(I-1)+B0(I))*(1.0/(4.0*PI))*(B0(I-B0(I-1))/
     4((R0(I+1-R0(I-1))*(N0(I-1)+N0(I))*MI))
      IF(ABS(AA(I)).LT. 1.0E-60) AA(I)=1.0E-60
    6 CONTINUE
      DO 2 I=1,10
C LIMIT TS SO SHELL THICKNESS IS NOT INCREASED BY MORE THAN A
C FACTOR OF 'A1'.
      RI=A1*(R1(I+1-R1(I))
      U=U1(I+1U1(I)+(TSI*(AA(I+1-AA(I))/2.0)
      AB=(AA(I+1-AA(I))/2.0
      AU=ABS(U)
      AAB=ABS(AB)
      IF(ABS(U).LT.1.0E-30) U=1.0E-30
      IF(AAB.LT.1.0E-50)AAB=1.0E-50
      IF(((4.0*AAB*RI)/(U**2)).GT.1.0E-02) GO TO 7
      TS=RI/AU
      GO TO 8
    7 DDIS=AU**2-4.0*AAB*RI
      SDIS=AU**2+4.0*AAB*RI
      IF(((U.GT.0.0).AND.(AB.GT.0.0)).OR.((U.LT.0.0).AND.(AB.LT.0.0)))
     1TS=(-AU+SQRT(SDIS))/(2.0*AAB)
      IF(((U.GT.0.0).AND.(AB.LT.0.0).AND.(DDIS.GT.0.0)).OR.((U.LT.0.0)
     1.AND.(AB.GT.0.0).AND.(DDIS.GT.0.0))) TS=(AU-SQRT(DDIS))/(2.0*AAB)
      IF(((U.GT.0.0).AND.(AB.LT.0.0).AND.(DDIS.LT.0.0)).OR.((U.LT.0.0)
     1.AND.(AB.GT.0.0).AND.(DDIS.LT.0.0))) TS=(AU+SQRT(SDIS))/(2.0*AAB)
    8 IF(TS.LT.TZ(2)) TZ(2)=TS
```

```
C LIMIT TS SO CELL ELECTRON AND ION TEMP. DOES NOT CHANCE BY MORE
C THAN A FACTOR OF 'A2' AND 'A3' RESPECTIVELY.
      T=2.0*(ABS(SNGL(TE1(I)-TE2(I))))
      IF(T.LT.1.0E-50) T=1.0E-50
      TS=(A2*TE1(I)*TSI)/T
      IF(TS.LT.TZ(3)) TZ(3)=TS
      TI1=TE1(I-DT1(I)
      TI=2.0*(ABS(TI1-TI2(I)))
      IF (TI.LT.1.0E-50) TI=1.0E-50
      TS=(A3*TI1*TSI)/TI
      IF(TS.LT.TZ(4)) TZ(4)=TS
    2 CONTINUE
C LIMIT TS SO VELOCITY DOES NOT CHANGE BY MORE THAN A FACTOR OF A5.
      DO 4 I=2,10
      IF(DABS(U1(I)).LT.1.0D-50) U1(I)=1.0D-50
      IF(DABS(U1(I)).LT.0.1D+06)A5=50.0
      IF(DABS(U1(I)).LT.0.1D+04) A5=0.1D+06/DABS(U1(I))
      AVEL=DABS(AA(I)/U1(I))
      IF(AVEL.LT.1.0E-50) AVEL=1.0E-50
      TS=A5/AVEL
      IF(TS.LT.TZ(5)) TZ(5)=TS
    4 CONTINUE
C  LIMIT TS SO RADIUS DOES NOT CHANGE BY MORE THAN A FACTOR OF A6.
      DO 5 I=2,10
      RI=A6*R1(I)
      U=U1(I)+(TSI*AA(I)/2.0)
      AB=AA(I)/2.0
      AU=ABS(U)
      AAB=ABS(AB)
      IF(ABS(U).LT.1.0E-30) U=1.0E-30
      IF(AAB.LT.1.0E-50)AAB=1.0E-50
      IF(((4.0*AAB*RI)/(U**2)).GT.1.0E-02) GO TO 17
      TS=RI/AU
      GO TO 18
   17 DDIS=AU**2-4.0*AAB*RI
      SDIS=AU**2+4.0*AAB*RI
      IF(((U.GT.0.0).AND.(AB.GT.0.0)).OR.((U.LT.0.0).AND.(AB.LT.0.0)))
     1TS=(-AU+SQRT(SDIS))/(2.0*AAB)
      IF(((U.GT.0.0).AND.(AB.LT.0.0).AND.(DDIS.GT.0.0)).OR.((U.LT.0.0)
     1.AND.(AB.GT.0.0).AND.(DDIS.GT.0.0))) TS=(AU-SQRT(DDIS))/(2.0*AAB)
      IF(((U.GT.0.0).AND.(AB.LT.0.0).AND.(DDIS.LT.0.0)).OR.((U.LT.0.0)
     1.AND.(AB.GT.0.0).AND.(DDIS.LT.0.0))) TS=(AU+SQRT(SDIS))/(2.0*AAB)
   18 IF(TS.LT.TZ(6)) TZ(6)=TS
    5 CONTINUE
C ONLY ALLOW TS TO INCREASE BY FACTOR OF A4 IN A SINGLE STEP
      TS=A4*TSI
      IF (TS.LT.TSF) TSF=TS
   99 CONTINUE
C     SET TSF EQUAL TO SMALLIST OF TZ(I).
      DO 20 I=1,6
      IF(TZ(I).LT.TSF) TSF=TZ(I)
   20 CONTINUE
C     WRITE(7,102) TZ(1),TZ(2),TZ(3),TZ(4),TZ(5),TZ(6)
C     WRITE(7,101) TSF
C 102 FORMAT('0',6E15.3)
```

```
C 101 FORMAT(' ',E11.3)
      RETURN
      END
      SUBROUTINE ETCOND(KE,NCELL)
C     SUBROUTINE CALCULATES ELECTRON THERMAL CONDUCTIVITY AT SHELL
C     CENTERS.
      REAL   TE(100),N(100),B(100),KE(100)
      COMMON/COMTH2/TE,N,B
      DO1 I=1,NCELL
      GA=2.9E-05*N(I)/TE(I)**1.5
      WCE=1.76E+07*B(I)
      KE(I)=2.356E+15*N(I)*TE(I)/(GA*(1.0+0.555*((WCE/GA)**2)))
    1 CONTINUE
      RETURN
      END
      SUBROUTINE ITCOND(KI,TI,NCELL)
C     SUBROUTINE CALCULATES THE ION THERMAL CONDUCTIVITY AT THE CELL
C     CENTERS.
      REAL   TE(100),TI(100),N(100),B(100),KI(100)
      COMMON/COMTH2/TE,N,B
      DO1 I=1,NCELL
      BE=1.414+0.175*(TI(I)/TE(I))**1.5
      GA=6.77E-07*N(I)/TI(I)**1.5
      WCI=9.56E+03*B(I)
      KI(I)=5.98E+12*N(I)*TI(I)/(BE*GA*(1.0+6.25*(WCI/(BE*GA))**2))
    1 CONTINUE
      RETURN
      END
      SUBROUTINE EITT(TEQ,NCELL)
C     SUBROUTINE EITT CALCULATES ION-ELECTRON THERMALIZATION TIME.
      REAL   TE(100),N(100),B(100),TEQ(100),LMDA
      COMMON/COMTH2/TE,N,B
      DO 1 I=1,NCELL
      IF(TE(I).LT.36.0) GO TO 2
      LMDA=9.31oE+10*TE(I)/N(I)**0.5
      GO TO 3
    2 LMDA=1.55E+10*(TE(I)**1.5)/N(I)**0.5
    3 TEQ(I)=3.16E+08*TE(I)**1.5/(N(I)*ALOG(LMDA))
    1 CONTINUE
      RETURN
      END
      SUBROUTINE ECOND(KR,NCELL)
C     SUBROUTINE CALCULATES C**2 X RESISTIVITY (STATOHMS.CM3/SEC2)
      REAL   TE(100),N(100),B(100),KR(100),LMDA
      COMMON/COMTH2/TE,N,B
      DO3 I=1,NCELL
      IF(TE(I).LT.36.0)GO TO 1
      LMDA=9.31oE+10*TE(I)/N (I)**0.5
      GO TO 2
    1 LMDA=1.55E+10*(TE(I)**1.5)/N(I)**0.5
    2 KR(I)=1.03E+07*ALOG(LMDA)/TE(I)**1.5
    3 CONTINUE
      RETURN
      END
      SUBROUTINE ENERGY(DT,NCELL,IE)
```

```
C       ENERGY SERVES AS A CHECK ON THE SIMULATION PROBLEM.  IN PARTICULAR
C       THE RATE AT WHICH THERMAL, KINETIC AND MAGNETIC ENERGY IS CHANGING
C       IN A CELL IS CALCULATED AND CAN BE COMPARED TO THE RATE AT WHICH
C       LASER ENERGY IS DEPOSITED IN THE PLASMA.
        REAL*8 UO(101),RO(101),TEO(100),DTO(100),NO(100),BO(100),DN(100)
        REAL   ETHO(100),ETH1(100),EKEO(100),EKE1(100),EBO(100),EB1(100)
       1,PABS(100),PB(100),PTH(100),PKE(100),HEAT(100),LIN(100)
        COMMON/COMHYO/UO,RO/CONTHO/TEO,DTO,NO,BO/COMLAS/LIN,HEAT/COMEN/DN
       1,ETHO,EKEO,EBO,PABS,PB,PTH,PKE,PABST,PTHT,PKET,PBT
C       CALCULATION OF THERMAL,KINETIC AND MAGNETIC ENERGY IN EACH CELL.
C       SET IE=0 IF THIS IS THE ONLY CALCULATION TO BE MADE.
        IF(IE.NE.0)GO TO 5
        DO6 I=1,NCELL
        ETHO(I)=2.4E-12*DN(I)*(2.0*TEO(I-DTO(I))
        EKEO(I)=2.091E-25*DN(I)*(UO(I)+UO(I+1))**2
        EBO(I)=BO(I)*BO(I)/8.0*(RO(I+1)*RO(I+1-RO(I)*RO(I))
    6   CONTINUE
        GO TO 7
    5   DO1 I=1,NCELL
        ETH1(I)=2.4E-12*DN(I)*(2.0*TEO(I-DTO(I))
        EKE1(I)=2.091E-25*DN(I)*(UO(I)+UO(I+1))**2
        EB1(I)=BO(I)*BO(I)/8.0*(RO(I+1)*RO(I+1-RO(I)*RO(I))
    1   CONTINUE
C       POWER CALCULATIONS.
        PABST=0.
        PBT=0.0
        PTHT=0.
        PKET=0.0
        DO3 I=1,NCELL
        PABS(I)=2.4E-19*DN(I)*HEAT(I)
        PB(I)=1.0E-07*(EB1(I-EBO(I))/DT
        PTH(I)=1.0E-07*(ETH1(I-ETHO(I))/DT
        PKE(I)=1.0E-07*(EKE1(I-EKEO(I))/DT
        PABST=PABST+PABS(I)
        PTHT=PTHT+PTH(I)
        PKET=PKET+PKE(I)
        PBT=PBT+PB(I)
    3   CONTINUE
C       ETHO,EKEO,EBO ARE SET TO THE LAST VALUES, IE. ETH1,...
    2   DO4 I=1,NCELL
        ETHO(I)=ETH1(I)
        EKEO(I)=EKE1(I)
        EBO(I)=EB1(I)
    4   CONTINUE
    7   RETURN
        END
        SUBROUTINE TPDATA
        REAL*8 RO(101),UO(101),TEO(100),DTO(100),NO(100),BO(100)
        REAL VS(102),TES(102),TIS(102),NS(102),RS(102),BS(102),TPS(102)
       1,TPO(100),TPF(100),TP2(100),E322(100),W3M1(100),TPARD(100),
       2W3M(100)
        INTEGER P
        COMMON PO,BZ,R,P,T,TF/COMHYO/UO,RO  /CONTHO/TEO,DTO,NO,BO
       1/PARAL/TPO,TPF,TP2,E322,W3M1,TPARD,W3M
C       SUBROUTINE PREPARES NUMERICAL DATA TO BE STORED ON TAPE FOR
```

```
C       PLOTTING.
        DO1 I=1,P
        TES(I)=SNGL(TEO(I))
        TIS(I)=SNGL(TEO(I-DTO(I))
        NS(I)=SNGL(NO(I))
        TPS(I)=TPF(I)
      1 CONTINUE
        N=P+1
        DO 2 I=1,N
        RS(I)=SNGL(RO(I))
        BS(I)=SNGL(BO(I))
        VS(I)=SNGL(UO(I))
      2 CONTINUE
        WRITE(3) T,TF,PO,R,BZ,P,RS ,TES,TIS,NS,VS,BS ,TPS
        RETURN
        END
        SUBROUTINE FLUX(P,BO,RO)
        REAL*8 BO(100),RO(101)
        INTEGER P
        TFLUX=0.0
        DO 1 I=1,P
        TFLUX=TFLUX + BO(I)*3.14159*((RO(I+1)**2) - (RO(I)**2))
      1 CONTINUE
        WRITE(6,2) TFLUX
      2 FORMAT(' ','TOTAL MAGNETIC FLUX IS',E14.6///)
        RETURN
        END
```

This routine plots data from magnetic tape of the M.H.D. routine.

```
        REAL RM(102),TE(102),TI(102),N(102),V(102),B(102) ,TP(102)
        INTEGER P
        COMMON R,BZ,PO,T,TF,P,RM/PLOTTN/TE,TI,N,V,B ,TP
C       TF IS TIME FOR FINAL PLOT.
C       TINC IS INCREMENT IN TIME BETWEEN PLOTS
C       TPL IS SET TO TIME FOR INITIAL PLOT.
        CALL PLOTS
        CALL PLOT(2.0,5.0,-3)
        TF=40.0E-09
        TINC=5.0E-09
        TPL=20.0E-09
      1 READ(2,END=2)T,TF,PO,R,BZ,P,RM,TE,TI,N,V,B ,TP
        IF(T.GE.TPL) GO TO 3
        GO TO 1
      3 TPL=TPL+TINC
        DO 4 I=1,P
      4 TP(I)=TP(I)+TE(I)
        CALL HYDPLT
        IF(T.GE.TF)  GO TO 2
        GO TO 1
      2 CALL PLOT(0.0,0.0,999)
```

```
      STOP
      END
      SUBROUTINE HYDPLT
C     SUBROUTINE CSALE FINDS SCALING PARAMETERS FOR COMPUTER PLOTTING
C     AND RESULTS APPEAR IN LOCATION (P+1) AND (P+2).
C     AN ORDINATE OF 7 INCHES IN A  PLOT IS ASSUMED.
      REAL TE(102),TI(102),N(102),B(102),V(102),RM(102) ,TP(102)
      INTEGER P,NLB(25)/68,69,85,98,73,99,104,64,77,103,113,112,46,113
     1,120,47,47,67,84,46,96,115,47,47,93/,VLB(29)/70,83,86,102,64,101
     2,69,83,86,67,73,99,104,64,77,61,113,112,46,118,47,47,67,84,97,98
     3,69,67,93/,VMAX
      COMMON R,BZ,P0,T,TF,P,RM/PLOTN/TE,TI,N,V,B ,TP
C     MXT,NOMAX,VMAX REPRESENT MAX. VALUES IN TEMP, DENSITY,AND VELOCITY
C     TO A POWER OF 10
C     ALL SCALING COEF. ARE CONTAINED IN LOCATIONS (P+1) AND (P+2).
C     MAGNETIC FIELD SCALING-  B/BZ X DENSITY (TIME=0)/MAX. DENSITY.
C     PLOT WINDOW, X-AXIS AND LABEL PARAMETERS.
      CALL HYDLBL
C     PLOT OF ELECTRON, ION, AND PARALLEL TEMPERATURE VS. RADIUS.
      CALL CSALE(TP,MXT,P,0)
      TE(P+1)=TP(P+1)
      TE(P+2)=TP(P+2)
      TI(P+1)=TE(P+1)
      TI(P+2)=TE(P+2)
      CALL AXIS(0.0,0.0,'TEMPERATURE (EV)',16,7.0,90.0,TP(P+1),TP(P+2)
     1,20.0)
      CALL DLINE(RM,TE,P,2,0.050)
      CALL DLINE(RM,TP,P,1,0.050)
C
C     PLOT OF PLASMA DENSITY VS. RADIUS.
      CALL CSALE(N,NOMAX,P,1)
      CALL AXIS(7.5,0.0,' ',-1,7.0,90.0,N(P+1),N(P+2),20.0)
      NLB(15)=102+NOMAX
      CALL LSYMB(7.9,2.5,0.12,NLB(1),90.0,-1)
      DO1 I=2,25
    1 CALL LSYMB(999.0,999.0,0.12,NLB(I),90.0,-1)
      CALL FLINE(RM,N,P,1,0,0)
C
C     PLOT OF MAGNETIC FIELD VS. RADIUS.
      B(P+1)=N(P+1)
      B(P+2)=N(P+2)
      DO2 I=1,P
    2 B(I)=7.0E+16*P0*B(I)/(BZ*10.0**NOMAX)+0.005
      CALL DASHLN(RM,B,P,1)
C
C
C     PLOT OF FLOW VELOCITY VS. RADIUS.
C     WINDOW PLUS LABELLING.
      CALL PLOT(-0.5,10.0,-3)
      CALL HYDLBL
C     COMPLETION OF GRAPH PLUS LABELLING.
      CALL SCALE(V,7.0,P,1)
      CALL AXIS(0.0,0.0,'FLOW VELOCITY (CM/SEC)',+22,
     17.0,90.0,V(P+1),V(P+2))
      CALL AXIS(7.5,0.0,'FLOW VELOCITY (CM/SEC)',-22,
```

```
     17.0,90.0,V(P+1),V(P+2))
      CALL PLINE(RM,V,P,1,0,0)
C
C     MOVE ORIGIN TO PREPARE FOR NEXT PLOT
      CALL PLOT(12.0,-11.0,-3)
      RETURN
      END
      SUBROUTINE HYDLBL
      REAL RM(102)
      INTEGER P
      COMMON R,BZ,PO,T,TF,P,RM
C     SUBROUTINE HYDLBL IS A LABELLING ROUTINE. GIVES A WINDOW (8 X 8.5),
C     THE X-AXIS AND THE FOLLOWING PHYSICAL CONSTANTS, TIME(NSEC),
C     FILLING PRESSURE (TORR), AND THE MAGNETIC FIELD (KG).
C     R= MAX. VALUE FOR R (CM)
C     T= TIME(SEC)
C     DRAWING OF A WINDOW.
      CALL PLOT(0.0,0.0,3)
      CALL PLOT(0.0,8.0,2)
      CALL PLOT(8.5,8.0,2)
      CALL PLOT(8.5,0.0,2)
      CALL PLOT(0.0,0.0,2)
C     DEFN OF A NEW ORIGIN.
      CALL PLOT(0.5,0.5,-3)
C     SCALING COEF FOR RADIUS.
      RM(P+1)=0.
      RM(P+2)=R /7.0
      CALL AXIS(0.0,0.0,'RADIUS (CM)',-11,7.5,0.0,RM(P+1),RM(P+2),14.29)
      CALL AXIS(0.0,7.0,' ',-1,7.5,0.0,1.0E+40,1.0,28.57)
C     PRINTING OF PLASMA PARAMETERS.
      BZKG=BZ*1.0E-03
      TNSEC=T*1.0E+9
      CALL SYMBOL(0.25,7.2,0.08,'TIME IS         NSEC.',0.0,19)
      CALL NUMBER(0.95,7.2,0.08,TNSEC,0.0,+2)
      CALL SYMBOL(2.1,7.2,0.08,'FILLING PRESSURE IS        TORR.',0.0,30)
      CALL NUMBER(3.687,7.2,0.08,PO,0.0,+1)
      CALL SYMBOL(4.85,7.2,0.08,'EXTERNAL FIELD IS       KGAUSS.',0.0,
     130)
      CALL NUMBER(6.25,7.2,0.08,BZKG,0.0,1)
      RETURN
      END
      SUBROUTINE CSALE(V,MX,P,SREQ)
      REAL V(102)
      INTEGER P,SREQ
C     SUBROUTINE SCALES VARIABLES FOR PLOTTING.
C     VALUES TO BE PLOTTED ARE NORMALIZED TO A POWER OF 10 (MX).
C     SL=SCALE LENGTH/INCH
C     SREQ= 0 (NO SCALING)  =1 IF SCALING IS REQUIRED.
C     SCALING PERFORMED ON BASIS OF 7 - INCH ORDINATE.
      X=0.
      DO1 I=1,P
      IF(X.LT.V(I)) X=V(I)
    1 CONTINUE
      DIFF=ALOG10(X)
      MX=IFIX(DIFF)
```

```
      DIFF=DIFP-MX
      IF(DIFP.LT.0.813)GO TO 3
      MX=MX+1
      DIFP=DIFP-1
    3 IF(SREQ.NE.1)GO TO 4
      SP=10.0**MX
      DO2 I=1,P
      V(I)=V(I)/SP
    2 CONTINUE
    4 IF(DIFP.GT.0.512)GO TO 5
      IF(DIFP.GT.0.204)GO TO 6
      SL=0.25
      GO TO 7
    5 SL=1.0
      GO TO 7
    6 SL=0.5
    7 IF(SREQ.NE.1)SL=SL*10.0**MX
      V(P+1)=0.0
      V(P+2)=SL
      RETURN
      END
      SUBROUTINE DLINE(X,Y,N,ICHAR,HT)
      REAL X(102),Y(102),X1(102),Y1(102)
C     X AND Y ARE VECTORS TO BE PLOTTED.  SCALING MUST BE ANNOTATED
C     N=NO. OF PTS. TO BE PLOTTED.  ICHAR=SYMBOL CODE. HT=CHARACTER HEIGHT.
      DO 1 I=1,N
      X1(I)=(X(I-X(N+1))/X(N+2)
    1 Y1(I)=(Y(I-Y(N+1))/Y(N+2)
      CALL SYMBOL (X1(1),Y1(1),HT,ICHAR,0.0,-1)
      DO 2 I=2,N
    2 CALL SYMBOL(X1(I),Y1(I),HT,ICHAR,0.0,-2)
      RETURN
      END
```

This routine calculates a grid of |K**2*D|.
Method of calculation depends on region in complex plane. The three methods are: 1. Integration as calculated by J. McMullin; 2. Asymptotic expansion as given on page 180 of Stix; or 3. Power series expansion as given on page 178 of Stix.

```
      COMPLEX*8 P,CMPLX
      REAL*8 A,B,WR,WI,K,DSQRT
      REAL FPLT(101,101),FPLT1(5050),FPLT2(5151)
      EQUIVALENCE(FPLT(1,1),FPLT1),(FPLT(1,51),FPLT2)
      K=2.0D0
      WMAX=10.0
      BASE=WMAX/100.0
      WRITE(7,8)
    8 FORMAT('1','   WR/WPE      WI/WPE       ALPHA        BETA
     1 FUNCTION              ABS       1/ABS'//)
      DO 1 I1=1,101
```

```
      DO 2 I2=1,101
      WR=BASE*(I1-1)
      WI=BASE*(I2-1)
      A=WR/(1.414213562*K)
      B=WI/(1.414213562*K)
      XRAD=DSQRT(A**2+B**2)
      BS=B
      IF(XRAD.LT.2.8) GO TO 3
      IF(BS.LT.0.2) GO TO 4
      CALL INTG(A,B,F,K)
      GO TO 5
    3 CALL EXPAN(A,B,F,K)
      GO TO 5
    4 CALL ASYMP(A,B,F,K)
    5 CONTINUE
      FPLT(I2,I1)=CABS(F)
      XINF=1.0/FPLT(I2,I1)
      IF((((I2/2)*2).NE.I2).AND.(((I1/2)*2).NE.I1))
     1WRITE(7,7)WR,WI,A,B,F,FPLT(I2,I1),XINF
    7 FORMAT(' ',2(D10.3,1X,D10.3,3X),2(E10.3,1X,E10.3,3X))
    2 CONTINUE
    1 CONTINUE
      WRITE(4) FPLT1
      WRITE(4) FPLT2
      STOP
      END
      SUBROUTINE INTG(A,B,F,K)
      COMPLEX*8 F,CMPLX
      REAL*8 A,B,X(10),W(10),INT1,INT2,F1,F2,F1M,F2M,XM,AB2,A2B2
     1,K,FR,FI,DEXP,DCOS,DSIN
      DATA X/0.2453407083009D0,0.7374737285454D0,1.2340762153953D0
     1,1.7385377121166D0,2.2549740020893D0,2.7888060584281D0
     2,3.3478545673832D0,3.9447640401156D0,4.6036824495507D0
     3,5.3874808900112D0/,
     4W/4.6224366960006D-1,2.866755053628D-1,1.090172060200D-1
     5,2.4810520887746D-2,3.243773342238D-3,2.28338636016 3D-4
     6,7.8025564785 32D-6,1.0860693707 69D-7,4.3993409922 73D-10
     7,2.2293936455 34D-13/
      INT1=0.0D0
      INT2=0.0D0
      DO 1 I=1,10
      F1=X(I)/((X(I-A)**2+B**2)*0.5641895835
      F2=F1*X(I)
      XM=-X(I)
      F1M=XM/((XM-A)**2+B**2)*0.5641895835
      F2M=F1M*XM
      INT1=INT1+W(I)*(F1+F1M)
      INT2=INT2+W(I)*(F2+F2M)
    1 CONTINUE
      AB2=2.0*A*B
      A2B2=A**2-B**2
      IF (A2B2.GT.150.0D0)A2B2=150.0D0
      IF(A2B2.LT.-150.0D0) A2B2=-150.0D0
      FR=K**2+3.544907702*DEXP(-A2B2)*(B*DCOS(AB2-A*DSIN(AB2))+INT2
     1-A*INT1
```

```
      PI=3.544907702*DEXP(-A2B2)*(A*DCOS(AB2)+B*DSIN(AB2)-B*INT1
      F=CMPLX(SNGL(FR),SNGL(PI))
      RETURN
      END
      SUBROUTINE EXPAN(A,B,F,K)
      COMPLEX*16 Z,DCMPLX,S,S1,F0,J,CDEXP
      COMPLEX*8 F
      REAL*8 K,A,B,DIV,CDABS
      J=DCMPLX(0.0D0,1.0D0)
      Z=DCMPLX(A,(-B))
      DIV=1.0D0
      S=DCMPLX(0.0D0,0.0D0)
      I=0
    1 I=I+1
      S1=((-1.0D0)**(I+1))*(Z**(2*I-1))*(2.0D0**(I-1))/DIV
      S=S+S1
      DIV=DIV*(2.0D0*I+1.0D0)
      IF(SNGL(CDABS(S1)).GT.SNGL(1.0D-3*CDABS(S))) GO TO 1
      F0=1.772453851*CDEXP(-(Z**2))+2.0D0*J*S
      F=K**2+1.0D0+J*Z*F0
      RETURN
      END
      SUBROUTINE ASYMP(A,B,F,K)
      COMPLEX*16 Z,DCMPLX,J,S,CDEXP,F0
      COMPLEX*8 F
      REAL*8 A,B,K
      J=DCMPLX(0.0D0,1.0D0)
      Z=DCMPLX(A,(-B))
      S=0.5D0/Z+0.25D0/(Z**3)+0.375D0/(Z**5)+0.9375D0/(Z**7)
     1+3.28125D0/(Z**9)
      F0=1.772453851*CDEXP(-(Z**2))+2.0D0*J*S
      F=K**2+1.0D0+J*Z*F0
      RETURN
      END
```

This routine makes a contour map of data from previous routine.
CCONTR is a subroutine in *CSLIB at computing center, U. of A.

```
      REAL A(101,101),CVAL(10),AR1(5050),AR2(5151),MINVAL
      INTEGER IOP(4)
      DATA IOP/1,1,0,0/
      EQUIVALENCE(A(1,1),AR1),(A(1,51),AR2)
      READ(4) AR1
      READ(4) AR2
      MINVAL=1.0
      DO 1 I=1,10
      CVAL(I)=I*MINVAL
    1 CONTINUE
      XSIZE=10.0
      YSIZE=10.0
      M=101
```

```
      N=101
      NC=10
      CALL PLOTS
C     CALL VRTWIN(0.0,13.78,0.0,10.5)
      CALL PLOT(5.0,5.0,-3)
      CALL CCONTR(XSIZE,YSIZE,A,M,N,CVAL,NC,IOP)
      CALL PLOT(0.0,0.0,999)
      STOP
      END
```

This routine makes a 3-D plot of data from previous routine.
CPLT3D is a subroutine in *CSLIB at computing center, U. of A.

```
      REAL A(101,101),AR1(5050),AR2(5151),MAXVAL
      EQUIVALENCE(A(1,1),AR1),(A(1,51),AR2)
      READ(4) AR1
      READ(4) AR2
      MAXVAL=1.0
      DO 1 I=1,101
      DO 2 J=1,101
      A(J,I)=1.0/A(J,I)
      IF(A(J,I).GT.MAXVAL) A(J,I)=MAXVAL
    2 CONTINUE
    1 CONTINUE
      M=101
      N=101
      CALL PLOTS
C     CALL VRTWIN(0.0,13.78,0.0,10.5)
      CALL PLOT(5.0,5.0,-3)
      K=3
      DIST=5.0
      YAW=330.0
      PITCH=30.0
      SIZE=10.0
      KODE=0
      MGN=2
      SCALE=1.0
      CALL CPLT3D(A,N,M,K,DIST,YAW,PITCH,SIZE,KODE,MGN,SCALE)
      CALL PLOT(0.0,0.0,999)
      STOP
      END
```

This routine calculates total energy in plasma from tape data.

```
      REAL VS(102),TES(102),TIS(102),NS(102),RMS(102),BS(102)
     1,TPS(102),RD(102),EB(102),EK(102),ET(102),ENT(102)
      INTEGER P,PM1
```

```
C     THIS ROUTINE READS MAG. TAPE AND CALCULATES TOTAL PLASMA ENERGY.
      WRITE(5,1)
    1 FORMAT(' ','ENTER IX=1 IF TAPE CONTAINS INFO. FROM NONLINEAR HEATI
     1NG, IX=2 IF INV. BREM. ONLY. ENTER TAPE RECORD NO.'/
     2' ','   IX   REC')
      READ(5,2) IX,NREC
    2 FORMAT(2I5)
      IZ=NREC-1
      IF(IZ.EQ.0) GO TO 3
      DO 12 I=1,IZ
      READ(3)
   12 CONTINUE
    3 CONTINUE
      GO TO (4,5),IX
    4 READ(3)T,TF,P0,R,BZ,P,RMS,TES,TIS,NS,VS,BS,TPS
      DO 101 I=1,P
  101 TES(I)=TES(I)+0.33333*TPS(I)
      GO TO 6
    5 READ(3)T,TF,P0,R,BZ,P,RMS,TES,TIS,NS,VS,BS
    6 CONTINUE
      EBT=0.0
      EKT=0.0
      ETT=0.0
      DO 8 I=1,P
      VS(I)=0.5*(VS(I)+VS(I+1))
      EB(I)=0.125*(BS(I)**2)*(RMS(I+1)**2-RMS(I)**2)
      EK(I)=2.62E-24*NS(I)*(VS(I)**2)*(RMS(I+1)**2-RMS(I)**2)
      ET(I)=7.54E-12*NS(I)*(TES(I)+TIS(I))*(RMS(I+1)**2-RMS(I)**2)
      EBT=EBT+EB(I)
      EKT=EKT+EK(I)
      ETT=ETT+ET(I)
    8 CONTINUE
      ENG=EBT+EKT+ETT
      WRITE(6,20)T
   20 FORMAT('0','TIME IS',E12.3,' SECS.')
      WRITE(6,9) ENG,ETT,EBT,EKT
    9 FORMAT(' ','TOTAL ENERGY = ',E12.5/' ','THERMAL ENERGY = ',E12.5/
     1' ','MAGNETIC ENERGY = ',E12.5/' ','KINETIC ENERGY = ',E12.5)
C     DO 10 I=1,P
C     ENT(I)=EB(I)+EK(I)+ET(I)
C     WRITE(6,11) ENT(I),ET(I),EK(I),EB(I),RMS(I)
C  11 FORMAT(' ',6E15.3)
C  10 CONTINUE
      STOP
      END
```